Synthesis, Properties and Structure Development of Variable Modulus Polyisocyanurate Materials for Damping Applications.

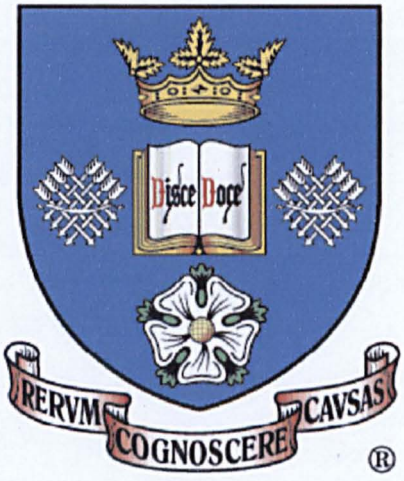

Anne-Louise Abbott

A Thesis Submitted to the
University of Sheffield
for the Degree of
Doctor of Philosophy

July 2003

Abstract

Damping vibrations in mechanical parts by the transformation into heat can be readily achieved by making use of the viscoelastic properties of polymer materials. The damping capability, tan δ, can be described as the ratio of the loss modulus, G", to the storage modulus, G'. This has a maximum around the glass transition temperature, T_g, for polymeric materials. Varying the composition of a polymer material is therefore a very important method of controlling the T_g. The use of polyisocyanurates gives good control of the T_g and the resultant materials have high thermal stability.

A series of poly(ether-isocyanurates) was synthesised by the end capping of hydroxyl-terminated polyoxypropylenes with methylene diphenyldiisocyanate (MDI), forming urethane links and leaving terminal isocyanate groups. The subsequent heat-activated, catalysed trimerisation of the isocyanate end groups gave the isocyanurate group which effectively cross-linked the material. Varying both the polyether (soft segment) chain length and the MDI (hard segment) content gave a range of samples with varied moduli. Morphology and subsequent mechanical properties are determined by the microphase separation of the hard and soft segments.

Bulk, layered and graded poly(ether-isocyanurates) were prepared and analysed by fourier transform infra-red microscopy and laser ablation mass spectroscopy. The formation of the gradient in modulus was attributed to a separation of the polymers due to density differences.

The morphologies of the poly(ether-isocyanurates) were investigated using synchrotron small angle x-ray scattering (SAXS). Development of this morphology was also studied by performing *in situ* time resolved experiments. Phase separation domain size varied with polyether chain length and with hard segment content. Microphase separation was observed to occur via spinodal decomposition (Cahn-Hilliard theory). The Teubner-Strey microemulsion model, based on a Ginzburg-Landau free-energy expansion, was applied to interpret the development of a bicontinuous morphology. The bicontinuity was preserved due to the vitrification of the polyisocyanurate domains.

Mechanical measurements were conducted using a nanoindenter. Static measurements gave values of indentation modulus from 5 MPa to 3 GPa. These results were modelled using a modified version of the Kerner equation. Phase inversion of glassy particles in a rubber matrix to rubber particles in a glassy matrix was observed for materials with a polyether soft segment number average molecular weight of 2200 with increasing hard segment content. The modulus variation of the gradient was studied by the positionability of the tip. Dynamic nanoindentation data were combined using time-temperature-superposition, and values of tan δ were evaluated over a range of frequencies for a number of samples.

Blends of polystyrene-polyisoprene-polystyrene triblock copolymer and homopolystyrene with well documented properties were also investigated to compare with the poly(ether-isocyanurate) elastomers, and similar changes in modulus and domain size with hard segment content were observed. Good correlations were found between microstructures from SAXS and the mechanical properties from nanoindentation measurements for both systems.

Acknowledgements.

I would like to express my sincere thanks to my supervisor Professor Anthony J. Ryan for his support, generosity and endless enthusiasm throughout the project. The opportunities that have been available for me throughout the research and write-up of this thesis will never be forgotten.

Grateful thanks are also expressed to Dr Michael L. Turner for his encouragement and patience.

I thank the staff of Daresbury laboratory, in particular Dr Nick Terrill and Mr Anthony Gleeson, for helping me get the best out of many a night shift.

Thanks also go to Mr Alan Cox for LAMS, Dr Geoff Cope for microtoming, and Dr Sasha Goruppa and Dr Simon Hayes for help and useful discussions regarding nanoindentation. I am grateful that they encouraged me to try new materials on the nanoindentor.

Thanks are also expressed to the technicians in the department of chemistry who have helped me during my years here, especially Mr Chris Lumley, Mr Richard Wilkinson, Mr Brian Watson, who made the moulds used in this work, and Mr Robert Hanson for help with the DSC.

Analysis of the scattering data would not have been possible without help from Dr Patrick Fairclough, Dr Ellen Heeley, Dr Alex Norman, Dr Shaomin Mai and Dr Wu Li, and for this I am extremely grateful.

I also thank everyone I have worked with, past and present, especially Kate, Rob, Paolo, Christine, Colin, Corinne, Jon, Andy, JC, Paul and Elizabeth.

Finally I would like to thank Mum, Dad and Paul who have offered unending support during this work.

Declaration

This thesis is based on the results of my own research and no portion of the work has been submitted for any degree or qualification at this or any other university or institution.

Department of Chemistry
The University of Sheffield
Sheffield
United Kingdom

May 2003

CHAPTER 1

INTRODUCTION

1.1 Polymers: Modern Materials

Polymers have become increasingly important for both high and low technology developments in today's society. This is because we are able to create materials with whatever properties we want simply by varying the chemical structure of the repeating unit, or by changing the organisation of the chains by processing. It is very important that the structure of the polymer on all length scales is known, as this has a considerable effect on the material properties of the polymer. Current research on polymeric systems includes; light emitting, light manipulating, and charge carrying polymers, smart materials responsive to environmental conditions, engineered plastics for packaging and the increasing demand for biodegradable waste, and polymers that are biocompatible - for use in the body as drug delivery systems or replacement body parts.[1] One of the main advantages of polymers used in the material industry is low cost, and the low density of polymers means that they are easy to transport.

The varying degrees of order on a range of length scales that polymeric systems may possess has meant that new techniques are still being developed to analyse the types of structures formed. *In-situ* measuring whilst processing is extremely valuable as it enables the real-time structure formation of the product to be established.

With the knowledge of how the chemical composition and processing affect the microstructure and the resulting properties, it is possible to tune the reactants and conditions to obtain the ideal mechanical properties needed for the desired application.

1.2 Damping

Vibrations are often triggered in machinery with moving parts. These are undesirable as they may generate unwanted noise, or cause fatigue, and hence

mechanical failure. Vibration can often be reduced by increasing the mass. This shifts the natural frequency to lower values, but added mass is often detrimental to the performance of the part. Vibration reduction may be attained by increasing the damping capacity; damping is the removal or reduction of mechanical vibrational energy by a transformation into heat.

Polymers with suitable properties, in particular their viscoelastic ones, may be applied to the vibrating substrate to increase the damping [2] and so reduce the noise and prolong the lifetime of the equipment.

A wide variety of damping polymers are already available, depending on the temperature and frequency range at which damping is required. Some of the most often used materials include: asphaltics, poly(vinyl acetate) and copolymers, acrylics, natural rubber, styrene butadiene rubber, silicone rubber and polyurethanes. Materials for vibration damping have been recently reviewed.[3]

Viscoelasticity is not the only mechanism for damping – defects such as phase boundaries, phase changes and various interfaces contribute to damping since these provide alternative mechanisms for the dissipation of energy.

Especially effective damping can be achieved by the use of multicomponent materials with microheterogeneous morphologies, and these include a number of polymer blends and block copolymers. Interpenetrating polymer networks are an easy way to achieve a desired morphology.[4]

Two practical methods of damping are of specific interest when polymers are involved:

Free layer damping. This is a cheap method where the system consists of two layers; the substrate to be damped and the polymeric damping layer. The viscoelastic polymer layer is deformed in extension and compression parallel to the substrate surface.

Constrained layer damping. A constrained layer damping system has three layers, the polymer being the middle one. Either the constrained layer can be part

of the system, for example gluing two sheets of metal together with the damping layer, or it can be applied afterwards. The most effective arrangements are when both the substrate and the constraining layer have high modulus (resistance to deformation) and the damping layer is soft (this is complicated by the fact that shear and strain components are not transmitted in the same ways through hard and soft materials – and is why such an arrangement is an effective damper).

In the presence of mechanical vibrations, vibrational energy may be dissipated by the polymer layer in the form of heat. In free layer damping the system becomes more effective as the layer thickness increases, and as the storage modulus and damping capability increase. In constrained layer damping, the principle deformation occurs as shear.

In order to design polymeric materials for vibration damping it is necessary to be aware of how polymers behave when subjected to stress. We can then make use of a range of structural features that polymers can adopt.

1.3 The Mechanical Properties of Polymeric Materials

The mechanical behaviour of materials can be investigated by the study of the deformations that occur under loading. Linear elastic materials follow Hooke's law, i.e. that stress is directly proportional to strain. Young's modulus, the modulus of elasticity, is the ratio of stress to strain when the deformation is totally elastic. Polymers, however, may behave differently from other solids, due to their viscoelastic nature – their behaviour exhibits the mechanical characteristics of viscous flow and elastic deformation.[5]

The shape of the sample and the way the load is applied is important, especially with polymer materials because the mechanical properties depend on the testing conditions (temperature and time).

The tensors in figure 1.1 describe the various directions of shear:

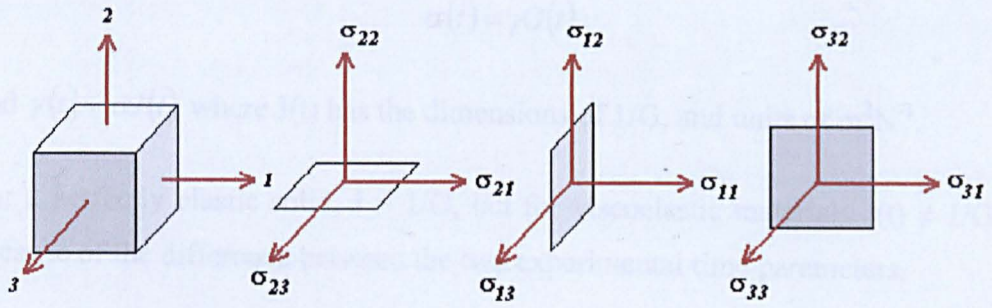

Fig. 1.1 Nomenclature for shear directions

The ratio of a stress to the corresponding strain is called a modulus. For a perfectly elastic solid the modulus G is defined as / , and G(t) is its time dependent analogue as measured in a dynamic experiment.

1.3.1 Static experiments

The effects of sequential changes in strain are additive. The stress is given by:

$$\sigma_{(21)}(t) \quad ^{t} G(t \quad t')\gamma_{(21)}(t')dt' \qquad 1.1$$

where $_{(21)}$ is the stress, γ_{21} $\frac{\gamma_{21}}{t}$ is the shear rate, the strain, and G(t) the relaxation modulus.

This can also be expressed in terms of the strain – a history of the time derivative of the stress:

$$\gamma_{21}t \quad ^{t} J(t \quad t')\sigma_{21}(t')dt \qquad 1.2$$

where σ_{21} $\frac{\sigma_{21}}{t}$ and J(t) is the creep compliance. Creep is a time dependent, permanent deformation that occurs under stress. Thus the ratio of the stress to the corresponding strain is equal to the modulus:

$$\sigma(t) = \gamma G(t) \tag{1.3}$$

and $\gamma(t) = \sigma J(t)$ where J(t) has the dimensions of 1/G, and units of m^2N^{-1}.

For a perfectly elastic solid, J = 1/G, but for viscoelastic materials J(t) ≠ 1/G(t) because of the difference between the two experimental time parameters.

1.3.2 Dynamic experiments

Further data can be obtained by varying the stress periodically. This is usually done by a sinusoidal alternation at a frequency ω. If the viscoelastic behaviour is linear, the strain will also alternate sinusoidally, but will be out of phase with the stress.

If $\gamma = \gamma^\circ \sin \omega t$ where γ° is the maximum strain amplitude, then

$$\dot{\gamma} = \omega \gamma^\circ \cos \omega t . \tag{1.4}$$

Substituting s for (t – t') in equation 1.1,

$$\sigma(t) = \int_0^\infty G(s)\omega\gamma^\circ \cos[\omega(t-s)]ds \tag{1.5}$$

$$= \gamma^\circ \left[\omega \int_0^\infty G(s) \sin \omega s ds \right] \sin \omega t + \gamma^\circ \left[\omega \int_0^\infty G(s) \cos \omega s ds \right] \omega t \tag{1.6}$$

The term in sin ωt is in phase with γ and the cos ωt term is 90° out of phase. σ is periodic in ω but out of phase with γ to a degree (depending on the relative magnitude of those terms).

In terms of time,

$$\sigma = \gamma^\circ [G' \sin \omega t + G'' \cos \omega t] \tag{1.7}$$

This introduces two new frequency dependent functions, G'(ω) is the shear storage modulus and G"(ω) is the shear loss modulus.

If the stress is written as the amplitude of stress $\sigma^{\circ}(\omega)$ and phase angle $\delta(\omega)$ between stress and strain then trigonometric relations show that:

$$\sigma = \sigma^{\circ} \sin(\omega t + \delta) = \sigma^{\circ} \cos\delta \sin\omega t + \sigma^{\circ} \sin\delta\omega s\omega t \qquad 1.8$$

Combining equations 1.7 and 1.8 give

$$G' = (\sigma^{\circ} / \gamma^{\circ}) \cos\delta \qquad 1.9$$

$$G'' = (\sigma^{\circ} / \gamma^{\circ}) \sin\ \delta \qquad 1.10$$

$$G''/G' = \tan\delta \qquad 1.11$$

How G', G" and tan δ vary in a real system is shown in figure 1.2, and the vectorial representation of each of the components is shown in figure 1.3.

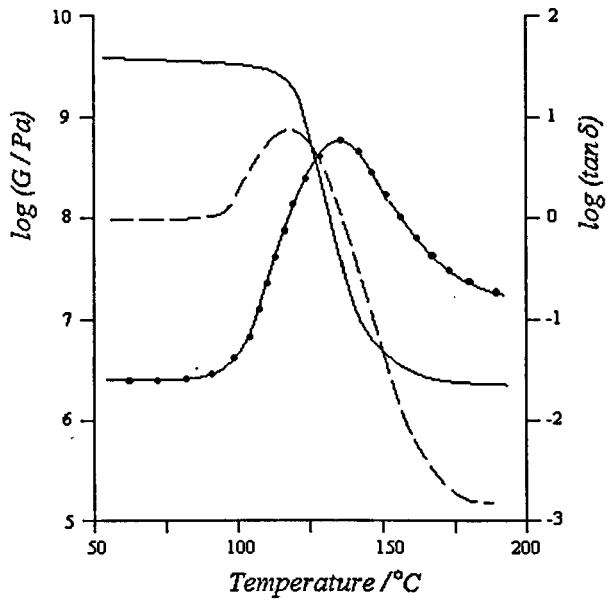

Fig. 1.2 The variation of tan δ (-•-), storage modulus (–) and loss modulus (- - -) with temperature for polystyrene [2].

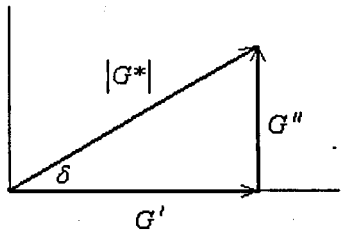

Fig. 1.3 The vectorial resolution of the components of the complex modulus in sinusoidal shear deformations

The sinusoidal varying stress is usually expressed as a complex number:

$$\sigma^* / \gamma^* = G^* = G' + iG'' \qquad 1.12$$

This is a vectorial resolution of components, represented in figure 1.3.

$$\left|G^*\right| = \sigma^\circ / \gamma^\circ = \sqrt{G'^2 + G''^2} \qquad 1.13$$

G′ is the ratio of the stress in phase with the strain to the strain, and G″ is the ratio of the stress 90° out of phase with the strain to the strain.

The complex compliance, $J^* = \gamma^* / \sigma^* = \frac{1}{G^*} = J' - iJ''$ 1.14

So,

$$J' = \frac{G'}{\left(G'^2 + G''^2\right)} = \frac{1/G'}{1 + \tan^2 \delta} \qquad 1.15$$

$$J'' = \frac{G''}{\left(G'^2 + G''^2\right)} = \frac{1/G''}{1 + \left(\tan^2 \delta\right)^{-1}} \qquad 1.16$$

$$G' = \frac{J'}{\left(J'^2 + J''^2\right)} = \frac{1/J'}{1 + \tan^2 \delta} \qquad 1.17$$

$$G'' = \frac{J''}{J'^2 + J''^2} = \frac{1/J''}{1 + \left(\tan^2 \delta\right)^{-1}} \qquad 1.18$$

1.3.3 Modelling Mechanical Properties

The modelling of mechanical properties is often performed by the spring and dashpot model, of which there are two main types, the Maxwell model and the Voigt or Kelvin model. Schematic diagrams of these models are given in figures 1.4 and 1.5.

For both of these systems, σ is defined as the force applied and γ the displacements of the terminals. Each spring is assigned a stiffness (force / displacement) termed G_i (shear modulus) and each dashpot is given a frictional resistance (force / velocity), termed the viscosity contribution, η_i.

For a viscoelastic liquid, $G_{(t)}$ approaches 0 as t tends towards infinity. For a viscoelastic solid $G_{(t)}$ approaches a constant, finite value, G_e.

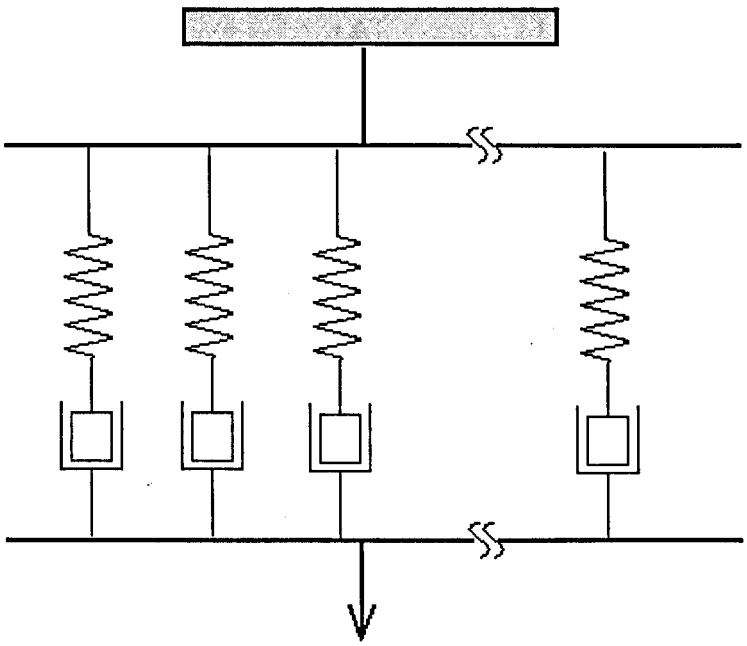

Fig. 1.4. The Maxwell Model

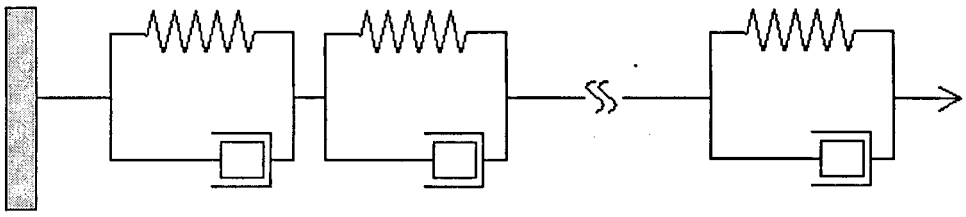

Fig. 1.5. The Voigt or Kelvin Model.

1.3.3.1 The Maxwell model

When a stress relaxation experiment is performed using the Maxwell model, the force on each dashpot relaxes exponentially. For a viscoelastic liquid system all the viscosities must be finite and for a solid system one viscosity must be infinite.

If a spring corresponds to shear rigidity, $G_i = 1 / J_i$, and a dashpot to viscosity ηi, then the relaxation time of an element is defined as $\tau_i = \eta_i / G_i$, and is a measure of the time required for stress relaxation.

So the values of modulus and creep become:

$$G(t) = G_i e^{-t/\tau_i} \qquad 1.19$$

$$G'(\omega) = Gi\omega^2\tau_i^2\left(1+\omega^2\tau_i^2\right) \qquad 1.20$$

$$G''(\omega) = Gi\omega\tau_i /\left(1+\omega^2\tau_i^2\right) \qquad 1.21$$

$$J(t) = Ji + t/\eta_i \qquad 1.22$$

$$J'(\omega) = Ji \qquad 1.23$$

$$J''(\omega) = Ji/\omega\tau_i = 1/\omega\eta_i \qquad 1.24$$

$$\eta'(\omega) = \eta_i/\left(1+\omega^2\tau_i^2\right) \qquad 1.25$$

$$\tan\delta = 1/\omega\tau_i \qquad 1.26$$

1.3.3.2 The Voigt model:

For a viscoelastic liquid one spring must have a modulus equal to zero, and for a viscoelastic solid, all springs must be nonzero.

For the Voigt model the spring and dashpot have the same definitions as for the Maxwell model, but their ratio, τ_i is defined as the retardation time. This is a measure of the time required for extension of the spring to its original length while retarded by the dashpot. So the functions then become:

$$J(t) = Ji(1 - e^{-t/\tau_i}) \qquad 1.27$$

$$J'(\omega) = Ji(1 + \omega^2\tau_i^2) \qquad 1.28$$

$$J''(\omega) = Ji\omega\tau_i/(1 + \omega^2\tau_i^2) \qquad 1.29$$

$$G(t) = Gi \qquad 1.30$$

$$G'(\omega) = Gi \qquad 1.31$$

$$G''(\omega) = Gi\omega\tau_i = \omega\eta_i \qquad 1.32$$

$$\eta'(\omega) = \eta_i \qquad 1.33$$

$$\tan\delta = \omega\tau_i \qquad 1.34$$

Importantly the Maxwell model cannot describe creep and the Voigt model cannot describe stress relaxation.

1.3.3.3 Relaxation Spectrum

In the Maxwell model the number of elements is increased without limit. This gives a continuous spectrum where each infinitesimal contribution to rigidity, F $d\tau$ is associated with relaxation times lying between τ and $\tau + d\tau$. A logarithmic

time scale is used for convenience, and the continuous relaxation spectrum is defined as H d lnτ.

The contribution to rigidity is associated with relaxation times whose logarithms lie in the range between lnτ and lnτ + dlnτ, a measure of the population of relaxation mechanisms with relaxation times in this interval.

The equation for the modulus can be written as:

$$G(t) = G_e + \int_{-\infty}^{\infty} H e^{-t/\tau} d\ln\tau \qquad 1.35$$

The G_e term allows for a discreet contribution with $\tau = \infty$ for viscoelastic solids. G_e is equal to zero for viscoelastic liquids. H has specific shapes for different classes of materials.

1.3.3.4 Retardation Spectrum

If the Voigt model is made to become infinite, then it represents a continuous spectrum of retardation times, L. The creep compliance can be written as:

$$J(t) = J_g + \int_{-\infty}^{\infty} L(1 - e^{-t/\tau}) d\ln\tau + t/\eta_o \qquad 1.36$$

J_g is a discrete contribution with t = 0, without it an instantaneous deformation would require an infinite stress.

Short time processes are revealed in detail in H and long time processes in L. Viscoelastic functions can therefore be calculated when the spectra are known.

1.3.4 Molecular Theory

Rouse theory [6] is based on the idea of representing the motion of polymer chains in a viscous liquid by a series of differential equations. Theories for the behaviour

of dilute solutions can be quite good at predicting the behaviour of pure polymers.

Rouse theory uses the bead and spring model, a schematic diagram of which is shown in figure 1.6.

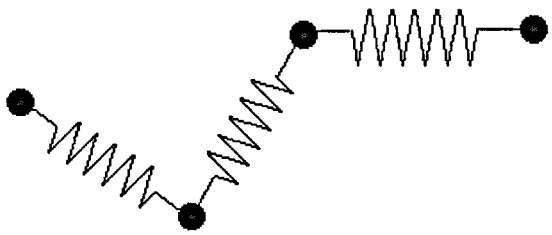

Fig. 1.6 Bead and spring model.

The springs used in Rouse theory are molecular chains of equal length. The separation of ends is around a Gaussian probability distribution. Only the beads interact directly with the solvent molecules. If a bead is displaced from its equilibrium position two forces act upon it: forces due to viscosity from interactions with solvent molecules, and forces due to the tendency of molecular chains to return to a state of maximum entropy by Brownian diffusion movements. There are distinct similarities between this model and the strain and displacement seen in the Voigt model.

Some adaptation to the ideal theory is required because the polymers being measured are far from ideal: they are not all of equal molecular weight, they posses entanglements, and the ones in this study in particular, contain a varying amount of cross-link units.

To improve the model, it has been proposed that we consider a cross-link with tetrafunctional connectivity. The representation of tri and tetrafunctionalities are shown in figure 1.7.

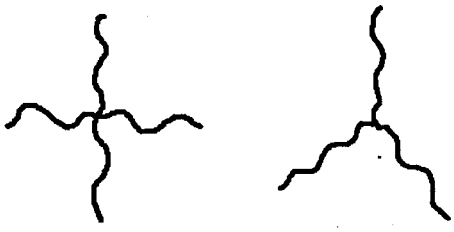

Fig. 1.7 Molecules with tetra- and tri-functionality

The arms are equal to the length of the chains in the Rouse model and there are no dangling chain ends. The density of cross-links is greater than the entanglement density before cross-linking occurred. The cross-links are fixed in that when the sample is deformed they will move in a similar way.

The Classical Theory of Rubber Elasticity states that the equilibrium shear modulus, G_e in infinitessimal deformations is given by:

$$Ge = g(\overline{r_E^2} / \overline{r_0^2})\nu RT \qquad 1.37$$

where ν is the number of moles of network strands per cm^3, g is a numerical factor of order 1, $\overline{r_E^2}$ is the mean square end to end distance of a strand, $\overline{r_0^2}$ is the mean square end to end distance that the strand would adopt if there were no cross-links. The ratio $\overline{r_E^2} / \overline{r_0^2}$ is of identity 1 at the conditions at which the network was formed. g Includes contributions from mobile cross-links that experience fluctuations instead of moving normally, (f-2) / f, where f is the functionality of the cross-link.

For a tetrafunctional cross-link this is equal to ½ and for a trifunctional it is equal to 1/3. The ν term is replaced by $(\nu - u)$ to describe the number of moles of junction points per cm^3.

In terms of a Rouse model of motion where the ends are fixed, ν is substituted for ρ / M and an additional contribution to the modulus with infinite relaxation time and magnitude νkT is added, i.e.:

$$G(t) = \nu RT\left[1 + \sum e^{-t/\tau}\right] \quad 1.38$$

$$G' = \nu RT\left[1 + \sum \omega^2 \tau_p{}^2 / \left(1 + \omega^2 \tau_p^2\right)\right] \quad 1.39$$

$$G'' = \nu RT \sum \omega \tau_p / \left(1 + \omega^2 \tau_p^2\right) \quad 1.40$$

$$\tau_p = a^2 P_c^2 \zeta_0 / 6\pi^2 p^2 kT \quad 1.41$$

where a is the characteristic length, P_c refers to the average degree of polymerisation of a network strand ($P_c = \rho / \nu M_0$ where M_0 is the monomer molecular weight), p is the summation index and ζ_0 is the translational friction coefficient per monomer unit. It is important to note that changing the cross-link density affects the chemical (and microstructural) composition of the polymer and hence the friction coefficient, ζ_0.

1.3.5 The Effect of Temperature on the Properties of Polymers

The viscoelastic nature of some polymers gives them their interesting properties, and this viscoelasticity is very temperature dependent.

1.3.5.1 Glass Transition Temperature.

Some materials exhibit a supercooled liquid state where the viscosity is greater than 10^{14} Nsm^{-2}. On heating, these materials do not melt, but soften over a range of temperatures, the mean of which is denoted the Glass Transition Temperature, or T_g. There is no latent heat involved as with first order transitions. Polymers that do not crystallise often exhibit a well defined T_g. The properties of the materials change drastically on passing through the T_g, from a brittle, glassy phase to a rubbery one. The measurement of the elastic modulus as a function of time can change by orders of magnitude. Other properties that undergo large changes include the refractive index, density, specific heat and dielectric constant.

The dramatic but reversible change in properties we see at the T_g, for instance elasticity and hardness, are due to changes in molecular motion within the polymer. At the T_g the chains get locked into the position that they were in when the T_g was reached. Below the T_g the available thermal energy is insufficient to overcome the rotational energy barriers within the polymer chain, and the polymer is in a glassy state and is likened to a frozen liquid with a random structure. The polymer behaves as though it were a stiff spring, storing all the energy in stretching (as potential energy) when work is done. If enough thermal energy is supplied, the chain segments can move, and a transition from glass-like to rubber-like state is observed. This can be likened to the difference between a weak spring and a stiff spring. As weak springs can only store a fraction of the potential energy that strong springs can, the rest is lost as heat. If the change from stiff to weak happens over an observable period of time, the energy loss is detected as mechanical damping.

The temperature at which the T_g occurs depends on the structure of the polymer. There are several architectural factors which affect the T_g. These include:

- Molecular weight – an indication of the length of the chain. Generally, the higher the molecular weight the higher the T_g.

- The presence of steric interactions caused by cis / trans double bonds. An all trans configuration (see figure 1.8, a)) will have higher T_g than all cis or cis / trans configuration (figure 1.8, b)).

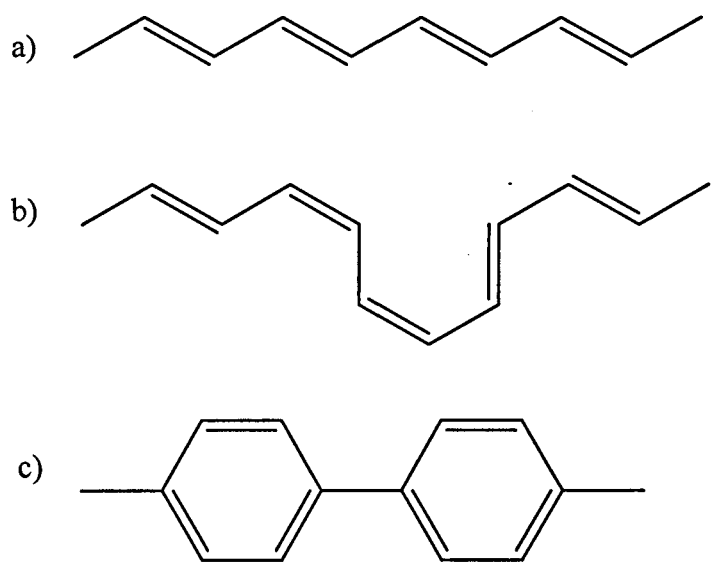

Fig. 1.8 Sections of backbones for 3 hydrocarbon polymers.

- The flexibility of the chain. A polymer with an inflexible backbone (eg polyphenylene - fig 1.8, c)) will have a higher T_g than e.g. polyethylene.

- Substituents. Side chain groups may have an effect if they provide additional interactions such as hydrogen bonds or dipole – dipole interactions.

- Cross-linking between the chains. The more branching or cross-linking the higher the T_g because of the reduced freedom of movement of the chains.

So, depending on the nature of the polymer, T_g can range from 170 to 500 K. Segmented (microphase separated) polyurethanes typically have two T_g's. The soft segment T_g is less than 250 K and the hard segment T_g is greater than 400 K. A comparison of the T_g arising from different polymer systems is given in table 1.1.

The T_g is well described using free volume theory, and may be located by following the change in volume against temperature, but is, however dependent upon the rate of cooling. Figure 1.9 shows that different T_g's may be obtained by varying the cooling rate.

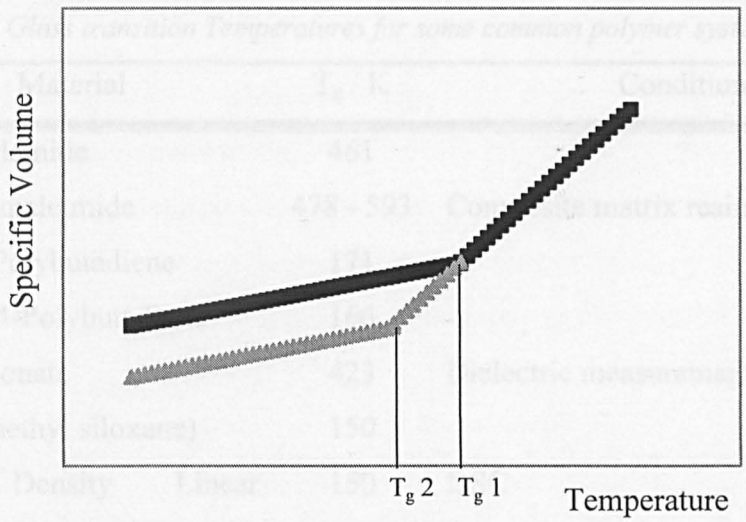

Fig. 1.9 *Change in specific volume with temperature to find* T_g

■ *faster cooling rate and* ▲ *slower cooling rate*

Cooling at a slower rate requires a lower temperature to stop chain motion. This is because of the time dependent nature of the T_g.

The Flory-Fox equation [7] (1.42) defines the free volume, v_f in terms of K, the free energy at absolute zero, T, the temperature of the system, and α_G, the cubic expansion coefficient when the polymer is in the glassy state and α_R the cubic expansion coefficient when the polymer is in the rubbery state.

$$v_f = K + (\alpha_R - \alpha_G)T \qquad 1.42$$

Table 1.1 *Glass transition Temperatures for some common polymer systems.* [5]

Material	T_g / K	Conditions,
Polyacrylamide	461	
Poly bis maleimide	478 - 593	Composite matrix resin,
Cis-1,4-Polybutadiene	171	
Trans-1,4-Polybutadiene	166	
Polycarbonate	423	Dielectric measurements, 10 Hz
Poly(dimethyl siloxane)	150	
High Density Linear Polyethylene	150	DSC
Low Density Polyethylene	140 - 170	
Poly(ethylene oxide)	160 - 184	Differential Microcalorimetry
Poly(ethylene terephthalate)	342 – 388	DSC
Cis-1,4-Polyisoprene	201	
Trans-1,4-Polyisoprene	205	
Poly(methyl acrylate)	284	
Poly(methyl methacrylate)	318, 379	Atactic, Isotactic
Poly(norbornene)	308 - 318	Vibration damping elastomer
Polypropylene	268	Atactic
Polypropylene	275	Isotactic
Poly(propylene oxide)	201	Amorphous, Atactic
Poly(propylene oxide)	265 - 321	Cross-linked with aromatic triisocyanate
Polystyrene	373	
Polyurea	215	MDI / Polyetheramine / DETDA
Polyurethane	363	MDI / Ethylene Glycol
Polyurethane	222 ss 470 hs *	PPG / MDI / BD

** 222K for soft segment (ss) and 470K for the hard segment (hs)*

1.3.5.2 The Importance of T_g for Damping Applications

Polymers can absorb mechanical energy and convert this partially into heat through viscous deformation. The most important mechanism of energy absorption is the conversion into heat by gain in internal rotational and vibrational energy through molecular relaxation processes. This can take place most effectively at the glass transition region, due to the onset of large segmental movements.

The T_g can be varied in a given polymer by the addition of plasticisers or fillers. The incorporation of fillers adds mass, which increases damping. Further advances in this field include the use of platelet fillers such as mica or graphite, which can act as mini constrained layer systems.

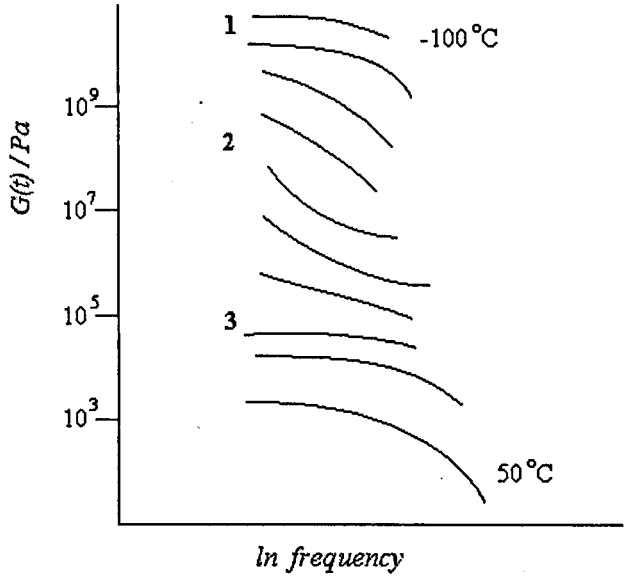

***Fig. 1.10** Stress relaxation curves for an elastomer e.g. polyisobutylene taken at different temperatures*

Below the T_g the polymer chain is not free to move therefore large changes in mechanical properties do not occur. Figure 1.10 shows how the modulus of an elastomer changes with frequency at different temperatures. There are distinct regions to curves such as this, some of which are marked on the figure.

In region **1** the compliance is low and does not change very much with frequency.

At higher temperatures a "plateau" is reached – region **3**. This is characteristic of a soft rubber, and mechanical properties only change very slowly with frequency.

It is in the "transition zone" **2** where the changes in mechanical properties with frequency are spectacular.

The retardation and relaxation times which constitute the viscoelastic spectra decrease rapidly with increasing temperature. At low temperatures no changes of configuration can happen within the period of deformation (all $\omega\tau_i >> 1$). At high temperatures, all $\omega\tau_i$ corresponding to mechanisms in the transition zone $<<1$, all configurational modes of motion can freely occur (within the confines of a virtual tube).

It would be very complicated to analyse the temperature dependence by using an analytical form for J'(T) at constant frequency, so a method of using reduced variables is employed – viscoelastic corresponding states. This separates the two principles of temperature and time (on which viscoelastic properties depend) and expresses these properties as a single function of each. It is then easier to see how the parameters that describe the temperature dependence are related to the molecular constitution and structure of the material in question.

All contributions to G' should be proportional to ρT and all relaxation times should have the same temperature dependence.

$$a_T = \left[a^2\zeta_0\right]_T / \left[a^2\zeta_0\right]_{T0} T \qquad 1.43$$

The temperature dependence is largely due to the change in the friction coefficient, although temperature enters again explicitly as a factor, and the mean square end to end distance per monomer unit, *a,* may change slightly.

Thus the effect of a change in temperature from T to T_0 is to multiply G' by $T_0\rho_0$ / $T\rho$ and multiply the frequency scale by a_T. The density ration is due to thermal expansion.

Each temperature curve is shifted to make a composite curve. This then represents the frequency dependence that would have been obtained over a much wider frequency range measured at a single temperature.

1.3.5.3 Glass Transition Temperatures for Polymer Blends

The T_g for miscible polymer blends varies with composition. For multiphase materials there will be multiple T_g's – and these will be close to the original values of the constituent homopolymers. For single phase blends, which include random and statistical copolymers as well as compatible blends there will be a single T_g lying between those of the corresponding homopolymers. Plasticisation (the addition of smaller molecules to a polymer) lowers the T_g, due to the effective addition of free volume to the system.

A prediction of the resultant T_g from a single phase mixture can be obtained by the use of the Fox equation 1.44:

$$\frac{1}{T_g} = \frac{w_p}{T_{gp}} + \frac{w_s}{T_{gs}} \qquad 1.44$$

where w is the weight fraction of each component and the subscripts p and s denote the polymer and the solvent.

For the same molecular architecture, the T_g increases with molecular weight until a plateau is reached. This will be dependent on the structure of the polymer.

$$T_g^{\infty} = T_g + K\sqrt{M_n} \qquad 1.45$$

where T_g^{∞} defines a polymer of infinite molecular weight and M_n is the number - average molecular weight of the sample. In the free volume assumption the excess free volume is associated with the chain ends and these become non existent for a polymer of infinite molecular weight.

The formation of a permanent network by the introduction of cross-links decreases the free volume available and therefore raises the T_g. The T_g may

become broad and poorly defined for high values of cross-linking. A linear relationship between the change in T_g with cross-link density can be formulated for the lower degrees of cross-linking:

$$\Delta T_g = AC_c \qquad 1.46$$

where C_c is the number of moles of cross-links per gram of polymer and A is a constant. This change in T_g with cross-link density becomes very important when dealing with complicated systems, for example those where the network is formed by curing. If a polymer is cured at a temperature, T_c, the increase in the glass transition, as the reaction proceeds, decreases the mobility of the monomers, and this slows the reaction down. As the T_g approaches the curing temperature, the reaction becomes diffusion controlled and may stop altogether due to vitrification. A complete cure can only be obtained by curing at temperatures above the glass transition of the final system. Often 'post-curing', where the temperature is increased significantly after the initial curing procedure, is adopted for many systems.[8]

1.3.5.4 The Williams-Landel-Ferry (WLF) Equation

The simplest way of applying a time – temperature equivalence is to produce a master compliance curve – choosing one temperature as a reference temperature and shifting results horizontally on a logarithmic temperature scale to give a smooth curve. It may also be necessary to apply a small vertical shift factor $T_0\rho_0 / T_r$ in the transition range. Molecular theories suggest that the equilibrium model changes with temperature in the transition range according to the theory of rubber elasticity.

The empirical relationship first provided by Williams, Landel and Ferry states that:

$$\log a_T = -C_1^0 (T - T_0) / C_2^0 + (T - T_0) \qquad 1.47$$

Therefore a plot of $(T-T_0)/\log a_T$ against $T-T_0$ gives C_1^0 = -1 / slope and C_2^0 = intercept / slope. A further criterion for satisfactory reduction is that the coefficients C_1^0 and C_2^0 should have magnitudes in accordance with experience when they are transformed to the values appropriate to the T_g as a reference temperature.

It was later proposed that this empirical equation had a more fundamental interpretation, and the theory according to free volume was established.

The fractional free volume, $f = n_f / v$ (which is very similar to the Flory-Fox equation, 1.42) is written as:

$$f = f_g + \alpha_f (T - T_g) \qquad 1.48$$

where f_g is the fractional free volume at T_g and a_f is the coefficient of expansion of free volume.

Relaxation times are given by expressions of the form $\tau = \eta / E$ (Maxwell). If the changes in modulus with temperature are ignored compared to the changes in viscosity, the shift factor a_T in going from T_g to some other temperature is given by:

$$a_T = \frac{\eta_T}{\eta_{T_g}} \qquad 1.49$$

Doolittle's viscosity equation [9] relates η to free volume in monomeric liquids and states that:

$$\eta = a \exp\left(\frac{b v}{v_f}\right) \qquad 1.50$$

where a and b are constants. It then follows that:

$\ln a_T = b\left\{\frac{1}{f} - \frac{1}{f_g}\right\}$, then substituting in $f = f_g + \alpha_f (T - T_g)$

gives

$$\log a_T = \frac{-(b/2.303 f_g)(T - T_g)}{f_g/\alpha_f + (T - T_g)} \qquad 1.51$$

which is the W-L-F equation.

1.4 Recent Attempts to Maximise Damping

Design principles for vibration isolation have been reviewed by Massot *et al* [10] and Harris *et al.*[11] An eloquent forward approach has been presented by Tomlinson.[12]

Recently, the main methods to maximise the damping capacity have been to fabricate a material that dampens over a wide range of frequencies by varying the composition of the material. This can be achieved by the addition of different types of filler.[13]

Use has been made of phase transitions other than the glass transition by Terentjev *et al* and Clarke *et al.*[14, 15] Phase transitions that liquid crystalline materials undergo also result in broad peaks in tan δ.

Hourston *et al* [16] use interpenetrating polymer networks to develop high performance damping materials with a broad range of T_g. IPN materials made from chemically - modified and compatabilised polyurethane and polystyrene were observed to have a broad transition between -12 and 125 °C. The resultant materials had very complicated morphologies: not only polyurethane domains in polystyrene matrix and polystyrene domains in polyurethane matrix but also polystyrene domains in polyurethane domains in polystyrene matrix

The modelling of new damping systems has been attempted by Tomlinson *et al.* [17]

1.5 Phase Separation

Why and how bulk demixing occurs in liquid and polymer systems is an area that has received great interest. Flory - Huggins theory is used in this section to explain why phase separation occurs and the process by which the two phases are formed is discussed by looking at two kinetic pathways.

1.5.1 Flory – Huggins Theory

The onset of phase separation can be predicted by the polymer solution theory of Flory and Huggins.[18]

Flory - Huggins theory divides each polymer molecule into chains of segments, with each segment being equal in size. The polymer molecule consists of X segments (X is given by the ratio of the molecular volumes of polymer and solvent) and the segments in the system are placed in a 3D lattice of identical cells each the size of the solvent molecules. Each segment is placed separately into the lattice, followed by another segment placed in an adjacent cell, hence a continuous sequence of chain segments occupy x cells. Figure 1.11 shows the lattice of cells in which polymer and solvent molecules have been placed.

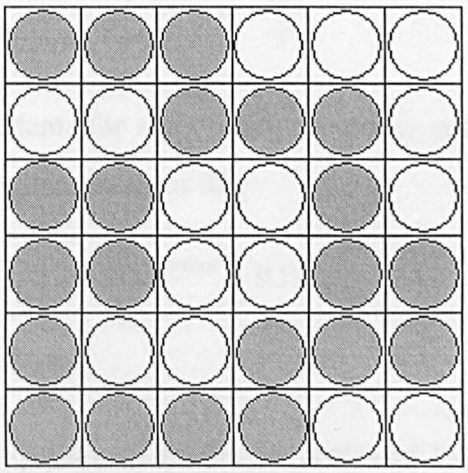

Fig. 1.11 *Diagram of polymer (filled circles) and solvent (empty circles) molecules placed in 2D lattice.*

The first quantity in the Flory - Huggins equation is the combinatorial entropy for an ideal solution – a positive variable, since when two molecules mix the number of spatial arrangements of the molecule increases.

$$\Delta G_m^{contact} = (z\text{-}2)N_1\phi_1\Delta g_{12} \qquad 1.52$$

where $(z\text{-}2)N_1\phi_1$ is the number of lattice sites adjacent to the polymer molecule that are occupied by polymer segments and Δg_{12} is the solvent segment interaction.

The lattice parameter and interchange energy are not accessible quantities, so a temperature dependent dimensionless quantity known as the Flory - Huggins interaction parameter, χ, is used to eliminate them.

$$\chi = \chi_{\Delta G} + \chi_{fv} \qquad 1.53$$

The first term is from the interchange energy contribution and the second term is from the free volume contribution.

The free volume can be negative (promoting demixing). The interchange energy is inversely proportionate to temperature while the free volume is independent of temperature,

$$\chi = \alpha + \frac{\beta}{T} \qquad 1.54$$

where α and β are constants for a polymer-polymer or polymer-solvent mixture. $\Delta G_m^{contact}$ can then be written in terms of χ:

$$\Delta G_m^{contact} = RTn_1\phi_2\chi \qquad 1.55$$

where $R = kN_A$ and $n_1 = N_1/N_A$

The Flory - Huggins equation of mixing is produced by a combination of the combinatorial entropy and the contact dissimilarity.

$$\Delta G_m = \Delta G_m^{contact} - T\,\Delta S_m^{combinatorial} \qquad 1.56$$

liberating

$$\Delta G_m = RT[n_1 \ln \phi_1 + n_2 \ln \phi_2 + n_1 \phi_2 \chi] \quad 1.57$$

The Flory - Huggins equation is used to predict the equilibrium behaviour of two liquid phases. If solvent 1 is a poor solvent for polymer 2 then miscibility will occur as long as the Gibbs free energy of mixing is less than the Gibbs free energy of the two components. Therefore as the temperature is lowered the Gibbs free energy of the two components becomes more favourable and phase separation occurs.

In reality Flory - Huggins theory does not work especially well for polymer solutions (for which it was derived), but the theory works well for polymer blends.

1.5.2 Phase Separation Kinetics

Development of structure and properties in materials is constrained by processing and polymerisation conditions. Phase separation into a hard, crystalline or glassy material that reinforces a soft rubbery phase is often desired for mechanical applications. Chemical structure, composition and processing conditions all affect the segregation of hard and soft segments. There is often complex structure formation – for example, in Reaction Injection Moulding there are competing polymerisation and phase separating processes.

Phase separation can occur via different pathways. This is important because their kinetics are different and so are compositions of the resultant phases.

For mixing to occur, the free energy of mixing must be negative.

The well known phase diagram for the stability of these systems with volume fraction and temperature is shown in figure 1.12. The binodal is obtained by equating the chemical potentials of the two phases.

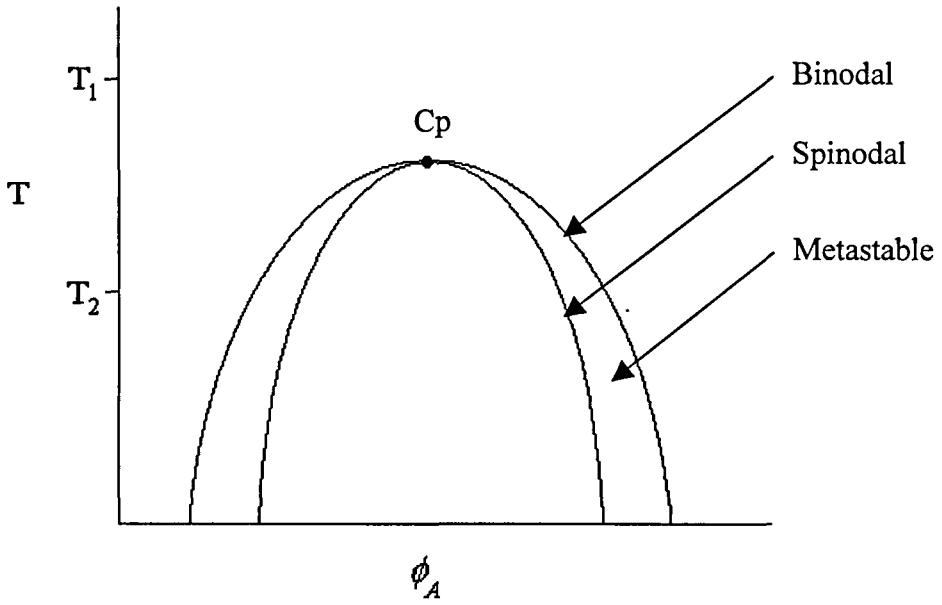

Fig. 1.12 Phase diagram for volume fraction against temperature.

At certain temperatures, for example T_1 in figure 1.13, for a 2 component mixture, the plot of the change in free energy of mixing, ΔG_m is concave throughout the composition range; i.e. the two components are miscible at all ratios.

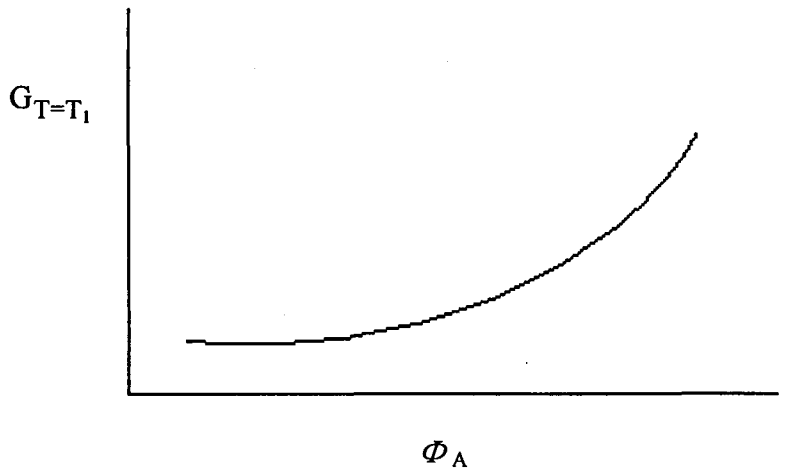

Fig. 1.13 G throughout composition range at T_1

This, however, is not always the case. ΔG_m may not be concave throughout the composition range.

Between ϕ_{s1} and ϕ_{s2} (where ϕ_{s1} is the volume fraction of component 1 on the spinodal), the free energy goes through a local maximum. The mixing of the two components is therefore undesirable as there is no thermodynamic barrier to the separation into two phases. This spontaneous separation is known as *spinodal decomposition.*

If the initial composition lies between ϕ_{b1} (the volume fraction of component 1 on the binodal)and ϕ_{s1} (or ϕ_{s2} and ϕ_{b2}), in the metastable region, then a nucleating agent is required for phase separation to occur. Separation into two phases with the composition defined by the binodal line is not spontaneous and is called *nucleation and growth.*

The spinodal line divides the metastable and unstable regions, so the equation of the spinodal (the boundary of these two conditions) is:

$$\frac{\partial^2 \Delta G_m}{\partial \phi^2} = 0 \qquad 1.58$$

For constant χ (interaction parameter), or temperature, Flory - Huggins theory gives the point of composition on the spinodal line as:

$$\frac{1}{N_A \phi} + \frac{1}{N_B (1-\phi)} - 2\chi = 0 \qquad 1.59$$

and the critical condition as:

$$\phi_C = \frac{N_B^{1/2}}{N_A^{1/2} + N_B^{1/2}} \qquad 1.60$$

Conditions for the different phase separation mechanisms are shown in figure 1.14

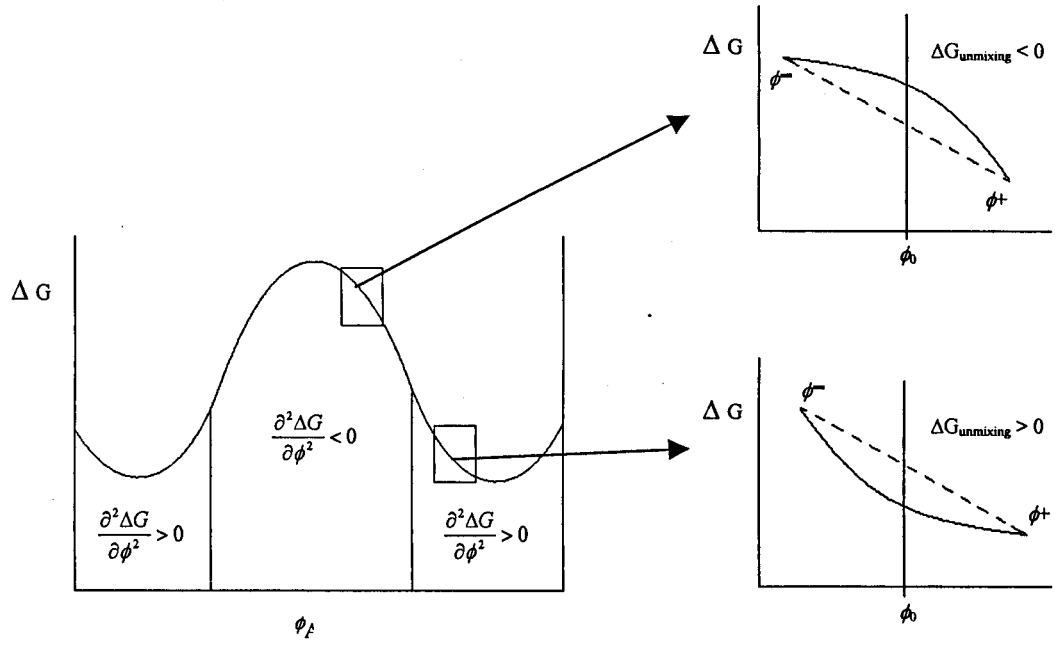

***Fig. 1.14** Conditions leading to different methods of phase separation*

Spinodal Decomposition

We can view composition as a function of a spatial coordinate with a small fluctuation about a fixed value of composition (top right diagram in figure 1.14). If a very small fluctuation occurs, what happens to the free energy? The free energy change is negative for an arbitrarily small fluctuation in composition, such that one part of the system gets more concentrated at the expense of the other. The system is inherently unstable and phase separation proceeds as in figure 1.15.

The spinodal decomposition process occurs when the polymer mixture is quenched from a homogeneous initial state in one-phase space to a final state in the unstable region, and occurs by a continuous and spontaneous process. Spinodal decomposition grows form a uniform composition by a diffusional flux against the concentration gradient – and therefore has a negative diffusion coefficient.

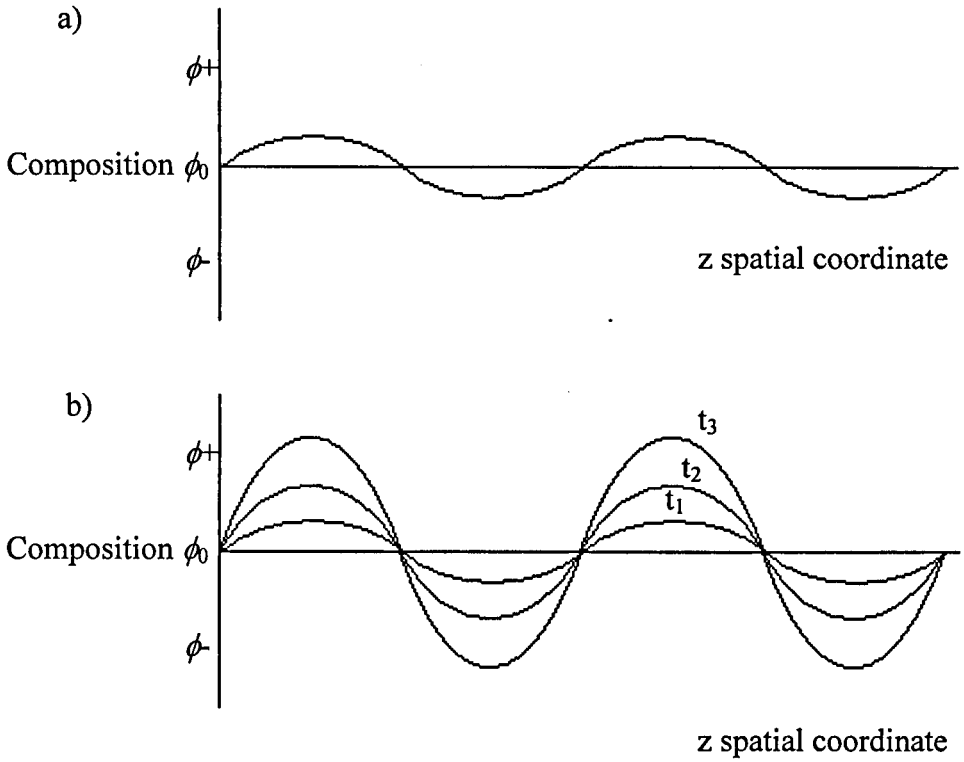

Fig. 1.15 *Composition profiles a) as a function of spatial coordinate with a small fluctuation about a fixed value of composition and b) at different times t_1, t_2 and t_3 during decomposition.*

Nucleation and Growth

The bottom right diagram in figure 1.14 represents the case where the system is stable with respect to small fluctuations i.e. metastable with respect to infinitesimal composition fluctuations. This type of system is unstable to the separation into the limiting compositions given by the common tangent construction. A large composition difference is required to nucleate the stable phase - see figure 1.16.

For nucleation – in contrast to phase separation by spinodal decomposition, - the new phase must initiate within a composition that is not near that of the parent phase. Nucleation is a phase transition that is large in degree (composition change) but small in extent (size), whereas spinodal decomposition is small in degree but large in size.

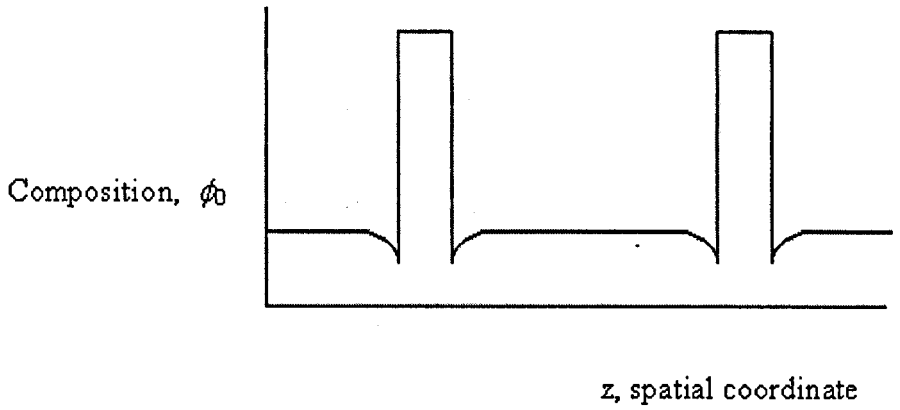

Fig. 1.16 Nucleation of an unstable phase.

A process requiring large composition fluctuations is called "nucleation". After the nucleus forms, the new phase grows, so together this is called nucleation and growth.

1.5.3 Reaction - Induced Phase Separation

Phase separation may be induced by chemical reaction – for example by polymerisation, where the increase in chain length and interaction parameter from an initial liquid – liquid mixture can result in a phase separated morphology.

Industrially, it is convenient to process materials from liquid starting materials. The structure of the final polymer formed is due to extremely complex competing processes that are occurring – polymerisation, gelation and vitrification, microphase separation and cross-linking. Variations in a number of factors, such as temperature or concentration of reactants therefore affect the morphology and thus the final physical properties.

The types of reactive processing vary from simple monomer or prepolymer casting, coating, to more complex reactive moulding procedures.

Reaction Injection Moulding (RIM) is a bulk synthesis route in which polymerisation and moulding occur simultaneously. It involves the fast production of complex plastic parts directly from low viscosity starting monomers. These liquids are combined by impingement mixing as they enter the mould. The flow rates are accurately controlled to provide the correct stoichiometry. A diagram of RIM equipment is given in figure 1.17.

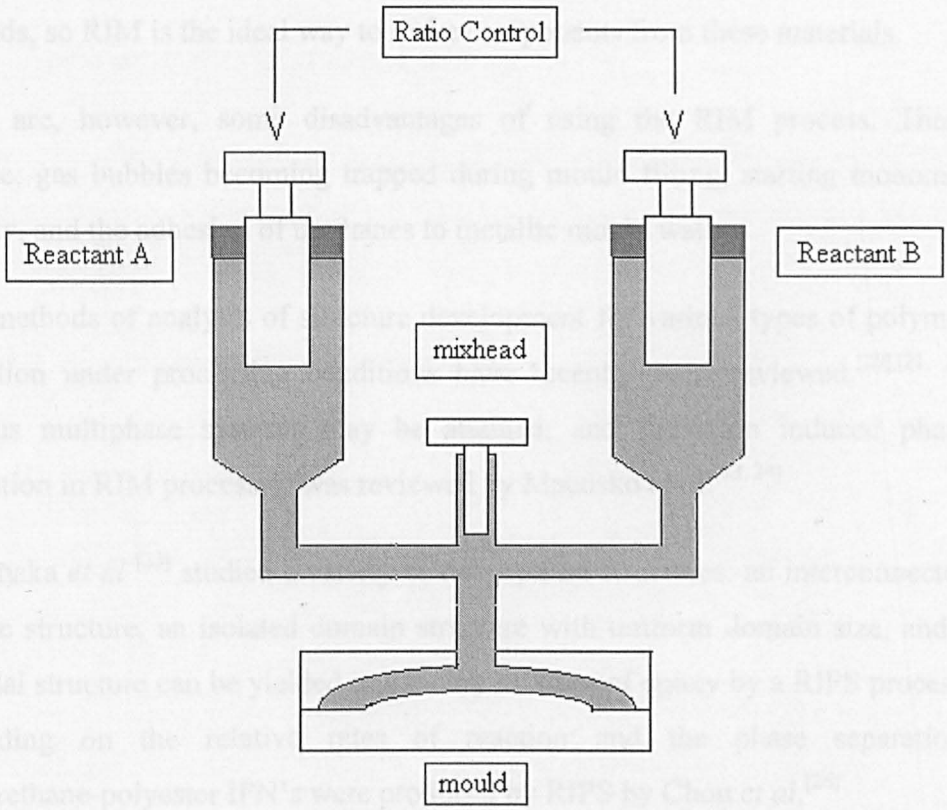

Fig. 1.17 Schematic diagram showing RIM set-up [19]

A solid polymer is formed by cross-linking or phase separation. This is one of the main differences between RIM and other sorts of injection moulding – e.g. thermoplastic injection moulding, where cooling rather than polymerisation is used to form the solid. In RIM it is purely the mixing which initiates the polymerisation, so the mould does not have to be heated to high temperatures.

95% of RIM products are made with polyurethanes or copoly(urethane-urea)s, and include car bumpers, armrests, steering wheels, snow boots, snowmobiles and golf carts.

Due to the low viscosities of the starting materials, RIM easily produces complex shapes with multiple inserts. Products are lighter (and therefore cheaper to transport), and mould pressures are kept down, so smaller clamps are needed, which also reduces the cost. Polyureas cannot be manufactured by normal methods, so RIM is the ideal way to make components from these materials.

There are, however, some disadvantages of using the RIM process. These include: gas bubbles becoming trapped during mould filling, starting monomer toxicity, and the adhesion of urethanes to metallic mould walls.

New methods of analysis of structure development for various types of polymer formation under processing conditions have recently been reviewed.[20],[21, 22] Various multiphase systems may be attained, and reaction induced phase separation in RIM processes was reviewed by Macosko *et al.*[23, 24]

Yamanaka *et al* [25] studied a variety of two - phase structures: an interconnected soluble structure, an isolated domain structure with uniform domain size, and a bimodal structure can be yielded in a binary mixture of epoxy by a RIPS process, depending on the relative rates of reaction and the phase separation. Polyurethane-polyester IPN's were produced by RIPS by Chou *et al.*[26]

It is very important that the complex competition between polymerisation and microphase separation is understood, and this is the reason that *in-situ* and time - resolved measurement techniques have become so useful.[27] Scattering techniques have been used to investigate the kinetics of structure formation.[28-34] Infra-red spectroscopy techniques [35] have been used to monitor the chemical changes that occur during reactive processing and rheological techniques have been used to monitor the mechanical properties. Combinations of these techniques [36] have provided even more useful information.

1.6 Single Phase Cross-linked Networks

Cross-linked networks comprise a wide range of very useful materials - from silicone elastomers to epoxy resins. From the structures of the reactants – their stiffness, functionality and mass, and the reaction conditions – stoichiometry and concentration we can predict the gel point and properties of the network structure.[37]

1.6.1 Network Formation Theory

For non - linear polymerisations to occur, at least one of the reactants has to have more than 2 functional groups, (f). This leads to macroscopic molecular growth which is only limited by the size of the reaction volume.

1.6.1.1 End-linking and cross-linking:

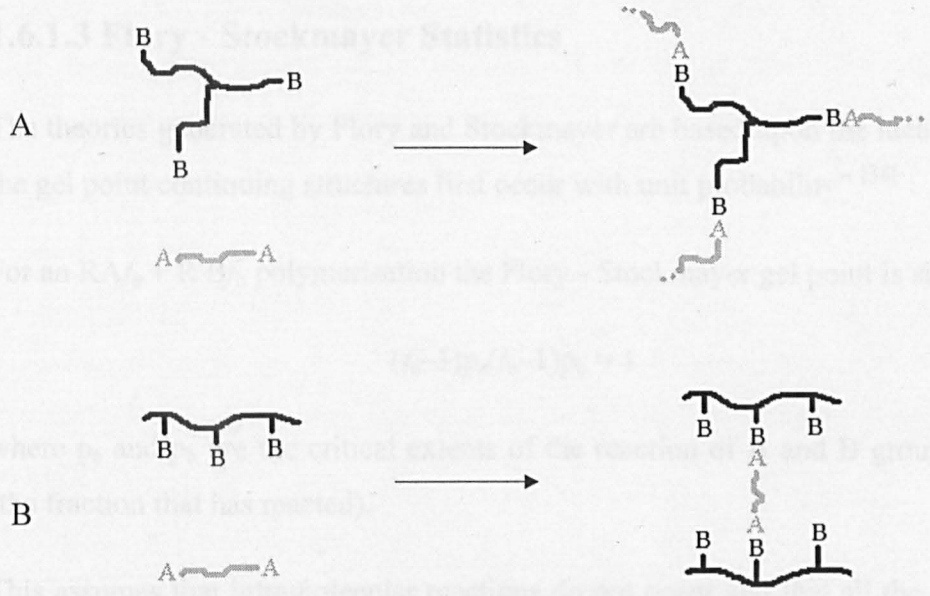

Fig. 1.18 End-linking (A) and Cross-linking (B)

The difference between end-linking and cross-linking is shown in figure 1.18. If the molecule A-A in figure 1.18.B is short then the product molecule is effectively tetrafunctional.

High values of f lead to gelation at a low conversion of reactive groups and to high amounts of cyclisation.

Reactants of low molecular mass, high functionality and stiff chains result in materials with high modulus due to the high density of junctions formed. Often these materials are glassy at ambient conditions. Reactants of high molecular mass with low functionality and flexible chains result in materials of low modulus, because the material has a low density of junction points with flexible chains between them.

1.6.1.2 Gel Point

The gel point is an extremely important transition that occurs during the formation of a network. It is at this point that the viscosity of the material changes dramatically. A liquid to solid transformation occurs, so after the gel point no liquid flow processing is possible.

1.6.1.3 Flory - Stockmayer Statistics

The theories generated by Flory and Stockmayer are based upon the idea that "At the gel point continuing structures first occur with unit probability".[38]

For an $RAf_a + R'Bf_b$ polymerisation the Flory - Stockmayer gel point is simply:

$$(f_a-1)p_a(f_b-1)p_b = 1 \qquad 1.61$$

where p_a and p_b are the critical extents of the reaction of A and B groups at gel (the fraction that has reacted).

This assumes that intramolecular reactions do not occur and that all the A and B groups have the same probability of reacting.

(f_a-1) is the number of paths which can lead from a randomly chosen A group on an RAf_a unit adjoining an $R'Bf_b$ unit. Stockmayer later used a general statistical reasoning [39] to formulate the gel point condition as:

$$(f_{aw}-1)p_a\bullet(f_{bw}-1)p_b = 1 \qquad 1.62$$

where p_a and p_b are the overall extents of A and B groups and f_{aw} and f_{bw} are the mass - average (weight - average) functionalities of A and B bearing reactants.

1.6.1.4 Cascade theory

Cascade theory was originally developed by Gordon [40] for cross-linking of polymer chains and chain cross-linking copolymerisation. It is a direct application of branching theory.

Equation 1.62 is the same as $\alpha_c = \frac{1}{P_{0w}-1}$ developed by Dusek and others for unequal reactivities (e.g. primary and secondary hydroxyls).

So, for polyfunctional polymer chains, the critical fraction of cross-linked units at gel point, α_c, is determined by the weight - average degree of polymerisation of primary chains (P_{0w}) irrespective of the type of their distribution because the chance of participation of a primary chain in structural propagation is proportional to the number of its segments.

1.6.1.5 Triplet polymerisations

"Triplet polymerisations" are often used to prepare networks, especially polyisocyanurates and polycyanurates. In a general case using *f*-functionalised reactants, RA*f* polymerising through reactions of triplets of functional groups [41] at gelation:

$$p_a\,2(f-1) = 1 \qquad 1.63$$

For three isocyanate groups forming an isocyanurate ring, $f = 2$, so $p = 0.5$ at the gel point.

1.6.1.6 Summary for cross-linked networks:

Relationships between chain concentration and junction points which assume perfect network structures are often used when interpreting the elastic properties of end-linked networks.

Flory - Stockmayer (F–S) statistics [18] (Rate theory), further developed by Stepto and Stanford [37] are used to express, with respect to the extent of the reaction (not time), the probabilities of the existence of subsets of structures based on the reactants. Compared with cascade theory where the connectivity of larger numbers of reactant units is accounted for locally, but outside the subset, all reactions are assumed to be intermolecular.

Gelation rarely occurs at the F–S gel point. The gel time is measured by monitoring the change in factors such as viscosity and modulus (see earlier). Delayed gelation will occur due to intramolecular reactions, and delayed or early gelation occurs due to non - equivalent reactive groups (Ahmed – Rolfes – Stepto (ARS) theory).[42]

1.6.2 Interpenetrating Polymer Networks (IPN's)

An Interpenetrating Polymer Network (IPN) is, "any material containing two polymers, each in network form".[43] The basic condition for eligibility as an IPN is: The two polymers are synthesized and / or cross-linked in the presence of the other. Originally it was proposed that an IPN had to consist of two polymers that were not dramatically phase separated,[44] but recently Lipatov [4] has provided arguments and evidence that this is not the case.

IPN's are distinguishable from blends and block copolymers in two ways; firstly an IPN does not dissolve in solvents, and secondly creep and flow are suppressed.

1.6.3 Graded Cross-Linked Materials made from IPN's:

Attempts at making materials with graded mechanical properties have been successful with the use of IPN's. Monomers are allowed to diffuse through a host network and then polymerised to create a gradient of guest polymer which depends on the reactant concentrations, the concentrations of cross-linker and the concentration of initiator.

Dror *et al* [45] prepared IPN's of poly(ether-urethane) with a gradient of polyacrylamide by the swelling of the poly(ether-urethane) films in an ethanolic solution of acrylamide, tetraethyleneglycol dimethacrylate (a branched reactant) and AIBN (initiator). This was followed by the polymerisation of the monomer resulting in a regular growth of polyacrylamide concentration through the poly(ether-urethane) creating a gradient IPN.

Lipatov *et al* [46, 47] measured the viscoelastic and mechanical properties of some gradient IPN's. These were prepared using a host polyurethane that was swollen in a mixture of butylmethacrylate, triethyleneglycol dimethacrylate, and an initiator which photopolymerised the monomers. This resulted in a gradient of the concentration of copolymer. Mechanical testing of these materials showed that their tensile strengths were much higher than those of the individual components.

1.7 Polyurethanes

Polyurethanes were discovered in the 1930's, and have generated an enormous amount of interest in the scientific world due to their adaptability to a whole range of applications. Their uses are wide, and include foams, fibres, elastomers, adhesives and coatings. At the present time, much research is being directed into the reactions and processing techniques of polyurethane foams and elastomers. [48]

Most modern polyurethane formulations use the reactions of isocyanates. Diisocyanates are required for polymerisation reactions. Figure 1.19 shows the

formation of a urethane link by the reaction of an isocyanate with an alcohol, a reaction that was first discovered by Bayer in 1937.

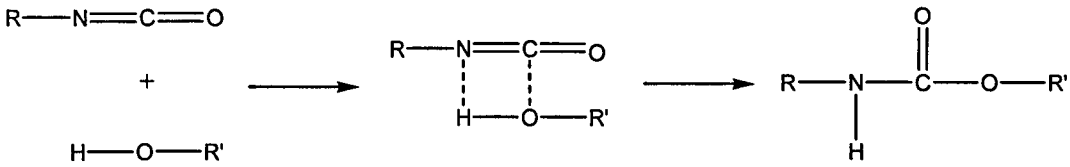

Fig. 1.19. The formation of a urethane bond.

The polymers formed by use of diisocyanates and diols in this reaction are linear, but can be branched or cross-linked with the use of multifunctional starting materials or through side reactions. The nature and stiffness of the isocyanate used and the R groups control the properties of the polyurethane formed, and ultimately the function of the material.

The basic chain growth is polyaddition, without the elimination of a small molecule, and is due to the highly electrophilic nature of the carbon atom in the isocyanate group.

1.7.1 Basic Reactions of Isocyanates in Polyurethane Chemistry:

Isocyanate groups undergo a number of reactions with the other species in the formulation. Figure 1.20 shows the reaction with alcohols to form urethanes, amines to form ureas, urethanes to form allophanates, and ureas to form biurets.

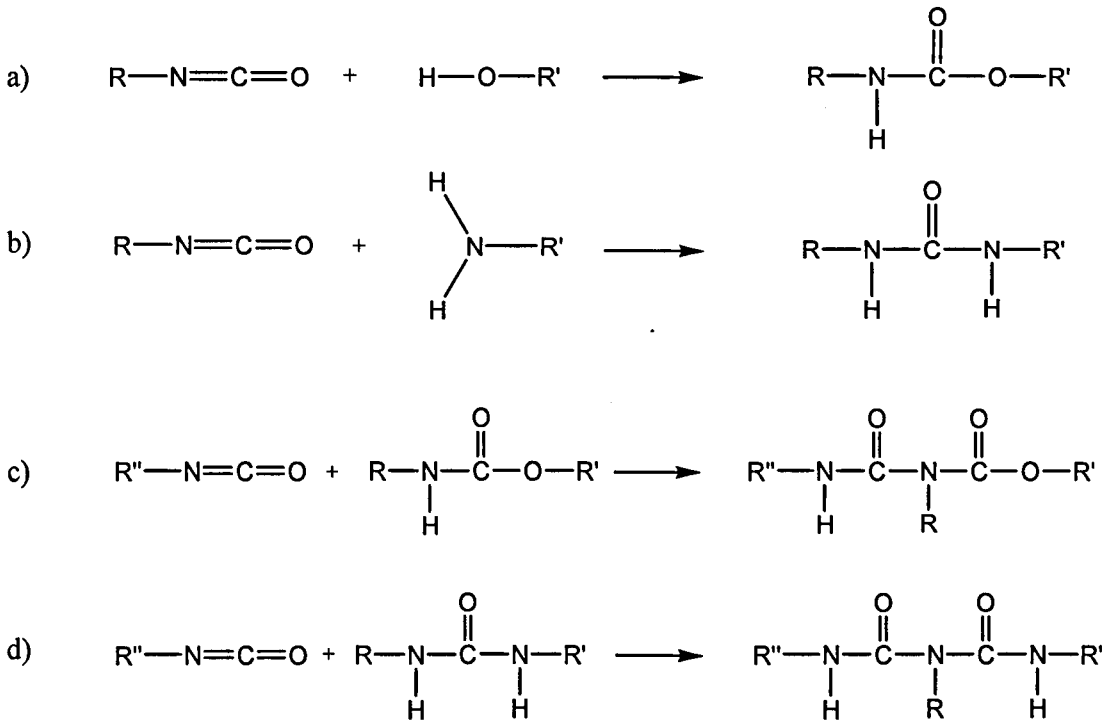

Fig. 1.20 Reactions of isocyanate groups with a) alcohols, b) amines, c) urethanes and d) ureas.

Complex chemical structures are formed from competing reactions in the formulation.

1.7.2 Cross-linking in Polyurethane Systems

Various chemical structures can form cross-linking groups in polyurethane formulations. Figure 1.21 shows the isocyanurate group, formed by the cyclisation of reactive isocyanate end groups.

Trisubstituted isocyanurates have a cyclical structure but unlike similar, related compounds there are no labile hydrogens in the aromatic series. This contributes to the thermal stability of isocyanurates bearing aromatic R groups. Therefore polyisocyanurates are useful materials for a variety of applications where a resistance to heat is required.

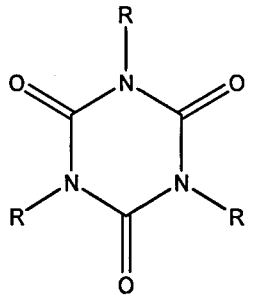

Fig. 1.21 The isocyanurate group

The most efficient way to prepare isocyanurates is through the catalytic cyclisation of isocyanates. Catalysts in use include various oxides, alkoxides, amines, carboxylates, hydrides and hydroxides of quaternary nitrogen.[48] A range of common catalysts is given in Table 1.2.

The general mechanism for the trimerisation of isocyanate groups is given in figure 1.22.[49] A - B represents the catalyst, which readily adds across the isocyanate C=N bond, giving intermediate (I). In excess diisocyanate, (I) reacts further to give (II) , which, on rotation of either CO-NR bond can give dimers (III) and (IV). Dimer (IV) is less stable and decomposes to form the carbodiimide (V), losing carbon dioxide. This can be an important reaction when dealing with polyurethane foam formulations. In the presence of more isocyanate, however, a third isocyanate group is incorporated into (II) to form intermediate (VI), which can either form a nylon polymer, (VII), or cyclise, eliminating the A – B catalyst to give the stable isocyanurate, (VIII). Trimer formation through the allophanate can also occur in the presence of basic catalysts, as shown in figure 1.23.[49]

***Table 1.2** Catalysts used for isocyanurate formation.*

Oxides	Hydrides	Alkoxides	Hydroxides of	Amines	Carboxylates
Li_2O	$NaBH_4$	$NaOCH_3$	N	$N(C_2H_5)_3$	$HCO_2^-Na^+$
$(Bu_3Sn)_2O$	R_3PbH	KO^tBu	P	$N(CH_3)_2CH_2C_6H_5$	$CO_3^{=}(Na^+)_2$
R_3AsO		Borates	As	$N_2C_6H_{12}$	$PhCO_2^-Na^+$
			Sb		$CH_3CO_2^-K^+$
					$(CH_3CO_2^-)_2$
					Alkali soaps
					Naphthenates

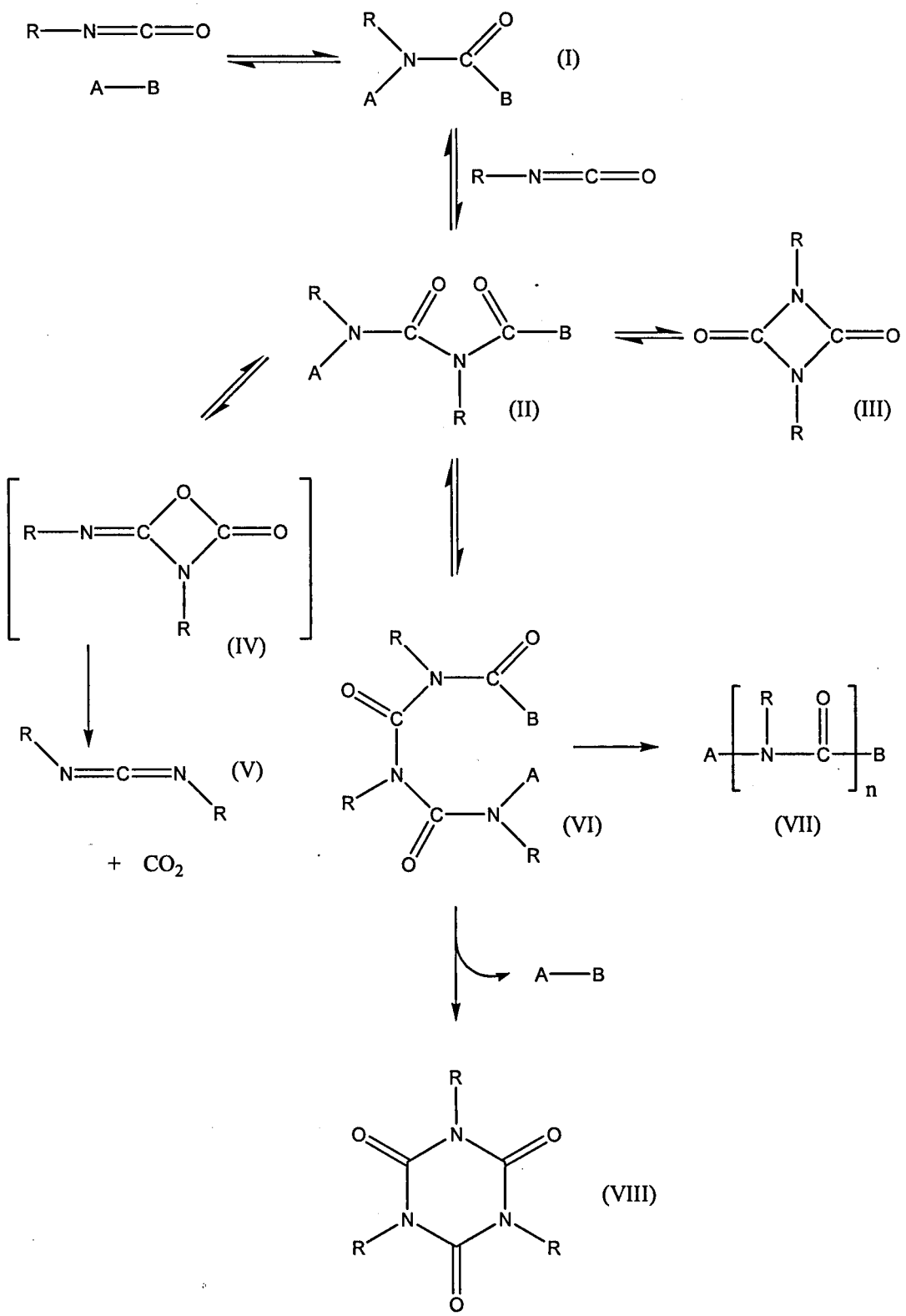

Fig. 1.22 General mechanism for isocyanate trimerisation

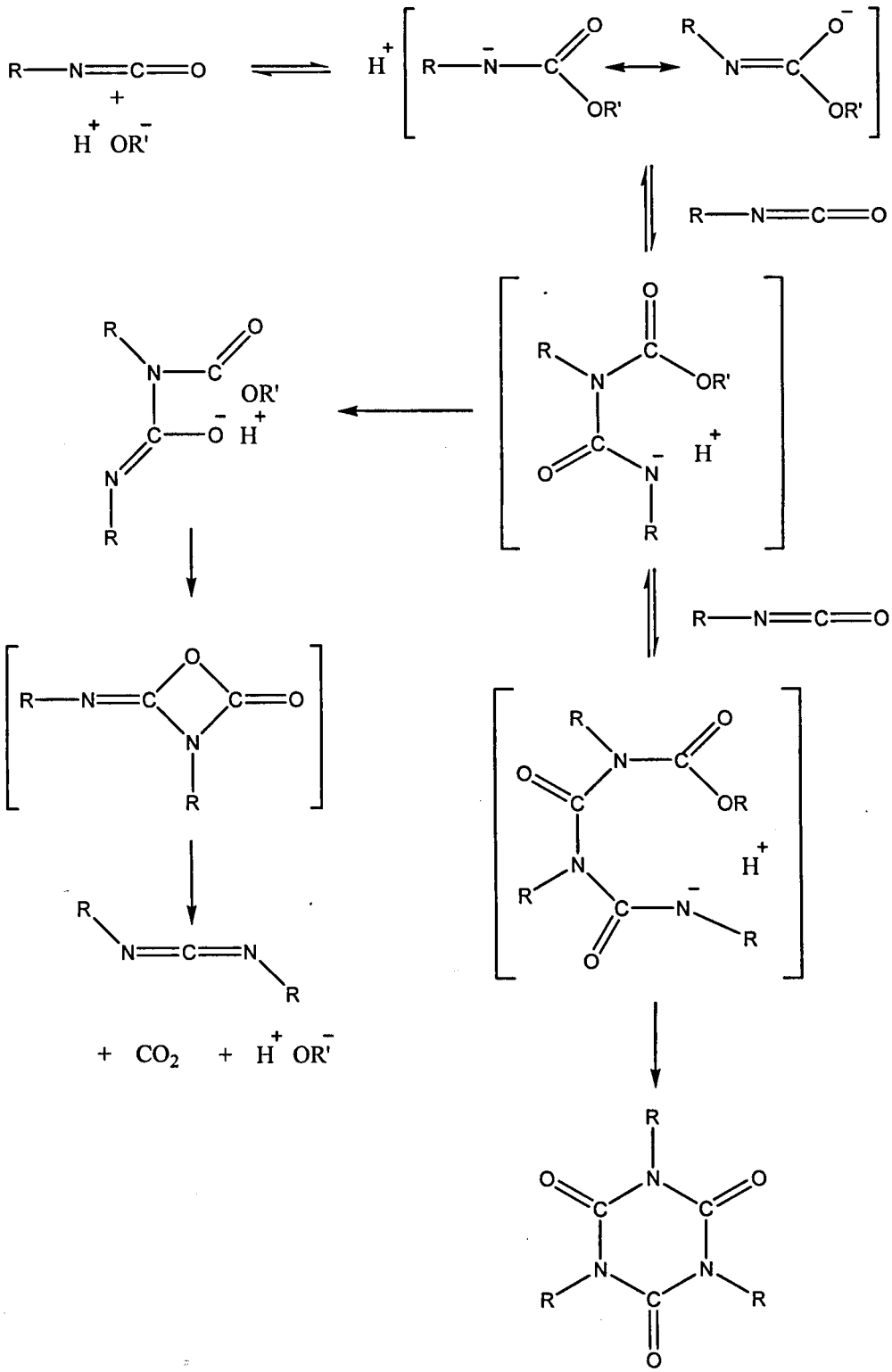

Fig. 1.23 Base - catalysed isocyanurate formation

1.7.3 Structure - Property Relationships

The processes involved in reaction - induced phase separation outlined in section 1.5.3 indicate the reasons why it is so important to understand how the morphology affects the material properties. Polyurethanes make good functional damping materials because they can achieve a phase - separated bicontinuous morphology, as shown in figure 1.24.

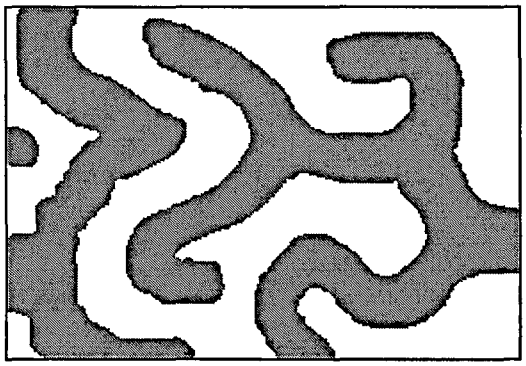

Fig. 1.24 Phase - separated structure in segmented copolyurethanes.

The morphology development in linear segmented block copolymers such as polyurethanes is very complex. During the reaction there is an increase in the degree of polymerisation, N, which changes χ; so the change in χN drives the system across the thermodynamic boundary and the homogenous disordered state becomes a microphase - separated, ordered state. This morphology (and thus the dependent properties) is therefore determined by the competition between the kinetics of polymerisation and the kinetics of microphase separation.[21, 22]

The dynamics of microphase separation were investigated by Yang *et al.*[50] Working with a system with 50% hard segment content, the analysis of the isocyanate conversion using FT-IR spectroscopy at different temperatures was conducted. The change in carbonyl peak intensity was used to determine the phase separation kinetics. The copolymerisation reaction initially followed second - order kinetics, but at higher conversion of isocyanate groups the reaction became diffusion controlled.

As mentioned in section 1.7.1, polyurethane chemistry centres around the chemistry of the isocyanate group. Phase-separated polyurethane structures consist of hard segments and soft segments. The rigid segments in polyurethanes contribute to the modulus, hardness, tear strength and ability to remain associated at elevated temperatures, and flexible segments give rise to the elastic nature of the materials and contribute to their low temperature performance. This hard / soft block composition leads to supramolecular organisation into aggregated structures of glassy domains in a rubber-like matrix. Therefore the thermal history before and after processing partially control the properties of polyurethanes.

1.7.3.1 Soft segments

Soft segments used in polyurethane chemistry are usually polyesters and polyethers. They are liquids or amorphous low - melting point solids that have a glass transition temperature below room temperature. Higher molecular weight polyester soft segments usually give rise to better tensile properties, but these have a tendency to crystallise. To prevent this polyethers are often used. They have weaker interchain interface forces than polyesters, which gives elastomers formed from them slightly inferior properties, but polyethers have better resistance to hydrolysis than polyesters due to the superior hydrolytic stability of ether groups over ester groups. Polyethers, therefore, are often used for systems where resistance to hydrolysis is required. Polyoxypropylene is commonly used as the side chain methyl group prevents the crystallisation of the flexible group.

1.7.3.2 Hard Segments

Hard segments in polyurethanes are formed by the reaction between diisocyanate with diol or diamine, often with the addition of chain extenders such as butane diol. Reducing the bulkiness of the diisocyanate used or increasing its flexibility results in a drop in modulus of the resultant elastomer.

The introduction of isocyanurate ring structures in the polyurethane system has a strong beneficial effect on the thermal stability of the elastomer.

1.7.4 Structure

The manufacture of polyurethanes consisting of hard and soft block components results in a two phase structure. The hard segments separate to form discreet domains in a matrix of soft segments. Rigid domains are seen both to form sites of physical cross-links and to function as reinforcing filler particles in the soft segment matrix.

The use of the hard / soft block polyurethane system enables us to modify the starting components and resultant cross-link density to give us the properties that we want, from micro to macroscopic scales.

Network formation theory gives us equation 1.64;

$$G = n_{e,c}RT \qquad 1.64$$

where G is the shear modulus at low frequency and low strain, $n_{e,c}$ is the concentration of elastic chains, R is the gas constant and T is the temperature, i.e. if intramolecular reactions form a significant number of inelastic chains and junctions, then $n_{e,c}$ and $n_{e,j}$ (the concentration of junction points) will be reduced below the values expected and the materials will have lower modulus and glass transition temperature.

The use of polyurethanes and polyisocyanurates for damping applications has received attention due to the ease of formation of a series of related materials by varying the hard and soft segments, and their ratio.

Cohn *et al* [51] performed HDI trimerisation using tributyltin oxide to form hard segments consisting of one or more isocyanurate rings, then the free NCO groups were reacted with polyether glycols (PEG, PPO). Mechanical properties varied as a function of soft and hard segment content and Young's modulus values of 5 – 10 MPa were obtained.

Stanford *et al* [52, 53] varied the soft segment functionality from two to four and observed complex effects of the soft segment structure on the kinetic competition

between phase separation and polymerisation processes that occurs during the formation of copolymers by RIM.

PPG and TDI were used by Askadskii *et al* [54] to make network polyisocyanurate systems with regulated chemical structure and therefore modulus.

The effect of soft and hard segment compositions of polyurethane on damping properties and transmission losses were studied by Yoon *et al* [55] by varying the content of butane diol and ethane diol.

Damping materials based on IPN's were investigated by Yu *et al*,[56] using dynamic mechanical spectroscopy to study the mechanical properties. SAXS and TEM were used as well as mechanical investigations to look at multiphase morphology and they concluded that when the weight ratio of polyurethane : polyacrylate was 1:2 the IPN had better damping properties.

Studies on the dynamic-mechanical and vibration damping properties of poly(ether – urethane) and epoxy composites were made by Huang *et al* [57]. They concluded that crosslink density was an important factor that influenced the loss factor of poly(ether-urethane) materials.

Hourston *et al* [16, 58, 59] have done extensive research into this area of polyurethane research.

Mechanical properties of polyurethanes made from copoly(propyleneoxide-tetrahydrofuran) were studied by Liu *et al* [60] who varied the processing history and hard segment content. It was found that a huge increase in modulus and other mechanical properties was obtained when PU were solvent cast, attributed to initial lower viscosity of the sample, allowing greater separation. The marked improvement of properties with 50% hard segment content was attributed to the formation of bicontinuous phases with an interlocking structure.[61]

1.8 Block Copolymers and Polymer Blends

A block copolymer is a polymer with sections made from different monomers. There are many types of block copolymers, some common architectures are shown in figure 1.25:

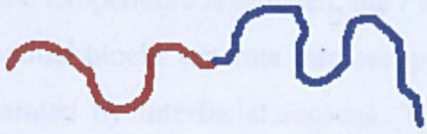

AB diblock copolymer

ABA Triblock copolymer

Multiblock copolymer

Fig. 1.25 *Schematic diagram of block copolymer structures*

Block copolymers are often made by sequential free radical anionic polymerisation of monomers such as styrene, isoprene, butadiene and methacrylic acid.

A short introduction to this area is included because polyurethanes are considered to be multiblock copolymers, and other block copolymers (for example ABS) are used as damping materials.

Block copolymers are considered to be amphiphilic in nature, and under the correct conditions will form lyotropic liquid crystals with morphologies as

described in the phase separation section, similar to the morphologies that low molecular weight surfactants can adopt. The experimental and theoretical aspects of self assembly of block copolymer systems has been reviewed recently.[62-65]

At high temperatures, there is a disordered phase where the blocks mix homogeneously, and as the temperature is reduced, the Flory - Huggins parameter χ is increased. The individual blocks separate microscopically into A and B rich domains which are separated by interfacial regions. The competition between interfacial tension and the entropic energy for stretching the polymer coils is caused by the mismatch in the coil size of the A and B blocks.

So, the phase behaviour of block copolymer systems are controlled by 3 main factors:

ϕ – composition
N – the overall degree of polymerisation
χ– the segment-segment Flory - Huggins interaction parameter.

Considering an AB diblock copolymer with $N = N_A + N_B$ chain units which occupy the same volume (v) and have the same statistical length, (b), then the theory predicts that the equilibrium phase behaviour depends only upon the product χN and composition defined by the mole fraction of A chain units.

$$\chi_A = N_A / N \qquad 1.65$$

In this, special case, b is determined by the radius of gyration of the copolymer,

$$R_g^2 = Nb^2 / 6 \qquad 1.66$$

where χ is the non - combinatorial Gibbs energy of mixing (see phase separation, equation 1.53). Unlike segments mix endothermically, giving the temperature dependence of χ. So at low values of χN the block copolymer is a single, disordered phase, but because the segments are bonded together this gives a characteristic length scaling as the radius of gyration (i.e. as $N^{1/2}$). Microphase separation is predicted to occur at $\chi N \approx 10.5$. Thus minimisation of the free

energy results in the formation of ordered structures dependent upon the composition.

Figure 1.26 shows some of the various different structures that can be formed:

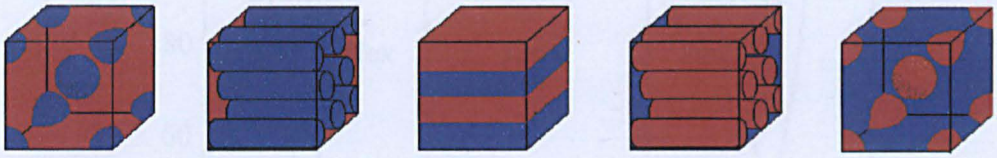

Body centred cubic spheres BCC | Hexagonal cylinders HEX | Lamellar layers LAM | Matrix-structure reversal

Fig. 1.26 *Representations of different ordered structures that may be formed by block copolymers that have undergone phase separation.*

Structures may be studied using scattering techniques, microscopy techniques and rheology. Using Landau - Ginzburg Theory, Leibler [66] calculated the phase diagram by comparing the free energy of the different ordered structures relative to that of the disordered phase. Matsen's unified phase diagram [67] is given in figure 1.27

The idea of blending together different polymers and yet conserving their individual properties in the final product seem extremely attractive; it would be an inexpensive way of obtaining new materials with a huge range of properties that could be precisely tuned by the variation in composition of the components of the blend. However, this method usually results in macrophase separation of the homopolymers and vastly inferior properties. The increase in compatibility needed to avoid macrophase separation can be obtained by the addition of a diblock copolymer which would act as a 'macromolecular surfactant'. The diblock segregates at the interface between the two homopolymers, reducing the interfacial tension between the two domains and stabilises the microscopic morphology.

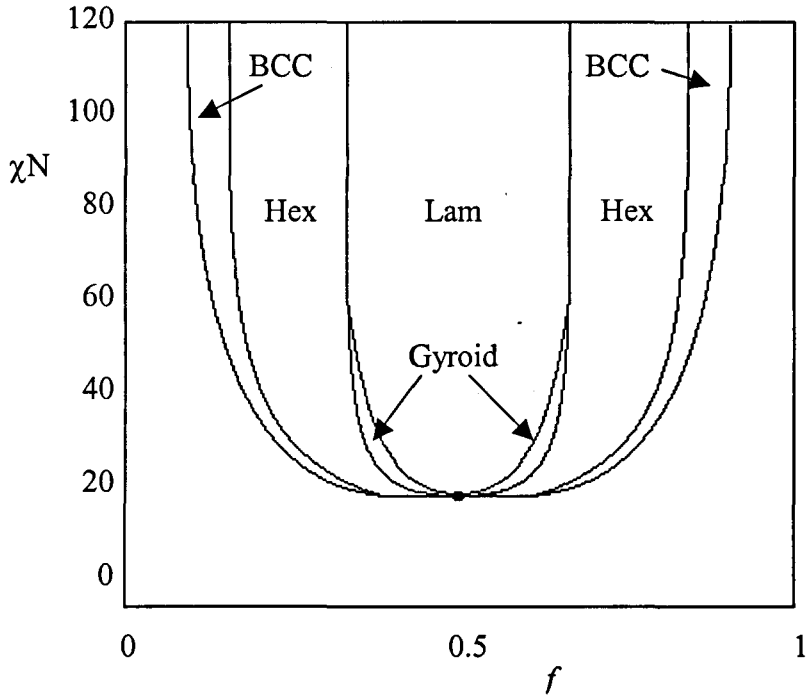

Fig. 1.27 Ideal phase diagram for diblock copolymers

Blends of amphiphilic block copolymers and corresponding homopolymers as solvents can be considered to model systems where the relative strengths of the interactions can be tuned.

1.9 Objectives

1.9.1 Summary of the Current Situation

The automotive, aerospace and white goods industries have considerable interest in developing thin conformal coatings that can effectively dissipate mechanical energy thus suppressing vibrations and noise. One of the methods often used for damping involves the exploitation of the loss processes in viscoelastic materials that dissipate energy in the form of heat in either free - or constrained - layer configurations. The main factors that these materials use for energy dissipation are the large losses observed in the glass transition region. The desired characteristics of the coating layer are reflected in the temperature dependence of the linear complex modulus $G^*(\omega)$, which is characterised by its real and

imaginary parts, the storage and loss moduli, G' and G", and their ratio G" / G' or loss factor, tan δ (where δ is the phase angle of G*). In general, it is desirable to have a large loss factor over wide temperature and frequency ranges. The damping capability of current materials, however, is limited to the particular conditions of temperature and frequency corresponding to the glass transition of the material. The design of novel materials should widen the transition considerably or make use of alternative mechanism for damping. In addition to this the material must have other attributes such as thermal stability, ease of coating complex shapes, good adhesion and make use of appropriate synthetic methods for large scale manufacture.

1.9.2 Experimental Approach

Requirements for material:

1. A versatile system, where it is easy to change the ratio of reactants and study how changing the chemistry affects the structure and therefore the mechanical properties of the material.

2. A system that provides adequate damping at useful frequencies. Machinery noise usually occurs at frequencies between 10 and 100 Hz.

3. The ability to change the macroscopic formulation within the sample to achieve graded mechanical properties.

4. Ease of processing – the gel time must be long enough for liquids to fill moulds.

5. A system that is conducive to different methods of analysis.

1.9.3 Aims of Project

This thesis describes the work involved in the synthesis and characterisation of novel network copolymers for use in damping applications. Synthesis routes

chosen were based on systems that started with liquid reactants that could be moulded into suitable sample shapes for chemical and mechanical investigation, thus following industrial processing techniques.

Isocyanurate network polymers were chosen because of their high thermal stability, and the ability to vary the cross-link density by the use of prepolymers with different chain lengths (polydimethylsiloxanes and polyethers), in formulations with different stoichiometric amounts of diisocyanate. This enabled the formation of a series of samples. The use of heat - activated catalysts allowed gradient formation and mould filling.

Materials with a graded cross-link density through the depth of the samples were prepared and studied by comparison with samples with layers of polyisocyanurate of different cross-link density. New methods of analysis were developed to investigate the gradient formed.

The structure – property relationships of bulk polyisocyanurates and the mechanism of morphology development were investigated.

1.10 References

[1] P. Ball, *Smart Stuff*, Channel 4 Television, London, **2002**.

[2] L. H. Sperling, *Vol. 425*, **1990**, p. 5.

[3] D. D. L. Chung, *Journal of Materials Science* **2001**, *36*, 5733.

[4] Y. S. Lipatov, *Phase-Separated Interpenetrating Polymer Networks*, The Ukranian State Chemical-Technology University, Ukraine, **2001**.

[5] J. D. Ferry, *Viscoelastic Properties of Polymers*, 3 ed., John Wiley and Sons, New York, **1980**.

[6] P. E. Rouse, *Journal of Chemical Physics* **1953**, *21*, 1272.

[7] P. J. F. Flory, P., *Journal of Applied Physics* **1950**, *21*, 581.

[8] C. L. Wang, D. Klempner, K. C. Frisch, *Journal of Applied Polymer Science* **1985**, *30*, 4337.

[9] A. K. Doolittle, Doolittle, D.B., *Journal of Applied Physics* **1957**, *28*, 901.

[10] C. Massot, H. Brusset, G. Rocherollesdeslignieres, *Rubber Chemistry and Technology* **1986**, *59*, 683.

[11] J. A. Harris, *Rubber Chemistry and Technology* **1989**, *62*, 515.

[12] G. R. Tomlinson, *Proceedings of the Institution of Mechanical Engineers Part C- Journal of Mechanical Engineering Science* **2000**, *214*, 103.

[13] R. P. Chartoff, E. H. Eriksen, D. E. Miller, I. O. Salyer, *Elastomerics* **1985**, *117*, 33.

[14] E. M. Terentjev, A. Hotta, S. M. Clarke, M. Warner, *Philosophical Transactions of the Royal Society of London Series a-Mathematical Physical and Engineering Sciences* **2003**, *361*, 653.

[15] S. M. Clarke, A. R. Tajbakhsh, E. M. Terentjev, C. Remillat, G. R. Tomlinson, J. R. House, *Journal of Applied Physics* **2001**, *89*, 6530.

[16] D. J. Hourston, F. U. Schafer, *High Performance Polymers* **1996**, *8*, 19.

[17] B. Bhattacharya, G. R. Tomlinson, J. R. House, *Proceedings of the Institution of Mechanical Engineers Part C- Journal of Mechanical Engineering Science* **2002**, *216*, 983.

[18] P. J. Flory, *Principles of Polymer Chemistry*, Cornell University Press, New York, **1953**.

[19] C. W. Macosko, *RIM Fundamentals*, Hanser, Munich, **1989**.

[20] J. L. Stanford, Ryan, A.J., Elwell, M.J.A., in *Processing of Polymers, Vol. 18* (Ed.: M. H.E.H.), VCH Verlagsgesellschaft mbH, Weinheim, **1997**.

[21] A. J. Ryan, U. R. Vaidya, W. Mormann, C. W. Macosko, *Polymer Bulletin* **1990**, *24*, 521.

[22] A. J. Ryan, J. L. Stanford, R. H. Still, *Plastics and Rubber Processing and Applications* **1990**, *13*, 99.

[23] R. E. Camargo, C. W. Macosko, M. V. Tirrell, S. T. Wellinghoff, *Polymer Engineering and Science* **1982**, *22*, 719.

[24] J. M. Castro, F. Lopezserrano, R. E. Camargo, C. W. Macosko, M. Tirrell, *Journal of Applied Polymer Science* **1981**, *26*, 2067.

[25] K. Yamanaka, Y. Takagi, T. Inoue, *Polymer* **1989**, *30*, 1839.

[26] Y. C. Chou, L. J. Lee, *Polymer Engineering and Science* **1994**, *34*, 1239.

[27] A. J. Ryan, J. L. Stanford, X. Q. Tao, *Plastics Rubber and Composites Processing and Applications* **1995**, *23*, 151.

[28] M. J. Elwell, S. Mortimer, A. J. Ryan, *Macromolecules* **1994**, *27*, 5428.

[29] M. J. Elwell, S. Mortimer, A. J. Ryan, W. Bras, *Nuclear Instruments & Methods in Physics Research Section B- Beam Interactions with Materials and Atoms* **1995**, *97*, 261.

[30] J. T. Koberstein, R. S. Stein, *Journal of Polymer Science Part B-Polymer Physics* **1983**, *21*, 1439.

[31] J. T. Koberstein, C. C. Yu, A. F. Galambos, T. P. Russell, A. J. Ryan, *Abstracts of Papers of the American Chemical Society* **1990**, *200*, 135.

[32] A. J. Ryan, S. Naylor, B. Komanschek, W. Bras, G. R. Mant, G. E. Derbyshire, in *Hyphenated Techniques in Polymer Characterization, Vol. 581*, Amer Chemical Soc, Washington, **1994**, pp. 162.

[33] A. J. Ryan, *Cellular Polymers* **1995**, *14*, 444.

[34] A. J. Ryan, M. J. Elwell, W. Bras, *Nuclear Instruments & Methods in Physics Research Section B- Beam Interactions with Materials and Atoms* **1995**, *97*, 216.

[35] M. J. Elwell, A. J. Ryan, H. J. M. Grunbauer, H. C. VanLieshout, *Polymer* **1996**, *37*, 1353.

[36] M. J. Elwell, A. J. Ryan, H. J. M. Grunbauer, H. C. Vanlieshout, W. Lidy, *Plastics Rubber and Composites Processing and Applications* **1995**, *23*, 265.

[37] R. F. T. Stepto, in *Polymer Networks Principles of their Formation, Structure and Properties*, 1 ed. (Ed.: R. F. T. Stepto), Blackie Academic and Professional, London, **1998**.

[38] J. L. Stanford, in *Polymer Networks, Principles of their Formation Structure and Properties*, 1st ed. (Ed.: R. F. T. Stepto), Blackie Academic and Professional, London, **1998**.

[39] W. H. Stockmayer, *Journal of Polymer Science* **1952**, *11*, 424.

[40] M. Gordon, *Proc. Royal Soc. London Series A.* **1962**, *268*, 240.

[41] K. Y. Fukui, T., *Journal of Polymer Science* **1960**, *XLV*, 305.

[42] H. Rolfes, Stepto, R.F.T., *Makromolekulare Chemie-Macromolecular Symposia* **1993**, *76*, 1.

[43] H. L. D. Frisch, Y. Schultz, M., *Interpenetrating Polymer Network (IPN) Materials*, 1 ed., Blackie Academic and Professional, London, **1998**.

[44] L. H. Sperling, *IPN's and Related Materials, Vol. Ch 1*, Plenum Press, **1981**.

[45] M. Dror, M. Z. Elsabee, G. C. Berry, *Journal of Applied Polymer Science* **1981**, *26*, 1741.

[46] Y. S. Lipatov, L. V. Karabanova, *Journal of Materials Science* **1995**, *30*, 2475.

[47] Y. S. Lipatov, L. V. Karabanova, *Journal of Materials Science* **1995**, *30*, 1095.

[48] C. Hepburn, *Polyurethane Elastomers*, 2 ed., Elsevier Science Publishers Ltd, Barking, **1992**.

[49] H. E. Reymore, Jr., P. S. Carleton, R. A. Kolakowski, A. A. R. Sayigh, in *Journal of Cellular Plastics, Vol. 11*, **1975**, pp. 328.

[50] W. L. P. Yang, C. W. Macosko, *Makromolekulare Chemie-Macromolecular Symposia* **1989**, *25*, 23.

[51] D. Cohn, K. Lane, *Polymer Communications* **1987**, *28*, 226.

[52] J. L. Stanford, R. H. Still, A. N. Wilkinson, *Polymer* **1995**, *36*, 3555.

[53] J. L. Stanford, R. H. Still, A. N. Wilkinson, *Polymer International* **1996**, *41*, 283.

[54] A. A. Askadskii, K. V. Konstantinov, L. M. Goleneva, K. A. Bychko, *Polymer Science Series A* **2002**, *44*, 335.

[55] K. H. Yoon, S. T. Yoon, O. O. Park, *Journal of Applied Polymer Science* **2000**, *75*, 604.

[56] X. Q. Yu, G. Gao, J. Y. Wang, F. Li, X. Y. Tang, *Polymer International* **1999**, *48*, 805.

[57] W. B. Huang, F. C. Zhan, *Journal of Applied Polymer Science* **1993**, *50*, 277.

[58] D. J. Hourston, F. U. Schafer, *Journal of Applied Polymer Science* **1996**, *62*, 2025.

[59] D. J. Hourston, F. U. Schafer, *Polymers for Advanced Technologies* **1996**, *7*, 273.

[60] Y. Liu, C. Y. Pan, *European Polymer Journal* **1998**, *34*, 621.

[61] R. W. Seymore, Cooper, S.L.,, *Rubber Chemistry and Technology* **1974**, *47*, 19.

[62] M. W. Matsen, R. B. Thompson, *Journal of Chemical Physics* **1999**, *111*, 7139.

[63] M. W. Matsen, F. S. Bates, *Journal of Chemical Physics* **1997**, *106*, 2436.

[64] M. W. Matsen, M. Schick, *Macromolecules* **1994**, *27*, 4014.

[65] M. Szwarc, *Advances in Polymer science, Vol. 49*, springer-Verlag, New York, **1983**.

[66] L. Leibler, *Macromolecules* **1980**, *13*, 1602.

[67] M. W. Matsen, F. S. Bates, *Macromolecules* **1996**, *29*, 1091.

CHAPTER 2

PREPARATION AND CHEMICAL ANALYSIS OF BULK ELASTOMERS

2.1 Introduction

The work described in this chapter details the reactants, formulations and experimental procedures used for the systems chosen that would allow control of the T_g.

A number of systems were investigated, working around the general theme of using the isocyanurate group to control the cross-link density. Criteria for the further analysis of the materials included: the ability to vary the components of the formulation to obtain different properties, ease of processing into suitable geometries for testing, high thermal stability and creep resistance.

Due to the very facile reaction of isocyanate groups with water releasing carbon dioxide it was essential that all starting materials were dry. Characterisation of starting materials was performed after the drying procedure had been completed.

2.2 Characterisation of Starting Materials

2.2.1 Characterisation Techniques

2.2.1.1 Fourier Transform Infra - Red Spectroscopy

Fourier Transform - Infra Red (FT-IR) spectroscopy measurements were made using a Perkin Elmer Paragon 1000 FT-IR spectrometer. Liquid samples were analysed in transmittance between sodium chloride plates. Solid samples were dissolved in dichloromethane and analysed in liquid cells.

2.2.1.2 Nuclear Magnetic Resonance Spectroscopy

Nuclear Magnetic Resonance Spectroscopy measurements were made on either a Brucker AC250 spectrometer equipped with an auto sampler or a Brucker AC400 spectrometer.

2.2.1.3 End Group Analysis (EGA)

End group analysis was performed to determine the equivalent weights of the polymers and isocyanates used in this study, where the equivalent weight, En is the molecular weight of a compound per reactive site.

$$En = \text{Molecular Weight} / \text{Functionality}$$

2.2.1.4 MALDI-TOF Mass Spectroscopy

Matrix Assisted LASER Desorption Ionisation – Time of Flight (MALDI-TOF) Mass Spectroscopy was performed on a Brucker MALDI-TOF mass spectrometer. This enabled the identification of any major impurities in the polymer starting materials.

2.2.2 Polymers

A number of liquid polymers were investigated in this study. The two main groups outlined below were chosen due to their lack of crystallinity, ease of water removal and reactive end groups for the formation of polyurethane, polyurea and polyisocyanurate groups

2.2.2.1 Polyoxypropylenes

The reaction between OH end groups and NCO groups forms urethane links. The molecular weights of the polyethers used in this study were 134, 192, 425, 725, 2200 4200 and 8200. Molecular weights of 725 and below were obtained from Aldrich, and 2200 and above were Acclaim™ polyol obtained from Acros Chemical Products. Figure 2.1 represents the structure of the higher molecular weight polyethers.

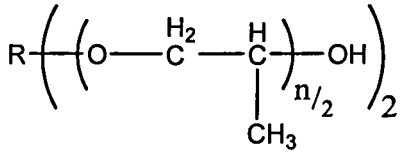

Fig. 2.1 Structure of polyoxypropylene diols.

The polyoxypropylene diols used were dried by azeotropic distillation with hexane.

2.2.2.1.1 Hydroxyl end - group analysis

Hydroxyl numbers for polyoxypropylenes were determined by acetylation of OH end groups, adapted from a method described by Sorensen [1], a schematic diagram of which is shown in figure 2.2.

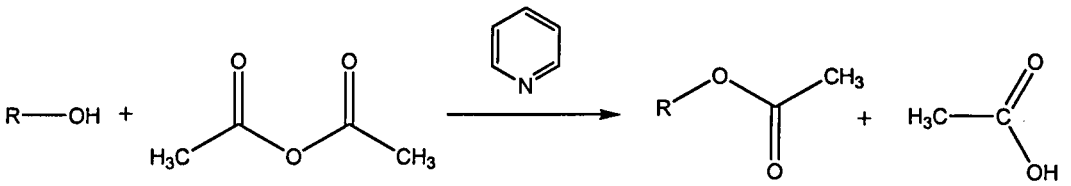

Fig. 2.2 Acetylation of OH end groups

To an accurately known mass of the polyol mixture was added 25 cm^3 of acetylating mixture (12 cm^3 acetic anhydride in 500 cm^3 pyridine). This solution was boiled under reflux for 3 hours, after which was added 10 cm^3 water, and the mixture heated for a further 5 minutes. 25 cm^3 of methanol was added through a condenser to wash the condensate into the flask. The resulting mixture was then titrated to a phenolphthalein pink end point using 0.5 molar sodium hydroxide. The results are shown in table 2.2.

- Hydroxyl number (OH number): The number of mg of KOH equivalent to the hydroxyl number in one gram of polyol.

  OH number = 56.1 x 1000 / En polyol

Table 2.1 Hydroxyl number data for polyols.

Polyol Mn	OH number (mg KOH g^{-1})	OH number (mg KOH g^{-1}) manufacturer's specification	Eq Weight (g mol^{-1} OH)
134	850 ± 10.0	n/a	66 ± 1
192	590 ± 5.0	n/a.	95 ± 2
425	275 ± 5.0	n/a	204 ± 4
725	160 ± 2.0	n/a	351 ± 5
2200	57 ± 1.0	56.4	984 ± 18
4200	30 ± 1.0	29.1	1870 ± 63
8200	14 ± 0.5	13.5	4007 ± 140

2.2.2.1.2 FT-IR

Figure 2.3 shows the FT-IR spectrum for polyoxypropylene with molecular weight 2200.

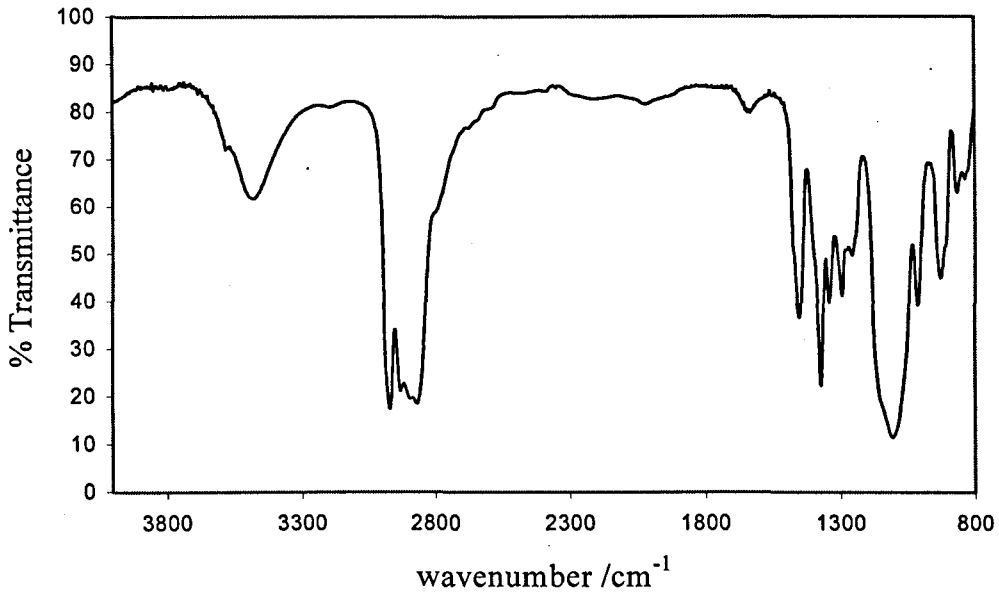

Fig. 2.3 FT-IR spectrum for polyoxypropylene Mw 2200.

The spectra of the polyols used are all quite similar. The broad band occurring at about 3500 cm^{-1} is due to the -OH stretch. The intense peaks at 2800 to 3000 cm^{-1} are due to sp^3 C-H stretches. The strong broad peak at 1100cm^{-1} is due to the C-O stretch in aliphatic ethers.

2.2.2.2 Amino - Terminated Polydimethylsiloxanes

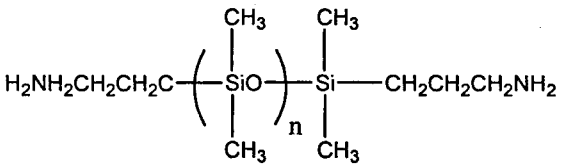

Fig. 2.4 Structure of amino - terminated polydimethylsiloxanes

Polydimethylsiloxanes (PDMS) terminated with propylamine groups were obtained from Gelest inc., and dried by azeotrophic distillation with hexane before use. Two samples were used, with molecular weights of approximately 1000 and 300, giving n in figure 2.4 to be approximately 10 and 37. The reaction of the terminal amino group with an isocyanate group forms a urea linkage.

2.2.2.2.1 Mass spectroscopy

It was difficult to obtain accurate mass spectroscopy data due to the similarities in refractive index between the solvents used and the polydimethylsiloxane polymers used. It was possible, however, to deduce from the mass spectroscopy results that there was a proportion of the sample of significantly lower molecular weight than the bulk of the sample.

2.2.2.2.2 ^{1}H and ^{32}Si nmr

NMR techniques provided more information regarding the structure and purity of the polydimethylsiloxane polymers. ^{1}H nmr, although dominated by the CH_3 methyl peak at δ 0.1 ppm, still showed a multiplet at δ 0.5 ppm - $CH_2CH_2CH_2NH_2$, a broad singlet at δ 1.25 ppm -$CH_2CH_2CH_2NH_2$, a multiplet at δ 1.4 ppm -$CH_2CH_2CH_2NH_2$ and a triplet at δ 2.6 ppm -$CH_2CH_2CH_2NH_2$. ^{32}Si nmr conducted on both samples showed many peaks between δ -20 and -22 ppm, and also a peak at δ 11.5 ppm attributed to shorter polydimethylsiloxane oligomers.

2.2.3 Isocyanates

The diisocyanate used in this study was 4,4'-methylenediphenyldiisocyanate (MDI), the structure of which is shown in figure 2.5.

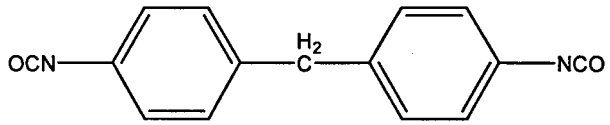

Fig. 2.5 Structure of 4,4' - methylenediphenyldiisocyanate

Obtained from Aldrich as flakes, pure MDI is a white crystalline solid. This was used in preference to toluene diisocyanate due to its ease of purification and lower toxicity.

2.2.3.1.1 NMR

^{1}H NMR in deuterated chloroform showed the expected two signals: a singlet at δ 3.9 due to CH_2 group, and a quartet at δ 7.1 due to C_6H_4 groups, in the ratio 2:8. Trace amounts of other isomers of MDI were seen.

2.2.3.1.2 IR

The FT-IR spectrum in dichloromethane is dominated by the very strong isocyanate peak at 2274 cm^{-1}. The peak at 1526 cm^{-1} is also attributed to the isocyanate group. The peaks at 3055, 1610 and 1578 cm^{-1} are due to aromatic C-H stretching bands, and the peak at 2987 cm^{-1} is due to sp^3 C-H stretching of the methylene CH_2 group.

2.2.4 Catalysts for Isocyanurate Formation

Catalysts used for the formation of isocyanurates were given in Chapter 1. Four catalysts were used in this study. These were compared to optimise both the high - temperature activated formation of the isocyanurate group and the ease of incorporation into the prepolymer formulation.

2.2.4.1 Dabco TMR

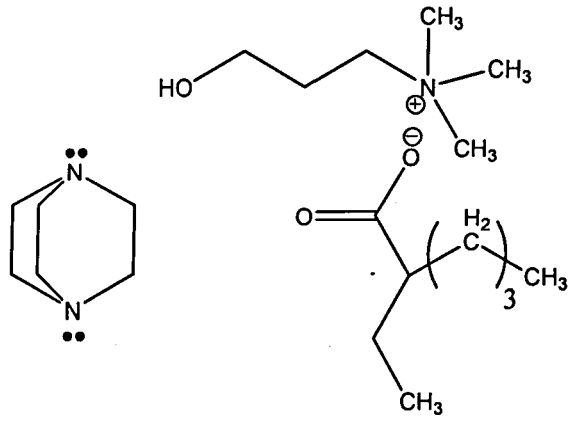

Fig. 2.6 Structure of Dabco TMR

Dabco TMR is the trade name for triethylenediamine (1,4-diazo-[2,2,2]-bicyclo-octane) N-hydroxypropyl-trimethylammonium 2-ethylhexanoate in ethylene glycol, the structure of which is shown in figure 2.6. This was obtained from Air Products and used as received.

2.2.4.2 Potassium Octanoate

Potassium octanoate, the structure of which is given in figure 2.7, was synthesised using the reaction between octanoic acid (Aldrich) and potassium hydroxide :

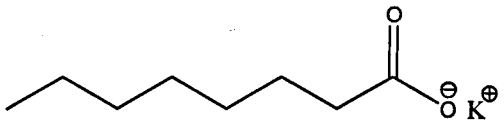

Fig. 2.7 Structure of potassium octanoate

14.42 g (0.1 mol,) of octanoic acid were added to a stirred solution of 5.61 g (0.1 mol, 1 equivalent) of potassium hydroxide in 100 cm^3 methanol. The solution was left to stir for 1 hour. The solvent was dried to remove water and evaporated to leave white crystals which were washed with hot hexane to give 16.35 g white solid, a yield of 90%.

2.2.4.3 Triethylamine

Liquid triethylamine was used as obtained from Aldrich.

2.2.4.4 Tetrabutylammonium acetate

The white crystalline solid obtained from Aldrich was dissolved in starting polymer to add to prepolymer prior to curing.

2.3 Synthesis of Polyisocyanurates

Polyisocyanurates were synthesised in a two-step method; the preparation of the end - capped prepolymer, then subsequent addition of trimerisation catalyst and curing to form the polyisocyanurate. Cast polyisocyanurate elastomers were formed in this way by Wang *et al* [2].

2.3.1 Prepolymer Formation

The liquid prepolymers for polyisocyanurate formation were synthesised by one of two general methods:

2.3.1.1 Solvent method:

The required amount of diisocyanate was dissolved in freshly distilled THF under nitrogen. The required ratio of dried polyether or polydimethylsiloxane was added drop - wise over a period of around 1 hour and the resulting mixture was left to stir at room temperature until the required OH / NCO number had been reached. The THF was then removed by vacuum distillation to leave the liquid prepolymer mixture.

2.3.1.2 Bulk method:

The required amount of diisocyanate was weighed into a round bottom flask. The flask was fitted to a schlenk line and heated to 70 °C, with stirring to melt all the diisocyanate. The required amount of dried liquid polymer was added drop - wise, under nitrogen, over a period of about 1 hour. The resulting mixture was left to stir for about 24 hours, until the required NCO conversion had been obtained. In general the bulk preparation method was preferred as it prevented the need to remove the solvent and the prepolymer could be transferred straight into the mould.

2.3.2 Polyisocyanurate Formation:

The solid catalysts (tetrabutylammonium acetate, potassium octanoate) were each dissolved in each of the starting polyethers and polydimethylsiloxanes, to give a concentration of 0.01 mol / L. In a glove box 0.1 ml of the required catalyst solution were added to the prepolymer and stirred vigorously for 10 seconds. The resulting mixture was then poured into a teflon mould (for specifications see appendix 1), which was sealed before removal from the glove box. Moulds were then placed in an incubator oven at 95 °C for 24 hours.

2.4 NCO End - Group Analysis

End - group analysis is performed to determine the end - group concentration and can be used to study the *rate* at which the reaction is proceeding. Titration is a convenient way of measuring composition; other methods for different systems include mass spectrometry, spectrophotometry, and magnetic resonance spectroscopy.

2.4.1 Method

Isocyanate end - group concentration was determined by titration, adapted from a method described by Stagg [3], shown in figure 2.8.

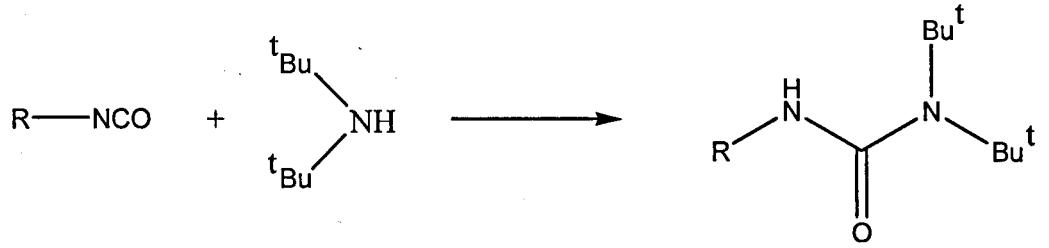

Fig. 2.8 Reaction of isocyanate with dibutylamine

To an accurately known mass of isocyanate (~0.3g) was added 25cm^3 of a 3% (v/v) of dibutylamine in butan-2-one. This solution was left to stand for 30 minutes to equilibrate before the addition of 25cm^3 of propan-2-ol to aid solubility. 5 Drops of bromocresol green (0.04% in propan-2-ol) were added and the blue reaction mixture titrated with 0.1 molar hydrochloric acid to a pale

yellow end point. Equation 3.1 is used to determine E_{niso}, the number of unreacted isocyanate groups:

$$E_{niso} = \frac{1000.m}{M(B-A)} \qquad 3.1$$

where, m is the mass of isocyanate in grams, M is the molarity of hydrochloric acid, A is the titre of hydrochloric acid consumed by the amine and isocyanate solution and B is the titre of hydrochloric acid consumed by the amine solution alone.

2.4.2 Isocyanate Conversion

The isocyanate conversion rate can be seen by the analysis of the results of end group analysis during the prepolymer synthesis.

Figure 2.9 shows the percentage isocyanate group as a function of time for two representative systems. The points on the chart are each the result of at least three measurements.

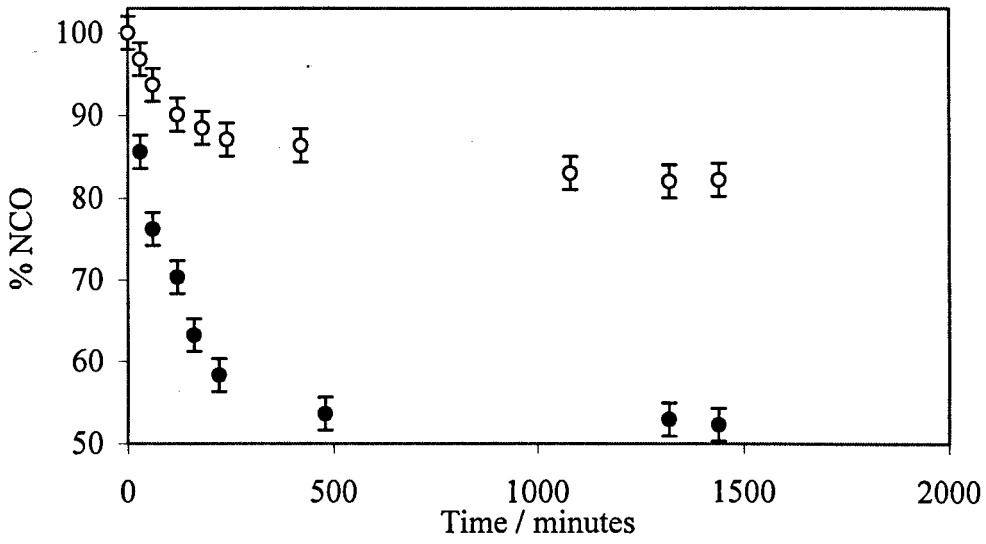

Fig 2.9 Rate of isocyanate conversion for 725 40 % (•) and 2200 40% (○) at 60 °C

Systems with a 2:1 (isocyanate: polyol) molar ratio approach 50 % isocyanate conversion, whereas there is still more than 50 % unreacted isocyanate in the

prepolymer systems with higher isocyanate ratio. Reactions with higher molecular weight polyethers proceed at a lower rate than shorter polyethers: this is because the concentration of reactive [-NCO] in mol kg^{-1} is reduced. There may also be a contribution due to the increased viscosity of the higher molecular weight polyether systems.

2.5 Samples Chosen and Nomenclature

2.5.1 Hard Segment Content

The hard segment (HS) is formed by the trimerisation reaction of isocyanate end groups and remaining unreacted MDI to form isocyanurate groups. The remainder of the material consists of soft segments (SS) formed from the polyol. The weight percent of hard segment content (HS%) is defined as:

$$\text{Weight HS\%} = \frac{\text{HS}}{\text{HS} + \text{SS}} \times 100$$

In this thesis the hard segment is calculated from the initial concentration of isocyanate added, and the soft segment form the initial concentration of polyether used.

2.5.2 Comparison of Polyether and PDMS Polyisocyanurates

In general the PDMS materials were fairly easy to prepare but shorter chain PDMS were unavailable so the T_g's obtained were well below room temperature. Increased isocyanate proportions in the poly(dimethylsiloxane-isocyanurate) polymers rendered them crumbly.

Poly(ether-isocyanurate) with varying polyether length and MDI content was the system chosen for thorough investigation.

2.5.3 Comparison of Catalysts

The gel point was reached too quickly with Dabco TMR– gelling occurred before moulding was possible. Moulding was possible with triethylamine, but this resulted in incomplete curing. This was attributed to the evaporation of triethylamine in the curing oven. Potassium octanoate gave good samples but had poor solubility in higher molecular weight polyols. Similarly tetrabutylammonium acetate gave good samples and also had better solubility in the higher molecular weight polyols.

2.5.4 Elastomer Formulation Tables for Systems Investigated:

The components and names for the poly(ether-isocyanurates) are given in table 2.3. Catalyst system 1 refers to tetrabutylammonium acetate, and catalyst system 2 refers to potassium octanoate. The general name for the poly(ether-isocyanurates) synthesised is Polyol Mw, %HS, catalyst system. Samples were catalysed by tetrabutylammonium acetate unless otherwise indicated.

***Table 2.2** Elastomer nomenclature for poly(ether-isocyanurates)*

Polyol Mw	Molar Ratio of NCO:Polyol	HS Wt %	Catalyst system	Name
134	2:1	78%	1	134 78%
192	2:1	72%	1	192 72%
425	2:1	53%	1	425 53%
425	2:1	53%	2	425 53%(2)
725	2:1	40%	1	725 40%
725	2:1	40%	2	725 40%(2)
725	5:1	63%	1	725 63%
725	6.5:1	69%	1	725 69%
725	10:1	77%	1	725 77%
2200	5:1	36%	1	2200 36%

Polyol Mw	Molar Ratio of NCO:Polyol	HS Wt %	Catalyst system	Name
2200	5:1	36%	2	2200 36%(2)
2200	6:1	40%	1	2200 40%
2200	9:1	50%	1	2200 50%
2200	10:1	53%	1	2200 53%
2200	11.5:1	57%	1	2200 57%
2200	20:1	70%	1	2200 70%
2200	24:1	73%	1	2200 73%
4200	7:1	30%	1	4200 30%
4200	10:1	37%	1	4200 37%
4200	11:1	40%	1	4200 40%
4200	17:1	50%	1	4200 50%
4200	20:1	54%	1	4200 54%
4200	25:1	60%	1	4200 60%
8200	10:1	23%	1	8200 23%
8200	13:1	29%	1	8200 29%
8200	16:1	33%	1	8200 33%
8200	20:1	37%	1	8200 37%
8200	33:1	50%	1	8200 50%

2.6 Block Copolymer Blends

The polyol / MDI system used in this work gives rise to a series of poly(ether-isocyanurate) elastomers with variable hard and soft segments. In order to be able to compare the results obtained from mechanical and structural investigations it was proposed that a model system be developed that possessed some similar qualities to the HS / SS system. The model system chosen consisted of a triblock copolymer of the form A-B-A where A was a polystyrene block and B was a polyisoprene block. Under the correct conditions this triblock copolymer is

known to phase separate with the polystyrene blocks forming a glassy (hard) phase and the polyisoprene forming a rubber (soft) phase.

Upon the addition of polystyrene homopolymer the sizes of the domains were expected to change so it was proposed that the proportion of hard and soft segments could be varied in a similar way to the poly(ether-isocyanurate) system. The triblock blend was then subjected to the same mechanical and structural analysis as the poly(ether-isocyanurate) system.

2.6.1 Triblock Copolymer

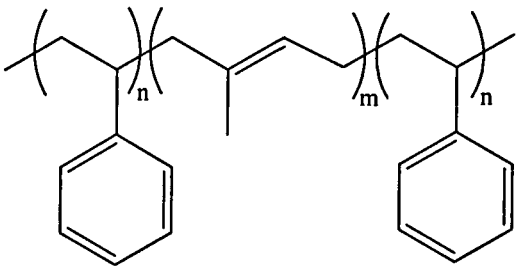

Fig. 2.10 Structure of Kraton D-1161

Polystyrene-polyisoprene-polystyrene symmetric triblock copolymer (Kraton D-1161) was used as obtained from Kraton. The molecular weight is 207000-237000, and contains 15 % polystyrene by weight. So in the structure shown in figure 2.10, n = ~ 160 and m = ~ 2775.

2.6.2 Homopolymer

Homopolystyrene with M_w ~ 5000 was synthesised by Phil Keegan [4] by Atom Transfer Radical Polymerisation (ATRP). A schematic diagram of the process used is shown in figure 2.11.

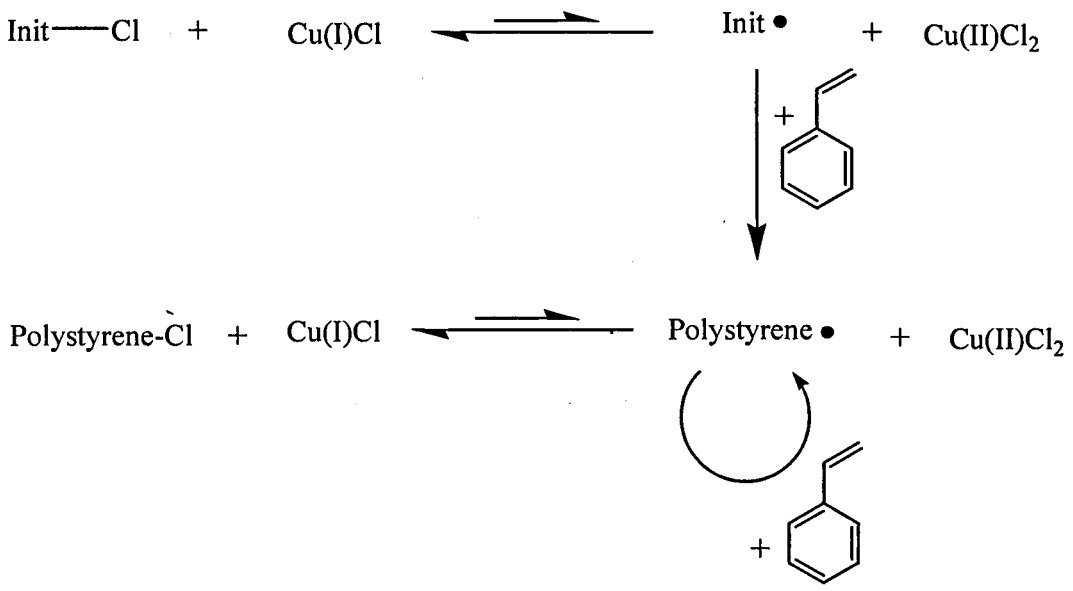

Fig. 2.11 The ATRP process used to synthesize polystyrene. The curly arrow represents chain growth.

In this synthesis the initiator used was 1-chloro-1-phenylethane (obtained from Acros), the ligand 2,2-bipyridine (Aldrich) was added to stabilise the copper complex, and the polymerisation was carried out at 130°C for 18 hours. The resulting dark brown viscous material was dissolved in THF at 50°C. Methanol was added, the slurry stirred for 20 hours, then filtered to yield white solid polymer. The molecular weight, obtained by G.P.C. was found to be 5200 and the polydispersity was 1.1.

2.6.3 Preparation of Polymer Blends

The required amounts of triblock and homopolymer were weighed out and dissolved in warm toluene with stirring. Solutions were then cast into 55mm diameter evaporating dishes and the toluene evaporated over period of 1 week. The resultant films were dried in the vacuum oven for 12 hours to remove remaining toluene. Table 2.4 shows the formulations for the prepared blends.

Table 2.3 Triblock copolymer blend formulations.

Wt % PS-PI-PS	Wt % HPS	Volume fraction PS	Name
100	0	0.114	PS-PI-PS / Wt_{HS} 0
90	10	0.183	PS-PI-PS / Wt_{HS} 10
80	20	0.255	PS-PI-PS / Wt_{HS} 20
70	30	0.332	PS-PI-PS / Wt_{HS} 30
50	50	0.496	PS-PI-PS / Wt_{HS} 50
0	100	1	PS-PI-PS / Wt_{HS} 100

The density of polystyrene is 1.25 gcm^{-3}, and the density of polyisoprene is 0.91 gcm^{-3}. The volume fraction is given by the quantity of material (weight %) divided by the density.

2.7 Characterisation of Elastomers.

The resulting polyisocyanurate plaques were characterised by FT-IR and DSC.

2.7.1 FT-IR

FT-IR was performed on thin films of the final samples. Examples of spectra obtained are shown in figures 2.12 and 2.13 The bands identified are shown in table 2.4:

Table 2.4 Infrared adsorption frequencies for polyurethane derivatives

Functional group	Wavenumber of band /cm^{-1}
N=C=O	2272 (very strong)
C=O Urethane	1740
C=O Isocyanurate	1690 – 1710
	1408 – 1429 confirmation band
C=O allophanate / biuret	1710 – 1751
C-O ether	1150 – 1170

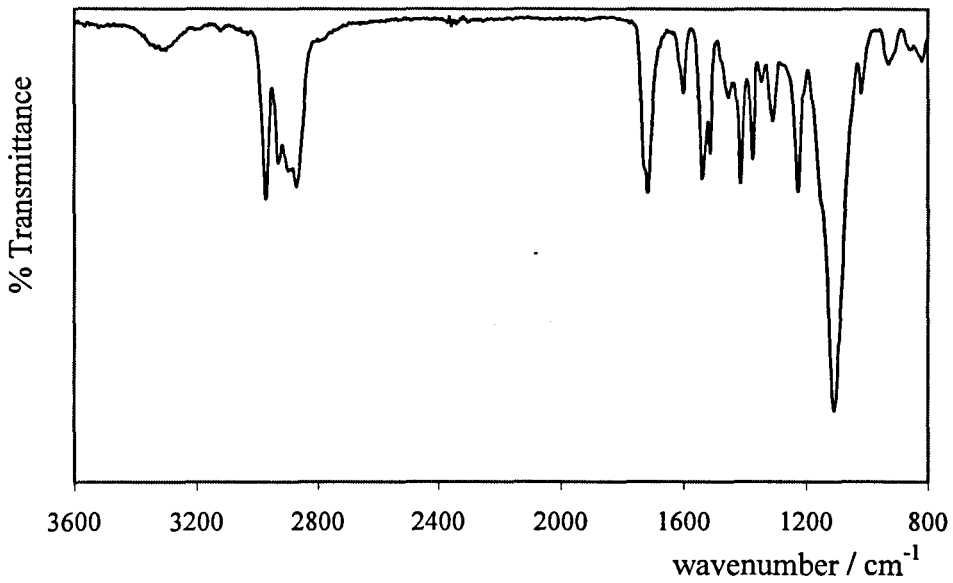

Fig 2.12 FT-IR spectrum for sample 2200 23%

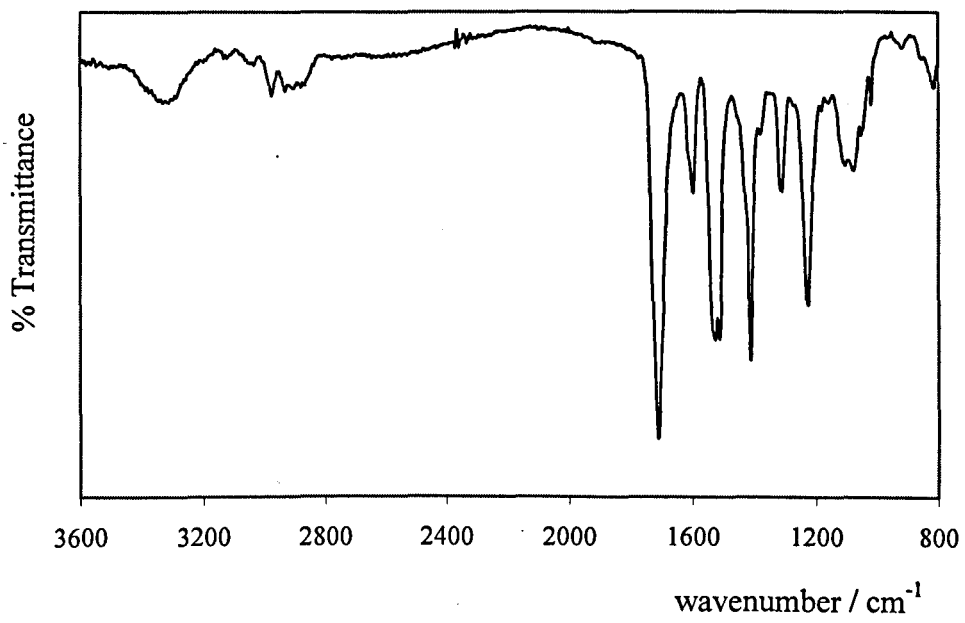

Fig 2.13 FT-IR spectrum for sample 192 72%

The carbonyl peaks in all spectra at 1710 – 1740 cm^{-1} are difficult to fully characterise. The samples contain urethane carbonyls, isocyanurate carbonyls and allophanate and biuret carbonyls. The presence of a peak at 1410 cm^{-1} indicates

that there are isocyanurate carbonyls present in the elastomers. The broad peak at 3300 cm^{-1} is attributed to N-H stretching band, and the presence of ether C-O indicated by the band at 1100 cm^{-1}, which is much more intense in the 2200 elastomer than the 192 elastomer. Peaks at 2900 – 3000 cm^{-1} are due to sp^3 C-H stretches. The intensity of this stretch is markedly less in the 192 elastomer than in the 2200 elastomer.

2.7.2 Differential Scanning Calorimetry, (DSC).

2.7.2.1 Introduction to the DSC technique

Differential Scanning Calorimetry is an important technique used to study different types of thermal transitions in a range of materials. Crystallisation, melting and other phase changes can be measured. DSC was used in this study to identify the Glass Transition temperature, T_g in the network polymers prepared.

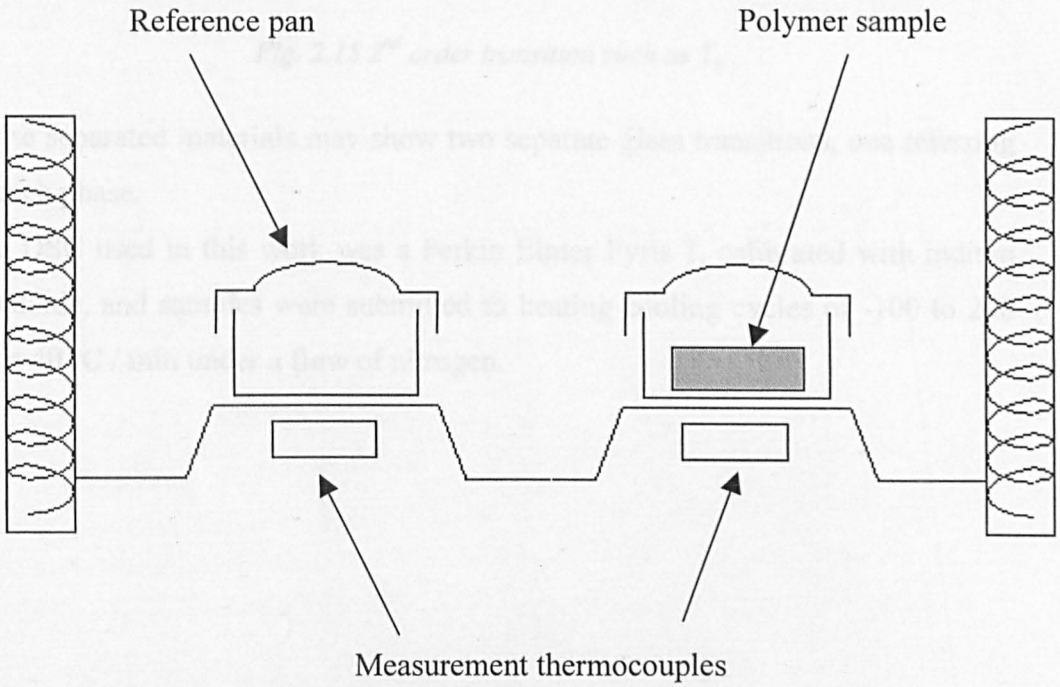

Fig. 2.14 Schematic diagram of the DSC set up.

Two pans, one containing the polymer sample and the other containing the reference sample are placed on platinum heaters, as shown in figure 2.14. The

computer controls the heaters to heat the two samples at the same, constant, rate. When a phase transition occurs in the sample there is an enthalpy change, either endothermic or exothermic, therefore to keep both the sample and reference pans heating at the same rate the heater has to supply more or less energy to the sample pan. This energy difference can be measured to give the enthalpy change of the transition. First order transitions such as crystallisation or melting show a peak whereas second order transitions such as the glass transition show a change in gradient, as shown in figure 2.15.

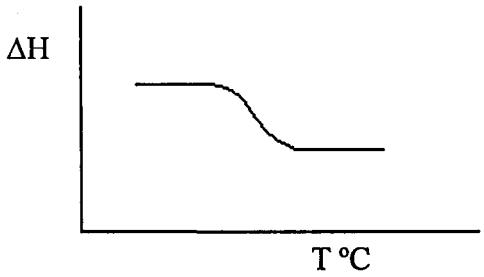

Fig. 2.15 2nd order transition such as T_g

Phase separated materials may show two separate glass transitions, one referring to each phase.

The DSC used in this work was a Perkin Elmer Pyris 1, calibrated with indium standards, and samples were submitted to heating cooling cycles of -100 to 200 °C at 40 °C / min under a flow of nitrogen.

2.7.2.2 DSC Results

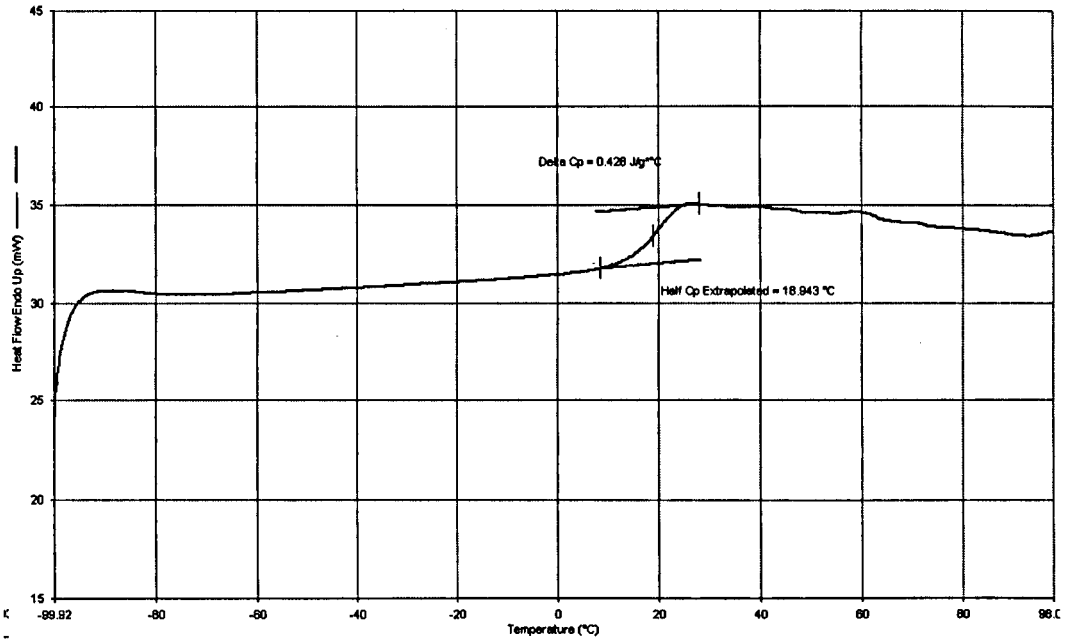

Fig. 2.16 DSC trace for sample 4200 37%

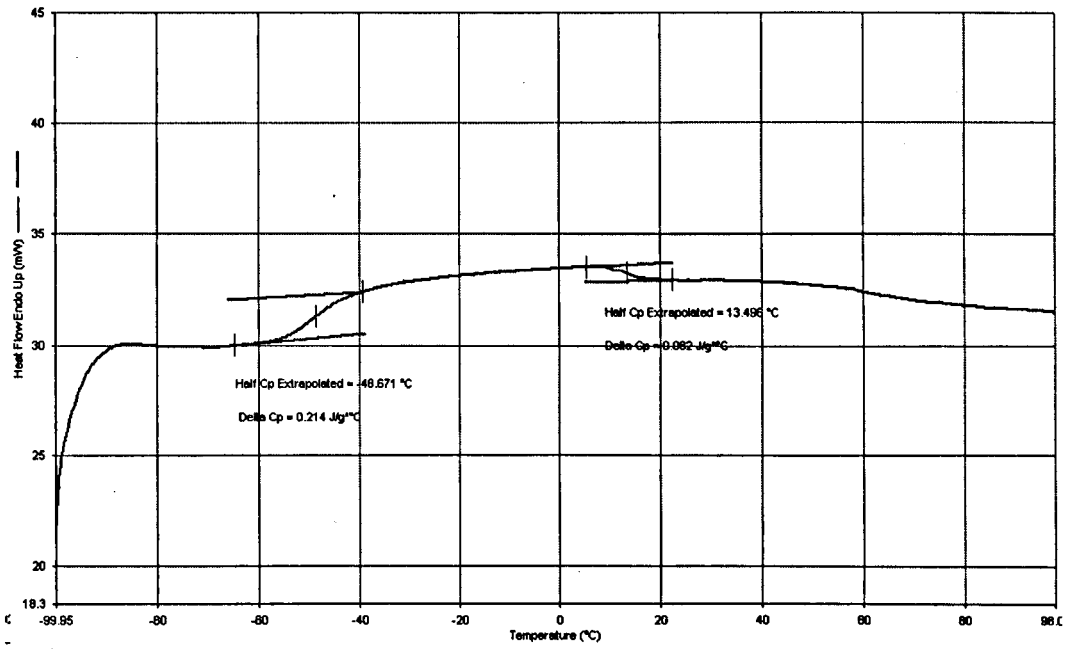

Fig. 2.17 DSC trace for e.g. 4400 50%

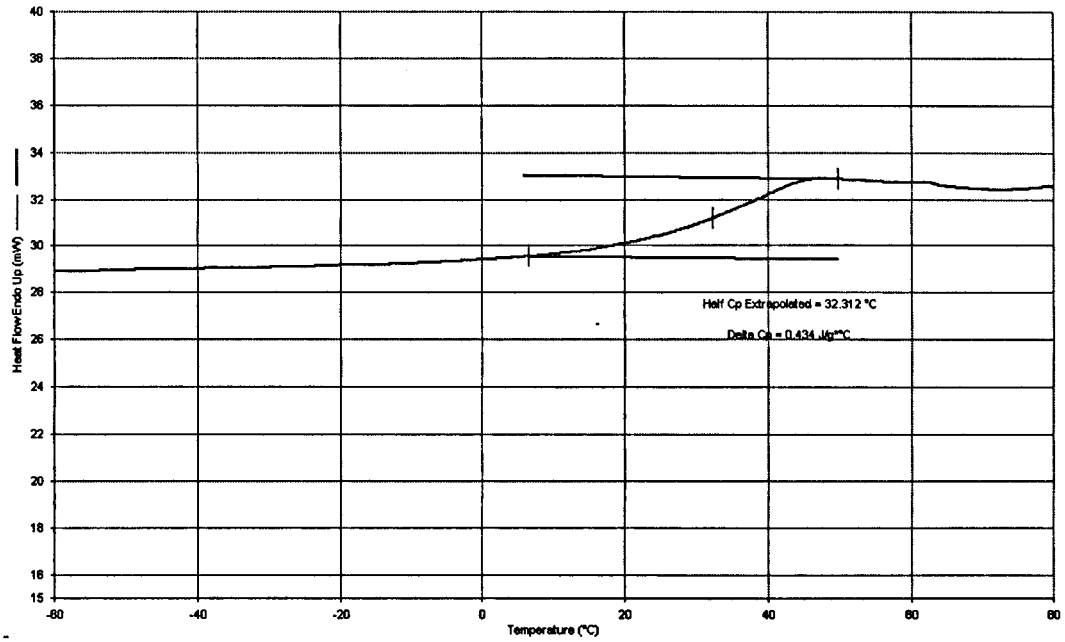

Fig. 2.18 DSC trace for sample 425 54%

Table 2.6 gives the results of the thermal transitions seen from DSC for a representative range of the network polymers synthesised. Further DSC traces may be found in Appendix 3.

Table 2.5 *T_g's of samples measured*

Polyisocyanurate	Glass Transition Temperature, °C
425 54% (2)	32
725 40% (2)	12
725 40%	4
2200 40%	-35 and 180
2200 50%	-35 180
2200 60%	-35 and 190
2200 70%	-35 190
4200 37%	19
4200 50%	-50 and 180
8200 33%	-60 and 180

In general higher T_g's were seen for poly(ether-isocyanurates) with shorter polyether segments and higher hard segment contents. Most of the samples made from polyether segments of M_w 2200 and higher showed two transitions, indicative of a two phase system in these samples. The exceptions to this were the low hard-segment content 4200 poly(ether-isocyanurates) 4200 30% and 4200 37% which displayed only one T_g. The higher T_g was often difficult to see.

2.8 Summary

Poly(ether-isocyanurate) was the system chosen for the focus of the work conducted during this study due to the capability of varying both the hard segment content and the polyether length, giving the ability to control the isocyanurate cross-link density in two different ways. The elastomeric end product could be processed from liquid starting materials, enabling mould filling to produce samples suitable for a variety of testing procedures.

2.9 References

[1] W. R. Sorenson, Campbell, T.W., *Preparative Methods of Polymer Chemistry*, Interscience Publishers inc, New York, 1961.

[2] C. L. Wang, D. Klempner, K. C. Frisch, *Journal of Applied Polymer Science* 1985, *30*, 4337.

[3] H. L. Stagg, *The Analyst* 1946, *71*, 557.

[4] P. Keegan, MChem dissertation, University of Sheffield, Sheffield, 1997.

CHAPTER 3

CHEMICAL CHARACTERISATION OF LAYERED AND GRADED SAMPLES

3.1 Sample Preparation

The solvent method of preparation described in the previous chapter was used to make end - capped prepolymers of various lengths with specific MDI contents. Each prepolymer was dyed a different colour to visually aid characterisation. Dyes chosen were Brilliant Crocein MOO, Lissamine Green and Bromocresol Green, all obtained from Aldrich. These dyes were chosen because they contained at least one hydroxyl group, which would react with the isocyanate end group and therefore would stay in the desired prepolymer.

5.56 mg / L of the dye Brilliant Crocein MOO, figure 3.1, below, was used to colour tripropylene glycol bright red. The end-capping reaction with 4,4'-methylenediphenyldiisocyanate was then completed as normal.

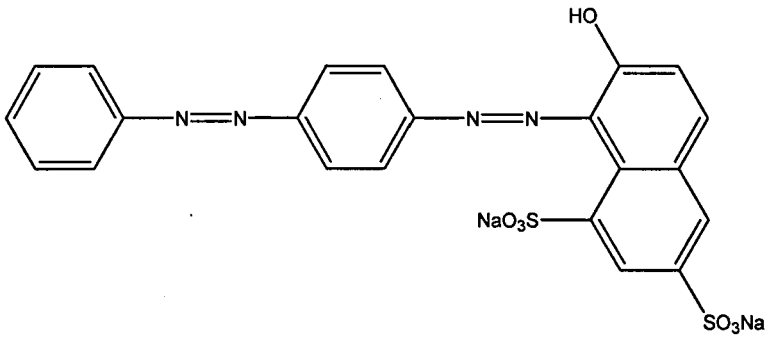

Fig. 3.1 Structure of Brilliant Crocein MOO

Similarly polyoxypropylene with a molecular weight of 725 was dyed blue with 5.76 mg /L of Lissamine green and the 2200 was dyed yellow with 6.98mg /L of Bromocresol green. The structures of these two dyes are shown in figure 3.2 overleaf.

The coloured prepolymers were then used to make polyisocyanurates with layered and graded modulus that could be distinguished visually.

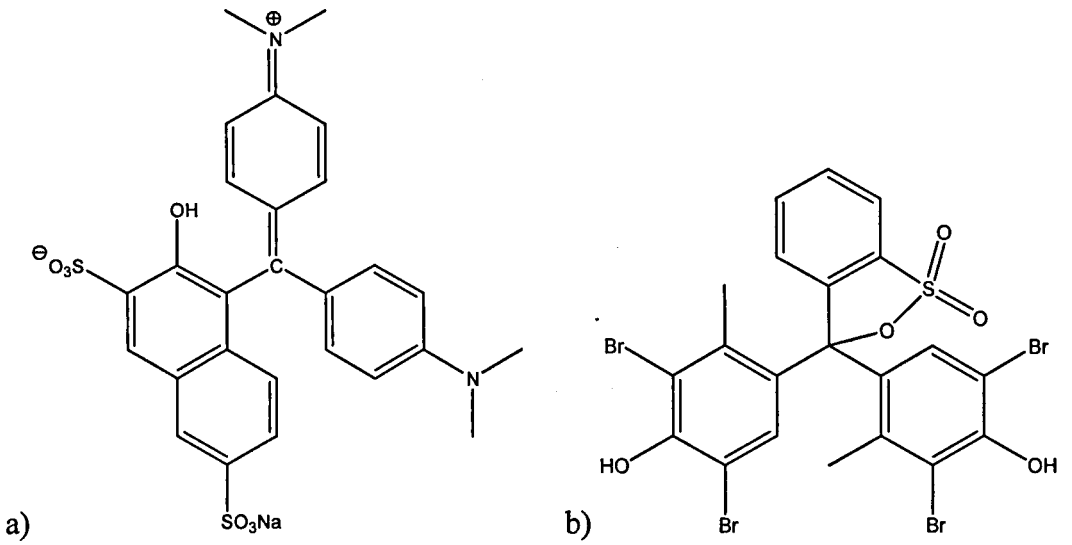

Fig. 3.2 Structure of a) Lissamine Green and b) Bromocresol Green

Layered samples were made similarly to the bulk samples previously described. Each layer was allowed to partially cure for 2 hours before the addition of the next layer. This prevented de-lamination but discouraged macroscale mixing.

Graded samples were made by mixing together two liquid prepolymers with tetrabutylammonium acetate catalyst and allowing the resultant mixture to stand in the sealed mould at room temperature for 24 hours. After this period the mould was placed in the curing oven and cured as before.

***Table 3.1** Layered and graded samples prepared*

Content –polyether length, moles MDI : POP	Architecture	Sample Name
192 72%, 2200 23%	Layered	L192-2200
192 72%, 725 40%	Layered	L192-725
725 40%, 2200 23%	Layered	L725-2200
192 72%, 2200 23%	Graded	G192-2200

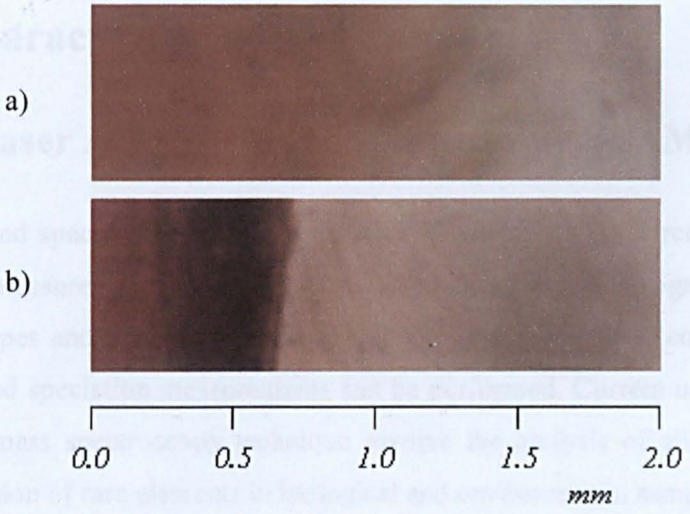

Fig. 3.3 *Photographs of cross sections of graded and layered samples (a) L192-2200 and (b) G192-2200, taken with an Olympus OM2 camera mounted on an Olympus BH-2 microscope. The 192 polyether appears on the left of the photographs.*

In order to characterise the resultant materials a cross section perpendicular to the layer stacking or gradient had to be made. Cryogenic microtoming was employed to obtain flat surfaces and thin films of the layered and graded materials. The sectioning temperature for each sample was chosen to be below the T_g of the softest part of the material but not so low as to make the hardest part brittle and crumbly. Cryogenic microtoming is commonly employed for dealing with biological samples so the sugar solution usually used to pick up the films was replaced with water so as not to interfere with later characterisation techniques. Samples were cut into 3 m thick films and placed onto barium fluoride plates. The same cross section samples were used for both characterisation techniques. The appearances of the cross sections for representative graded and layered samples are shown in figure 3.3. The photographs clearly show that there is no mixing between the layers in the layered sample and that the dyed red 192 prepolymer is present in decreasing concentration as distance from the sample surface nearest the bottom of the mould is increased.

3.2 Characterisation Techniques

3.2.1 Laser Ablation Mass Spectroscopy, (LAMS)

Laser based spectro - chemical measurements constitute an extremely important class of measurement system. High powered lasers can interrogate virtually all sample types and depending on laser technology and operating conditions, bulk, feature and speciation measurements can be performed. Current uses of the laser ablation mass spectroscopy technique involve the analysis of alloys [1] and the identification of rare elements in biological and environmental samples.[2]

For the LAMS technique, pulsed laser radiation is delivered to the sample surface through a near field optical probe, and the ablation plume is sampled through a capillary orifice and analysed by standard Mass Spectroscopy methods. A spatial resolution of less than 200 nm is obtained.

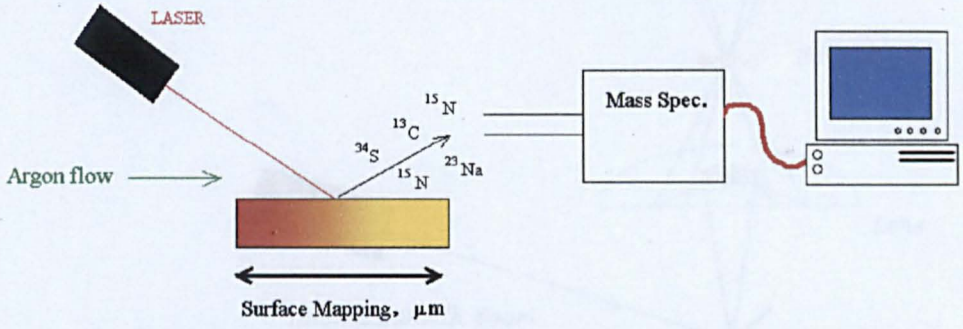

Fig. 3.4 Schematic diagram of Laser Ablation Mass Spectroscopy set up

The set up shown in figure 3.4 describes the LAMS technique. The sample stage moved at 10 m / s. The mass spectrometer analysed the relative intensity of carbon and nitrogen. Both layered and graded samples were investigated in this way.

3.2.2 Fourier Transform Infra Red Microscopy

Figure 3.5 shows the apparatus for the FT-IR experiments. 3 m film samples were analysed in transmittance. BaF_2 plates obtained from Crystran Ltd were

employed rather than the usual NaCl because BaF_2 has a low solubility (0.17g / 100g water at 23 °C) and would not be dissolved by the water used for sample retrieval during cryogenic microtoming. BaF_2 was chosen over other low solubility materials for the large transmission range of 0.15 to 12.5 m in the IR region. IR spectra were taken at intervals of 100 m for a distance of 1000 m.

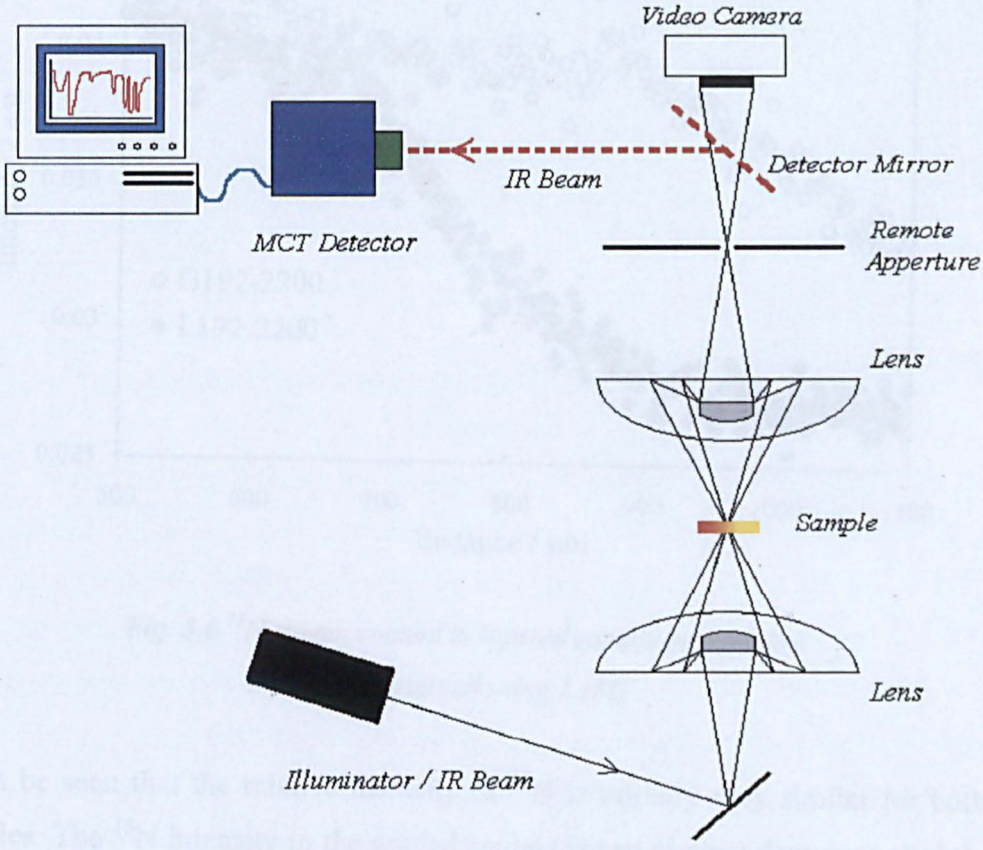

***Fig. 3.5** Schematic of FT-IR microscope set up*

3.3 Results

3.3.1 Laser Ablation Mass Spectroscopy Results

The results obtained for the variation in the intensity of ^{15}N isotope in both the layered and graded samples L192-2200 and G192-2200, are shown in figure 3.6.

In both cases the scan has started at the lower molecular weight polyoxypropylene 192 part of the sample and moved towards the 2200 polyoxypropylene region.

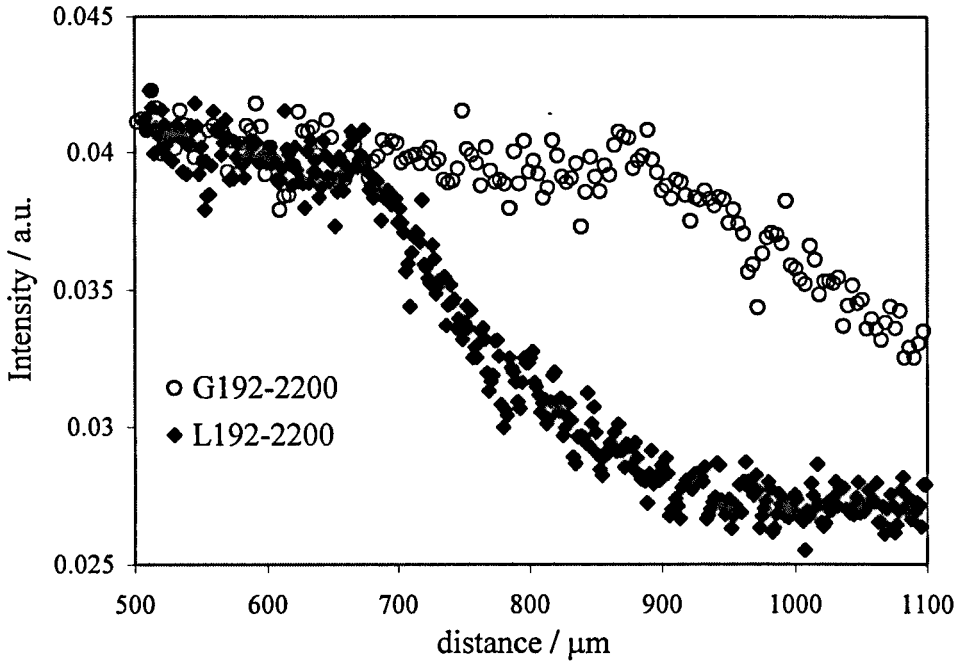

Fig. 3.6 ^{15}Nitrogen content in layered sample and graded sample observed using LAMS.

It can be seen that the relative intensity of ^{15}N is initially very similar for both samples. The ^{15}N intensity in the graded sample (open circles) decreases slightly until 870 μm, after which it decreases more rapidly. The layered sample, however, experiences a sharp fall in intensity at 675 μm and the intensity plateaus off before the edge of the sample is reached. Results for all isotopes tested and for other samples may be found in appendix 4.

3.3.2 IR-Microscope Results

Figure 3.7, below, shows a linescan image obtained from sample G192-2200 using the FT-IR microscope. The image is presented as wavenumber against

distance, where blue is low intensity and yellow is high intensity The IR spectra that make up this image are presented in appendix 2.

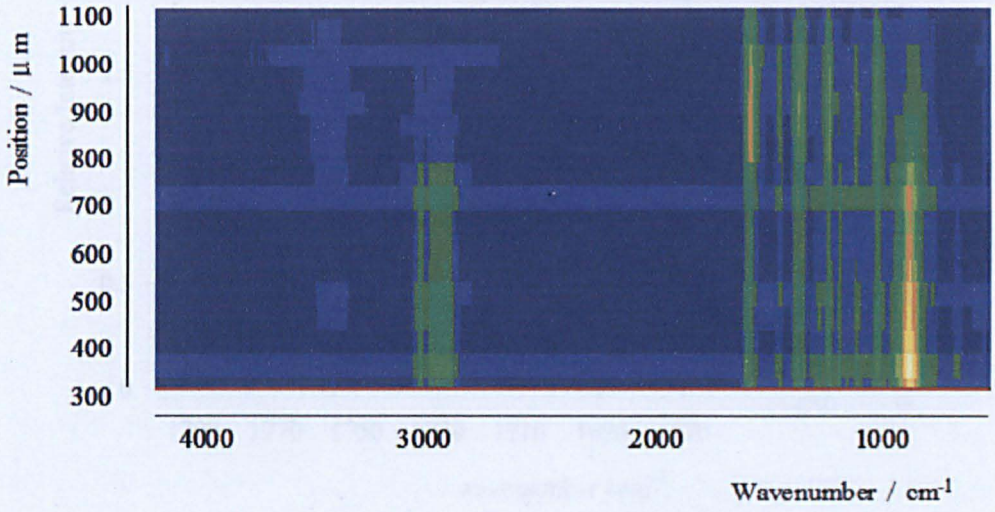

Fig. 3.7 *Linescan image of G192-2200 obtained from the FT-IR microscope*

IR bands solely present in the cross-link or the soft polyether segment can be analysed to see how their intensity changes with distance. Shorter chains with a higher cross-link density contain a much higher proportion of urethane groups whereas longer polyether chains, with a lower cross-link density have a much higher proportion of sp^3 carbons.

Figure 3.8, shows the IR spectra for the carbonyl region of the linescan image shown in figure 3.7. The spectra have been offset by a value of 0.1 of the relative intensity for clarity. The carbonyl peaks are difficult to separate, but the peak at lower wavenumber (1705 – 1720 cm^{-1}) is attributed to the carbonyls in the cross-links –isocyanurate, allophanate and biuret, and the peak at higher wavenumber (1725 – 1740 cm^{-1}) to the carbonyl in the urethane groups. Figure 3.9 shows the variation of intensity of these two bands across the section. The relative intensity of the peak due to the carbonyls in the cross-links increases as the scan progresses from the 2200 rich component of the cross section to the 192 rich component, and the relative intensity of the C-H_2 stretches at 2900 cm^{-1} decreases from the 2200 rich component to the 192 component.

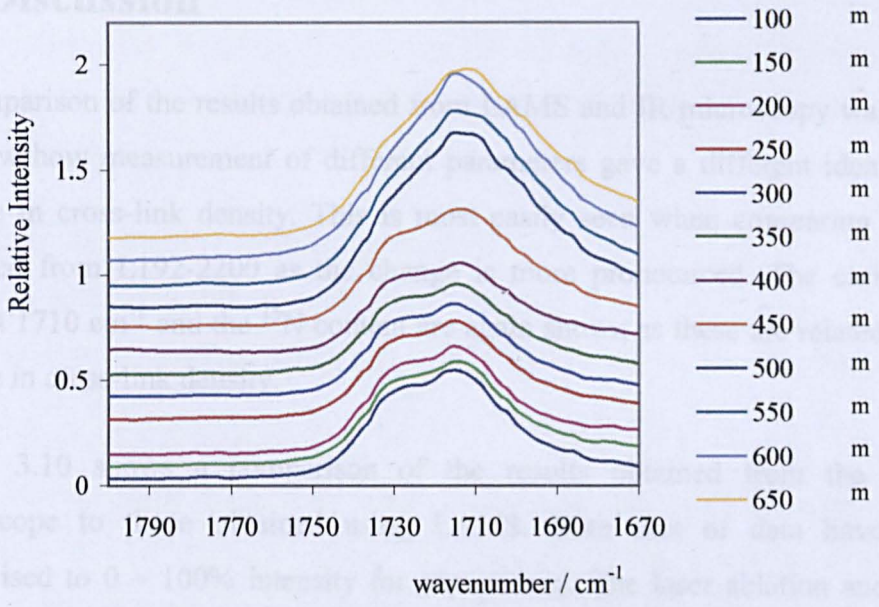

Fig. 3.8 *IR spectra of carbonyl region for sample G192-2200*

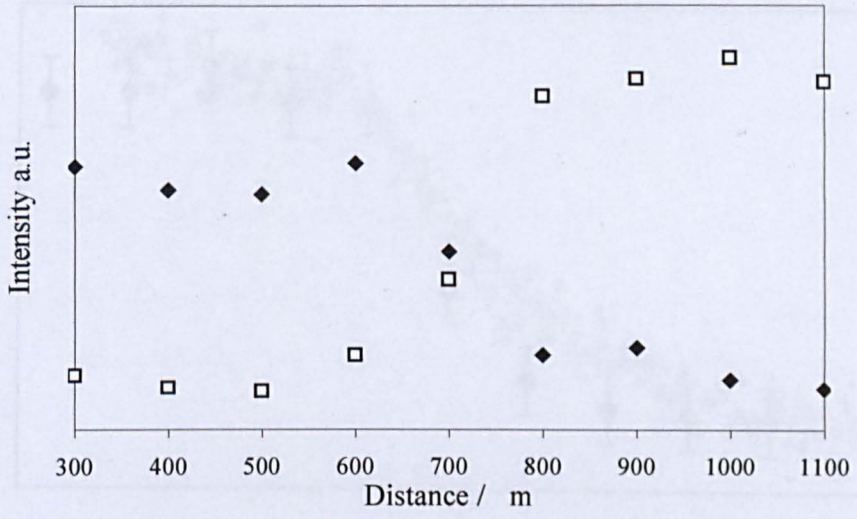

Fig. 3.9 *Intensity of C=O stretching frequency at 1714 cm^{-1} (□) and C-H_2 at 2900 cm^{-1} (♦) along cross section of sample G192-2200*

3.4 Discussion

A comparison of the results obtained from LAMS and IR microscopy was made to show how measurement of different parameters gave a different idea of the change in cross-link density. This is most easily seen when comparing results obtained from L192-2200 as the change is more pronounced. The carbonyl's peak at 1710 cm^{-1} and the ^{15}N content are again shown as these are related to the change in cross-link density.

Figure 3.10 shows a comparison of the results obtained from the FT-IR microscope to those obtained using LAMS. Both sets of data have been normalised to 0 – 100% intensity for comparison. The laser ablation and mass spectroscopy techniques have different resolution functions due to the different physical principles upon which each technique is based.

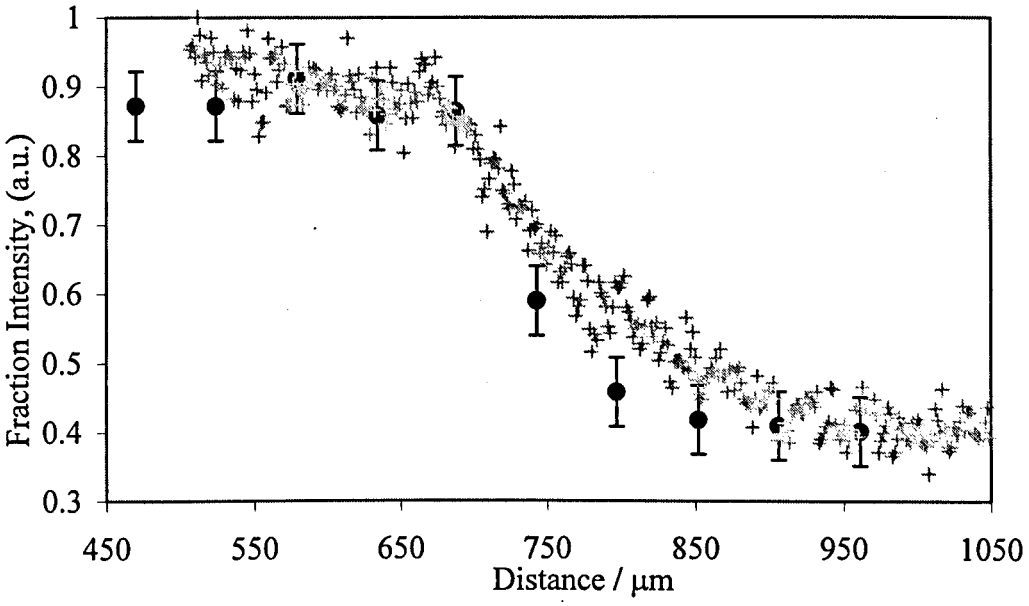

***Fig. 3.10** Comparison of the two techniques for sample L192-2200. • represents the carbonyl intensity at 1710 cm^{-1} using the IR microscope and + represents the ^{15}N intensity obtained from LAMS.*

The intrinsic scatter in the LAMS is shown by the data and the error bar in the carbonyl intensity is given. These data demonstrate clearly that the dramatic change in intensity due to the interface between the two layers occurs at exactly the same position.

It appears that there is a certain amount of 'drag' in Laser Ablation. The time taken for ablated atoms to reach the mass spectrometer means that there is a significant error involved when trying to pinpoint the original position of the atom.

Some atoms can be difficult to identify. There is a limit to the sensitivity of machine – this technique is usually used to look at much heavier atoms, and polymer systems consisting of carbon, oxygen, hydrogen and nitrogen are not well investigated. It may be possible to look at the atoms in the dye molecules, for example bromine, as long as these are not masked by the gases used for transportation.

In order to perform quantitative measurements on the FT-IR microscope, very thin, very even, slices obtained from the microtome are needed. Uneven sample thickness, and rucking / folding of the sample give very misleading results.

There were great difficulties with the sample preparation; both cutting to prepare for sample characterisation and generating the correct bulk sample geometry for mechanical testing. Layered samples gave curved plaques, attributed to differences in thermal expansion of the various prepolymers.

Both LAMS and FT-IR microscopy results gave insight into the gradient achieved in sample G192-2200. By comparison with results from the layered sample L192-2200 in figure 3.6 it can be seen that there is an almost pure 192 component at the start of the scans, - this component is at the bottom of the moulds. This 192 rich phase continues for 870 μm; after this point there is a mixture of 192 and 2200 polyoxypropylene soft segment, and the decrease in ^{15}N intensity progresses linearly.

We have speculated on the mechanism of this separation to form the graded sample, and have proposed that it be due to gravity. The thick layer of harder (more dense) 192 polymer sinks to the bottom of sample, then grading starts. Any surface driven separation would not extend as far as 1000 μm.

3.5 Summary

The work described in this chapter describes the preparation and characterisation of layered and graded samples. It was proposed that the structural features and mechanical properties be investigated for the bulk polyisocyanurate systems that made up the layered and graded systems to see how the chemical structure of each sample could contribute to the mechanical properties. If the separation was indeed due to gravity then it would be important to know how the separate components contributed to the final properties.

3.6 References

[1] A. M. Leach, G. M. Hieftje, *Journal of Analytical Atomic Spectrometry* **2002**, *17*, 852.

[2] K. Watanabe, T. Iguchi, *Journal of Nuclear Science and Technology* **2002**, *39*, 312.

CHAPTER 4

STRUCTURE DEVELOPMENT

4.1 Introduction

Phase separation plays an extremely important part in the development of structure in reactive systems, and the theory was outlined in chapter 1. The advantage of having a phase separated damping system is that there are additional ways for the vibrational energy to be dissipated, due to the inhomogeneity of the material.

This part of the work includes an investigation of how the ratio of soft and hard blocks and the polyether soft segment length affect the phase separation and how the phase separation develops in this reactive system. Structures were obtained for different volume fractions of added homopolymer in the model triblock copolymer blend system.

4.1.1 Small Angle X-Ray Scattering (SAXS)

The microstructure of these types of materials is conveniently probed using X-ray radiation. The electron density difference between the phases scatters X-rays and Small Angle X-Ray Scattering (SAXS) measures structures with lengths from 20 to 1000 Å – ideally suited to the length scale of the systems under investigation.

Synchrotron radiation is used because of the increased speed of data acquisition due to the high intensity beam. A laboratory X-ray source requires such long exposure times to obtain good quality data, that only static measurements are possible. This use of synchrotron sources enables time resolved experiments to be performed in a variety of sample environments.

The driving force of microphase separation is still in the subject of current research, and we can pose the questions, "What is the mechanism by which these materials microphase separate during rapid, bulk copolymerisation?" and "how do different phenomena (i.e. microphase separation and, for example, vitrification / gelation) interact to affect the relevant morphology?"

To answer these questions it is necessary to probe the phase - separation dynamics by conducting real - time SAXS measurements during rapid bulk copolymerisation that results in the formation of a segmented polyisocyanurate.

4.1.2 Theory of X-ray Scattering

When a beam of X-ray radiation hits a sample the electrons in the sample resonate at the frequency of the incident X-rays and emit secondary waves which can interfere with each other. This generates a SAXS pattern – the result of interference between the scattered waves generated by individual electrons in the sample.

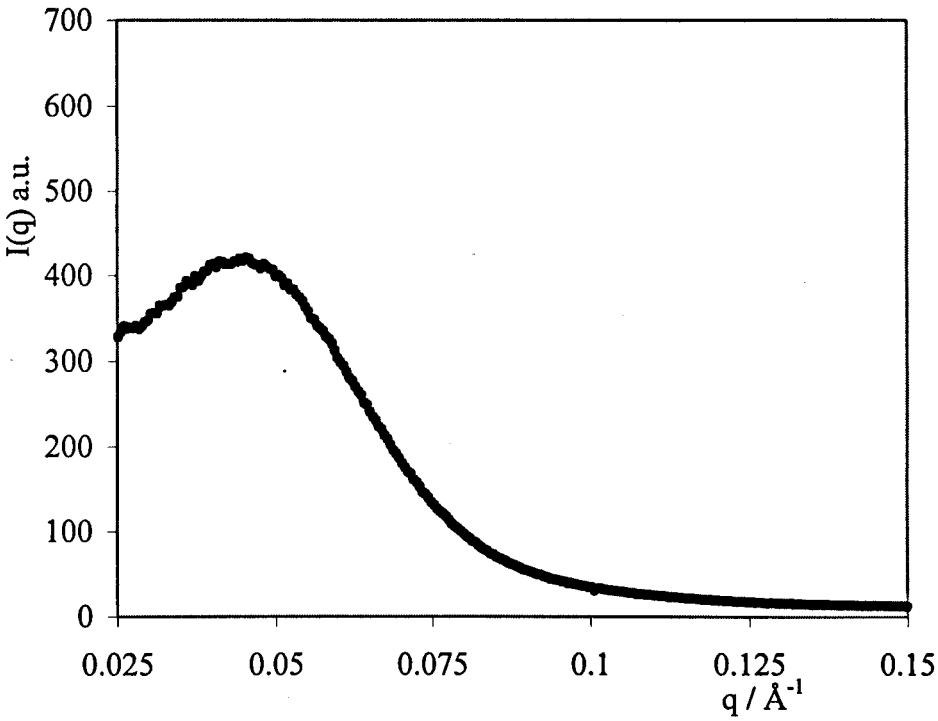

Fig. 4.1 A typical scattering profile for a phase - separated polyurethane elastomer.

The angular dependence of the scattered intensity can, after analysis, provide information about the morphology of the sample as the pattern is related to the magnitude and periodicity of the electron distribution. The scattering pattern for a

typical phase separated polyurethane elastomer is shown in figure 4.1, which plots scattering intensity (I(q)) against scattering vector, q, in $Å^{-1}$.

The intensity is related to the degree of microphase separation and the breadth of the intensity provides information on the size distribution of the inhomogeneities in the sample. The appearance of a maximum in the intensity is indicative of a periodic structure, and the position of this maximum provides information on the inter domain spacing (the d-spacing).

A common method for the determination of the structure is to use Bragg's law (equation 4.1).

$$d = \frac{\lambda}{2\sin\theta_{max}} = \frac{2\pi}{q_{max}} \qquad 4.1$$

where d is the interdomain spacing, q_{max} is the peak position at maximum intensity, θ_{max} is angle of reflected X-rays and λ is the wavelength of the beam of X-rays.

It is often convenient to perform a Lorrentz correction as the structure can be thought of as globally isotropic but locally lamellar – this corrects for this 3D to 1D transformation. This is done by plotting $I(q).q^2$ against q.

The *relative invariant*, Q', can be calculated by performing a summation under the $I(q).q^2$ against q curve between the first reliable data point, $q = q_1$ and the region in which $I(q).q^2$ becomes constant, $q = q_2$.

$$Q' = \int_{q_2}^{q_1} I(q)q^2 dq \qquad 4.2$$

In terms of morphology Q' represents the degree of phase separation. It is a relative value and has arbitrary units.

4.1.3 Instrumentation, Beamlines and Detectors.

The SRS operating parameters are 2 GeV, 100-200 mA with a flux of 4×10^{13} photons s^{-1} at the sample position. The intensity is 3 orders of magnitude higher

than conventional sources, so the rate of data collection is hugely increased enabling *in situ* measurements.

The vacuum chamber between the sample position and the detector reduces air scattering and absorption. The beam exit and vacuum pipe entrance are equipped with 15 μm mica windows, and 10 μm Kapton ™ windows. A Beamstop is mounted just before the exit window to prevent the direct beam hitting the detector. Cameras have different detectors depending on beamline / conditions. Parallel plate ionisation chambers are mounted before and after the sample so that corrections can be made for changes in sample thickness.

Station 16.1 [1, 2] is a fixed wavelength (1.41Å) X-ray diffraction station installed on a superconducting wiggler, specifically designed for time resolved studies of non-crystalline and fibrous materials at low measurement angles. The camera is the multiwire area RAPID [3] detector, which measures intensity in the radial direction. The spatial resolution of RAPID is 500 μm and maximum count rate is 20 000 000 counts s^{-1}.

Station 8.2 [4] was equipped with a multiwire quadrant detector, with a maximum count rate of 250 000 counts s^{-1}. The camera length was 3.2 m. For both stations the data acquisition software / system generated an acquisition time frame of 6 seconds with a wait time of 10 μs.

4.1.4 Previous Studies

Synchrotron radiation has been a valuable tool for probing how the morphology and its evolution is controlled by the chemical building blocks of the material, ultimately aiding property improvement.

Bonart [5] was amongst the first researchers to identify the orientation of a periodic structure under tensile deformation.

Koberstein *et al* [6, 7] investigated the thickness of the hard segment controlled by the shortest hard segment chain insoluble in the soft segment domain. This was

the first use of combined DSC / SAXS and DSC / WAXD of the multiple endotherms occurring in polyurethane elastomers that clearly showed that the intermediate temperature endotherm was associated with the onset of a microphase mixing transition. Real - time synchrotron SAXS and WAXS measurements of the kinetics of microphase separation and crystallisation have demonstrated that the competition between these two processes was responsible for determining the final structure.

Chu [8] studied the microphase separation kinetics of two segmented polyurethanes where the hard segment for each was MDI and 1,4-butane diol, but compared the two soft segments poly(tetramethylene oxide) and poly(propylene oxide) – poly(ethylene oxide). The difference obtained in absolute scattering intensity; and the difference in the relative invariant indicating more phase separation could not just be explained using thermodynamic arguments. They concluded that there was a significant thermodynamic factor, but also that the hard segment mobility, system viscosity and hard segment interactions were the three controlling factors for phase structure formation.

Synchrotron radiation was used by Ryan *et al* [9] in time resolved experiments to study the evolutionary dynamics of microphase separation during the bulk formation of some copolyurethanes. The hard segment comprised MDI and 1,4-butane diol and the soft segment was a poly(ethylene oxide) – poly(propylene oxide) diol with a molecular weight of 2000. A small reaction injection moulding (RIM) device was used in the experimental hutch to record data for the entire procedure. It was seen that higher temperatures gave rise to a faster rate of microphase separation, but ultimately resulted in a lower degree of phase separation. The induction time decreased with increasing temperature.

Copoly(isocyanurate –ureas) formed by RIM were investigated by Ryan *et al* [10] using a 2:1 mass ratio of polyisocyanurate to polyoxypropylene-polyamine. The effects of the polyether / polyamine functionality and chain extender on the final morphology were investigated by performing static SAXS measurements related to the resulting thermal and mechanical properties. Moduli between 1.5 and 0.7

GPa were obtained for the materials indicative of a glassy matrix. The isocyanate groups trimerised at a rate determined by catalyst content and temperature, and the addition of chain extender prevented full development of the electron density difference and reduced the d-spacing producing tougher materials. DMTA confirmed the existence of the microphase morphology, the scale of which was determined by TEM and SAXS analysis.

Musselman *et al* [11] synthesised and characterised, using SAXS and DSC, some polyurethane-urea elastomers. These had been synthesised via a specific route which gave well defined, less polydisperse hard segment lengths. Blundell *et al* [12] performed simultaneous measurements of 2D SAXS patterns and stress during tensile deformations, using synchrotron X-ray sources. Using samples with different distributions of hard and soft block length, they observed contrasting behaviour in, and mechanisms of deformation, attributed to the differences in sequence distribution.

Wilkinson *et al* [13] performed synchrotron SAXS studies of the structure development of RIM copoly(isocyanurate-ureas) and observed that the microphase separation occurred at a critical isocyanate group conversion and with kinetics associated with spinodal decomposition. This microphase separation was stopped by the vitrification of the polyisocyanurate giving a co-continuous morphology the size of which was approximately 100 Å. The maximum in scattered intensity appears after about 20 seconds then increased in intensity as the phase separation developed. The induction times decreased with increasing temperature following an Arrhenius rate dependence and the peak maximum (q*) was independent of temperature, in accordance with Leibler's theory.[14] From the observation of the structure development in real time it is seen that the dominant phase separation mechanism is spinodal decomposition forming a non equilibrium co-continuous morphology of two interconnecting networks. A plot of the log of the peak intensity as a function of time follows the Cahn - Hilliard theory of simple liquid-liquid phase separation.[15]

The reactive processing of model flexible polyurethane foams by *in-situ* studies of structure development using combined IR / SAXS and rheology / SAXS performed by Elwell *et al* [16]. Three distinct regions were observed in the $I(q_{max})$ versus time plot: I – low intensity, due to homogeneous liquid mixture, II – the appearance of the microphase separation temperature – a rapid increase in intensity and slope give amplification rate (R(q)) of composition fluctuations, and III – the onset of vitrification – after this the scattered intensity remains constant. The SAXS relative invariant, Q', appears to start to increase before the rapid growth in the concentration of hydrogen - bonded urea carbonyls, and the growth in the elastic shear modulus lags behind the relative invariant, i.e. hydrogen bonds "fix" the structure formed by microphase separation, then vitrification occurs.

Foam systems were also investigated by Li *et al*,[17,18] where TDI and MDI foaming systems were compared. The SAXS intensity increased early on in the microphase separation data – in good agreement with Cahn - Hilliard theory, i.e. separation of urea hard segments proceeds via spinodal decomposition during the formation of flexible polyurethane foam. The data were then fitted to the Teubner-Strey microemulsion structure factor, which extracts morphological characteristics, and it was concluded that the microemulsion structure was formed in a manner similar to the spinodal decomposition of non - reactive polymer blends under isoquench depth.

The aim of the work presented in this chapter is to investigate the morphology of poly(ether-isocyanurate) systems and polystyrene-polyisoprene-polystyrene / homopolystrene blends from static scattering experiments. The development of structure and phase separation mechanisms of the poly(ether-isocyanurate) systems will also be investigated by the analysis of the data obtained from time resolved experiments.

4.2 Experimental

All experiments were conducted at beamlines 8.2 and 16.1 at Daresbury Laboratories, Warrington, UK, and the Dubble beamline at the ESRF, Grenoble, France. Static, constant temperature experiments were performed on preformed samples to investigate their final morphologies. Dynamic temperature ramps were performed on liquid prepolymer samples so that phase separation during curing could be studied and fitted to recent theories.

4.2.1 Calibration

Sample to detector distance was calibrated using wet rat tail collagen, the scattering pattern of which is shown in figure 4.2.

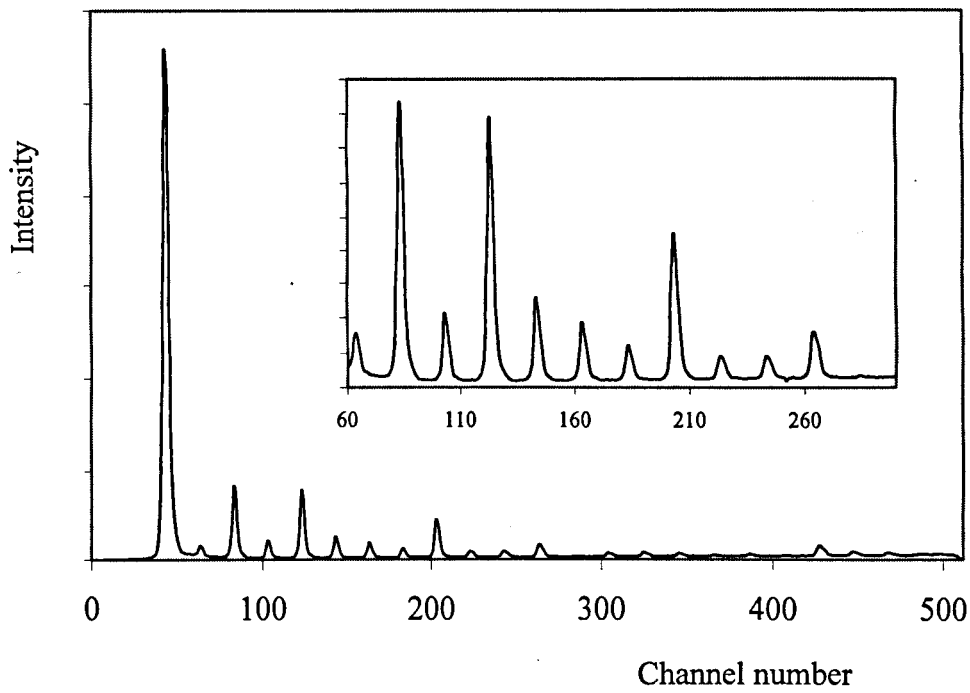

Fig. 4.2 Highly - orientated scattering pattern obtained from wet rat - tail collagen. Insert is a magnification of channels 60 to 300.

The d-spacing for collagen is 670 Å and it is used because of its many higher order peaks. The values of the higher order reflections are used to determine the

scattering vector, then using the equation $q=2n\pi/d$, the linear relationship between the scattering vector and the channel number can be established.

Experimental data was corrected for background scattering (empty pan and camera) and the detector response (taken using an Fe^{55} source).

4.2.2 Static Experiments

Solid samples of poly(ether-isocyanurates) and PS-PI-PS / PS blends were cut into pieces with a thickness of 1 mm and secured in the path of the beam with Kapton ™ tape. Data were collected for ten six second frames. The background "empty cell" of Kapton was removed.

4.2.3 Dynamic Experiments

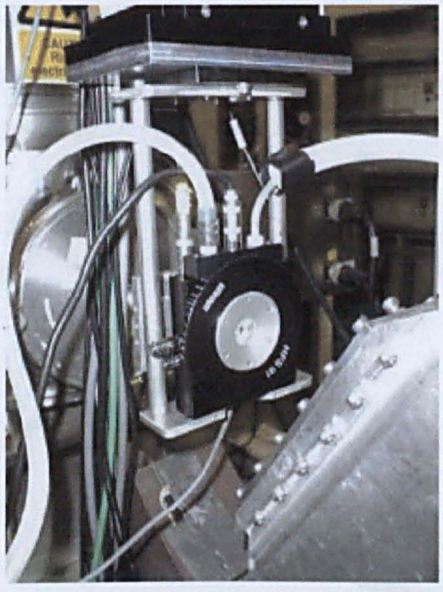

Fig. 4.3 *Photograph of the DSC hot-stage positioning on the beamline.*

Liquid samples of isocyanate end capped polyether prepolymers were mixed with the required catalyst system in an inert atmosphere. A sample of this mixture was placed into a punched aluminium DSC pan that had been fitted with mica windows, an aluminium spacer bar was added, and the pan sealed and placed in

the DSC. The experimental sample cell environment is pictured in figure 4.3. The temperature of the sample was lowered to –20 °C to prevent reaction occurring. The DSC was then mounted in the path of the X-Ray beam.

Temperature ramps were performed on a range of different samples with different hard segment contents.

4.3 Analysis of Results and Discussion

4.3.1 Static SAXS Patterns

4.3.1.1 Polyisocyanurates.

All polyisocyanurates with soft segment polyether molecular weight 2200 or greater showed a characteristic scattering pattern: examples for 4200 30 and 50% polyisocyanurate samples are shown in figure 4.4.

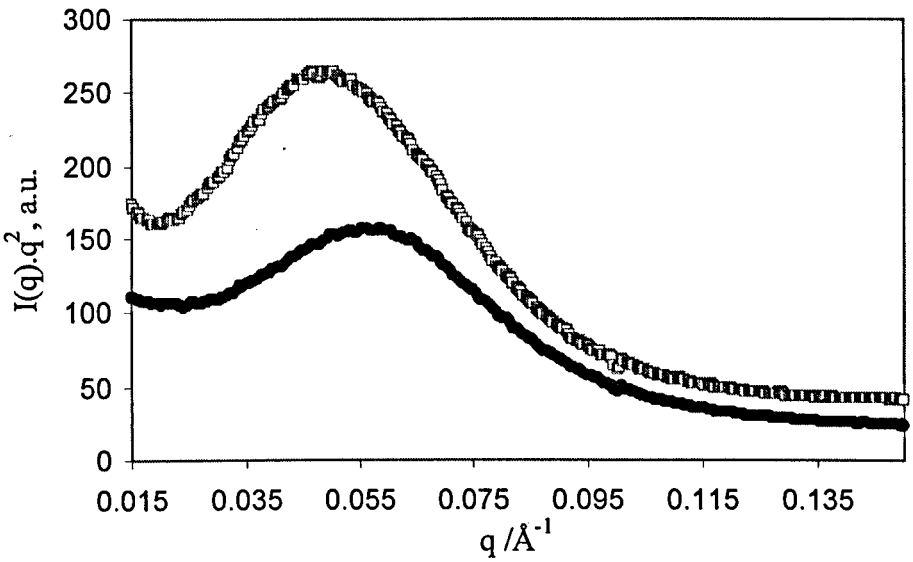

Fig. 4.4 Lorrentz - corrected scattering patterns for preformed polyisocyanurates with polyether segment Mw 4200 and hard segment contents of • 30 % and □ 50 %.

A further example with a shorter polyether soft segment length is shown in figure 4.5.

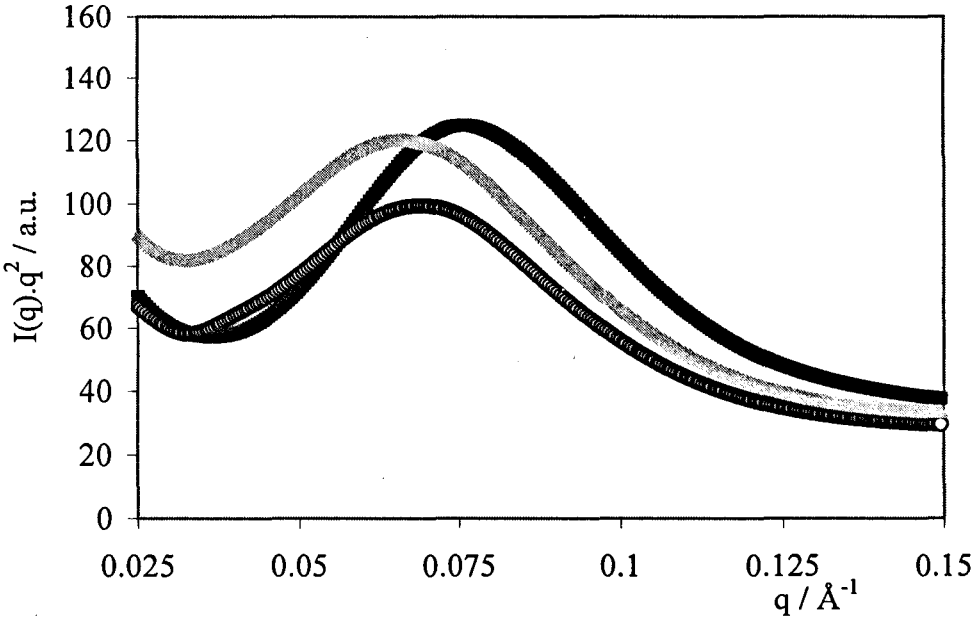

Fig. 4.5 Lorrentz - corrected scattering patterns for preformed polyisocyanurates with polyether segment Mn 2200 and hard segment contents of ■ 40 %, ○ 50 % and ▲ 60 %.

***Table 4.1** d-spacings for poly(ether-isocyanurates)*

Sample	Lorentz Corrected d-spacing, Å ± 2 %
2200 36 %	69.9
2200 40 %	81.6
2200 50 %	89.7
2200 53 %	90.1
2200 57 %	92.1
2200 60 %	96.6
4200 30 %	110.0
4200 37 %	115.1
4200 50 %	127.9
4200 54 %	130.2
8200 29 %	121.2
8200 37 %	131.1
8200 50 %	154.8

d-spacings for all poly(ether-isocyanurate) samples investigated are given in Table 4.1.

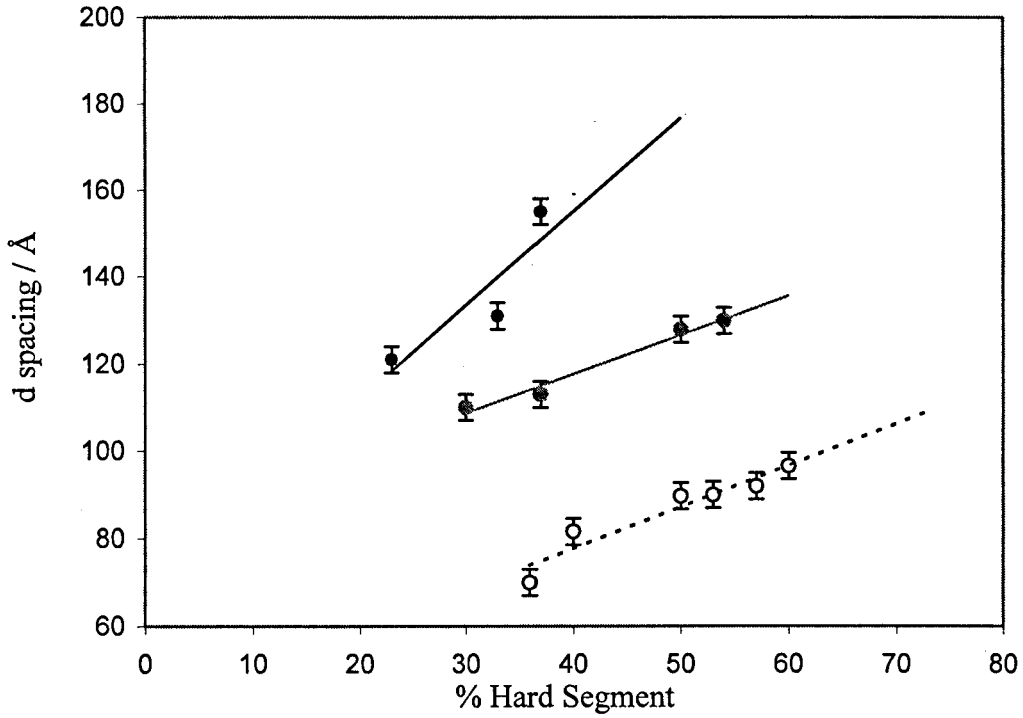

***Fig. 4.6** Variation in d-spacing with hard segment content with polyether soft segments ○ 2200 • 4200 • 8200.*

The variation in d-spacing with hard segment content is plotted in figure 4.6. It can be seen that d spacing increases with hard segment content and with polyether Mn.

4.3.1.2 Static Triblock Copolymer Blends

The scattering patterns obtained at station 16.1 for Polystyrene-polyisoprene-polystyrene / polystyrene blends are shown in figure 4.7. Table 4.2 gives the *d*-spacings for the polymer blends.

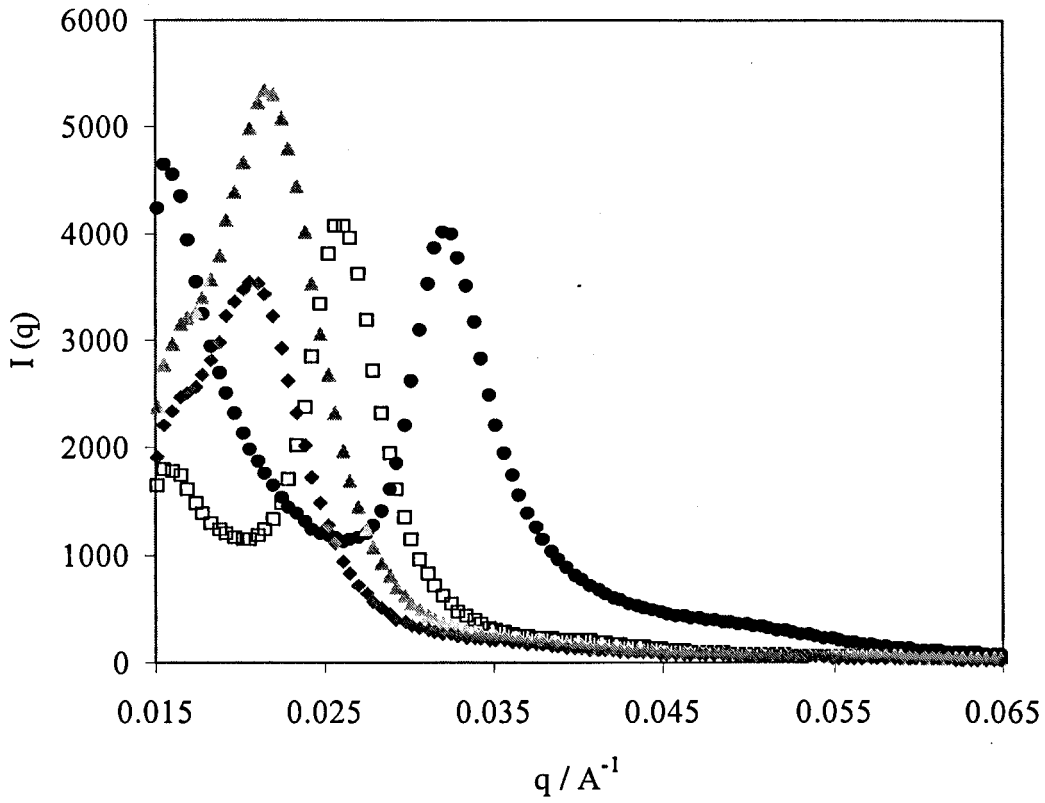

Fig. 4.7. *Scattering patterns obtained from Kraton® triblock copolymer blended with polystyrene. Amount of added polystyrene: • 0%, □ 10%, ▲ 20%, ♦ 50% by weight.*

Table 4.2 *d-spacings for PS-PI-PS / PS blends*

Added polystyrene, weight %	Total Volume fraction polystyrene, %	d-spacing, Å ± 2%
0	0.11	193
10	0.18	241
20	0.25	292
50	0.49	305

4.3.2 Time - Resolved SAXS Patterns

The developments of phase separation at elevated temperature can be seen by an increase in peak intensity, a typical example of which is shown in figure 4.8.

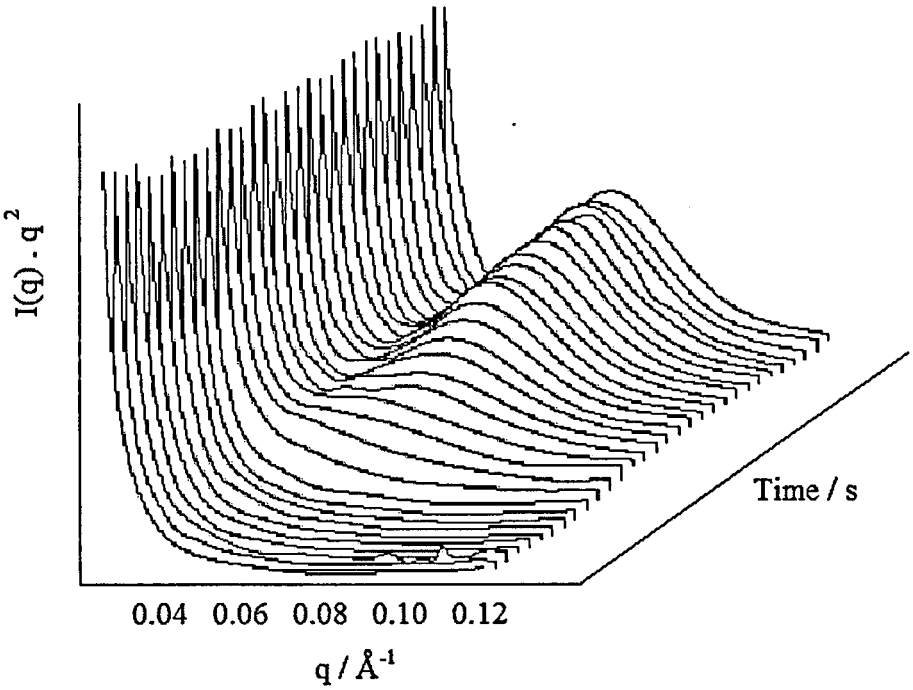

Fig. 4.8 The development of phase separation for 2200 40% shows every 4th frame (24seconds), with a curing temperature of 95 °C.

Evolution of phase separation is shown in figure 4.8. The absence of any scattering profile in the first 10 frames is due to liquid-liquid mixing of components. After 216 seconds the scattering pattern begins to form as structure is developed, reaching a maximum peak intensity after 504 seconds. The position of the peak maximum, q* remains constant during structure formation and there is no shift to lower q values once the structure is formed.

The position of q* and therefore the d-spacing of the samples formed in the beam is slightly different to samples moulded in the lab. This is probably due to the higher proportion of catalyst in the prepolymers used in the dynamic experiments, and the attainment of the curing temperature more rapidly in the DSC set-up.

After the experiments had been performed the DSC pans were opened and the sample inspected. There were no traces of bubble formation in the samples, indicating that dry conditions had been maintained throughout the procedure.

The maximum peak intensity can be monitored as the reaction progresses, as shown in figure 4.9, which displays the plot of I(q*) vs t with different regions, I, II and III.

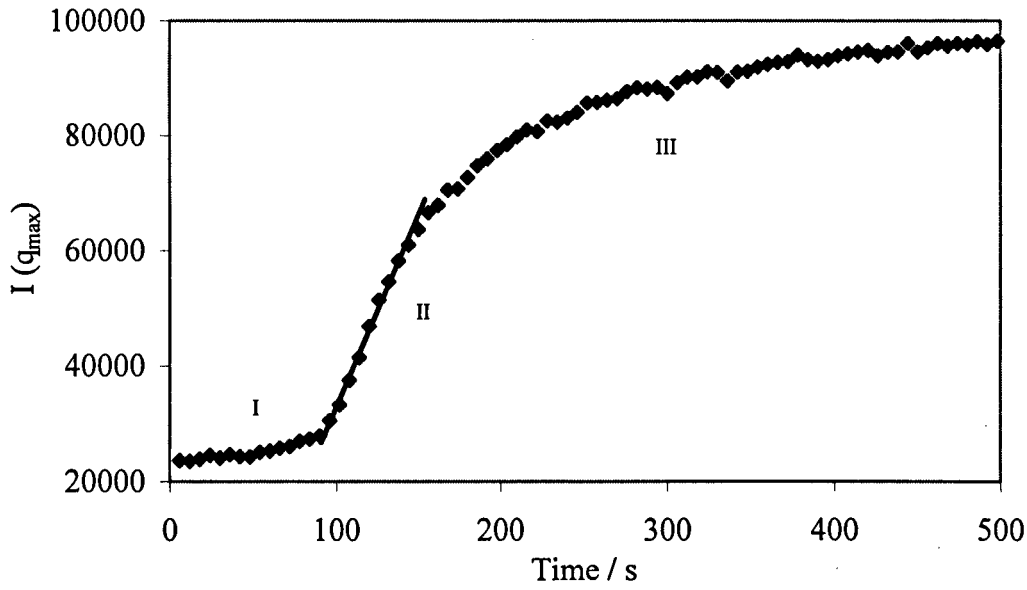

Fig. 4.9 Maximum peak intensity as phase separation proceeds for sample 2200 40% at 110 °C

The three regions can be described as

I: homogeneous liquid mixture of prepolymer, excess isocyanate and trimerisation catalyst. At approximately 90 seconds, the hard segment and molecular weight build up reach a critical value and the system becomes thermodynamically unstable.

II: the onset of microphase separation, with associated rapid increase in scattered intensity. The slope of this line is the amplification rate (R(q)) of the composition fluctuations. At this stage there is a high degree of interconnectivity between the phases of the microphase separating components. The molecular weight, N is the driving force for the thermodynamic quench enabling the system to pass from

disorder to order. Temperature is proportional to $1/\chi N$ (see introduction chapter), so as the molecular weight increases the chains get less compatible.

III: after 200 seconds the peak intensity begins to level off, and eventually becomes constant. Microphase separation has been stopped by the vitrification of the hard segment phase in the system.

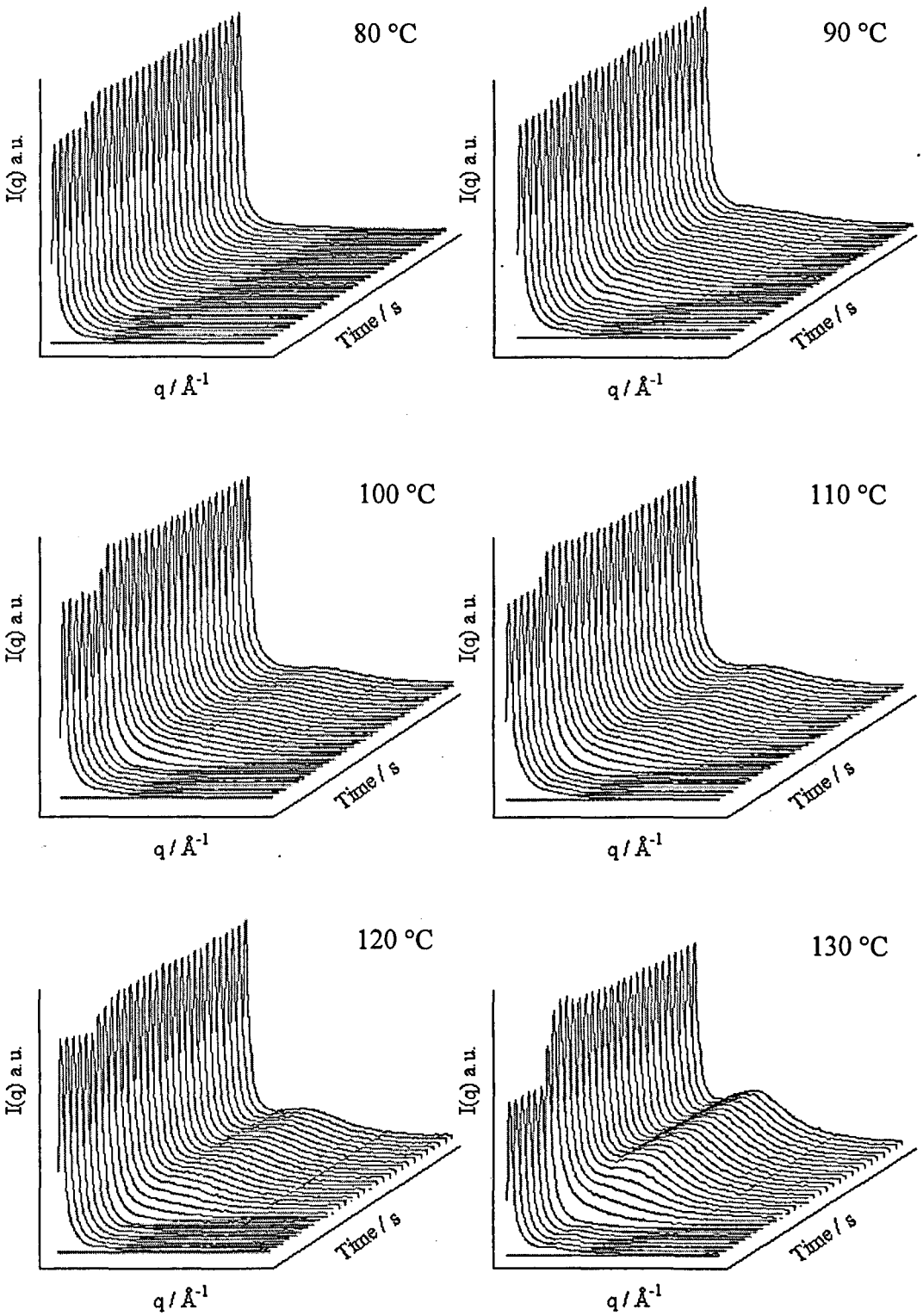

Fig. 4.10 Scattering profiles for 2200 40% at different temperatures.

Sample 2200 40% was cured at 6 different temperatures, the scattering profiles of which are shown in figure 4.10. For all time resolved data a background of the first frame of data was removed. The intensity of the peak maximum for three of these curing temperatures are plotted in figure 4.11 and the rates displayed in table 4.3.

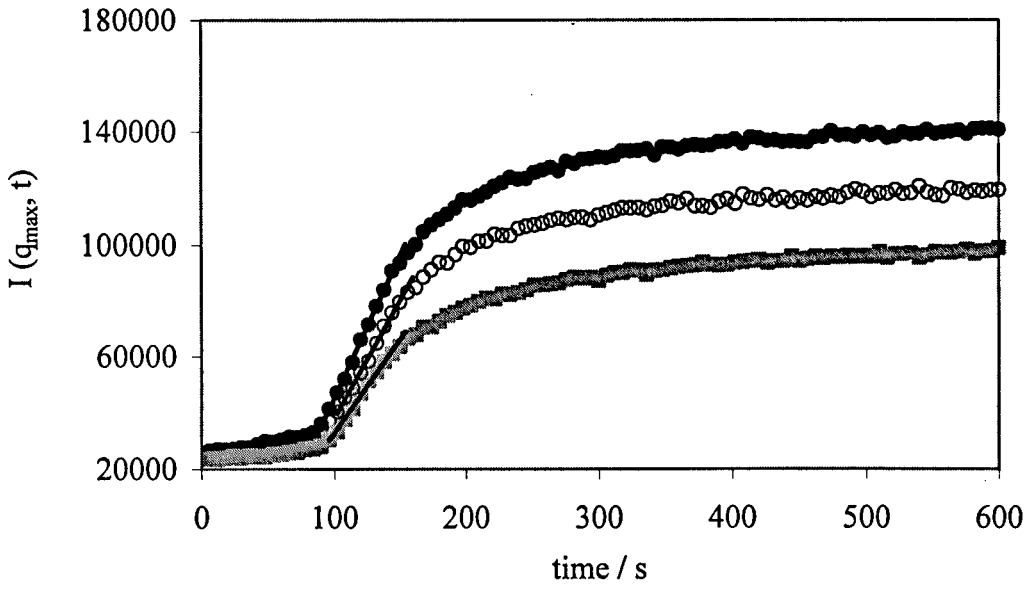

Fig. 4.11 2200 40% at different temperatures – different growth rates, where ■ represents 110 °C, ○ 120 °C and ♦ 130 °C cures

Temperature of cure °C	Gradient of growth / s
110	668.23
120	845.27
130	1024.2

***Table 4.3** Growth rates for 2200 40% at different curing temperatures*

For these 10 degree increases in temperature the onset of microphase separation occurs at the same time, at about 90 seconds. At higher temperatures the degree of polymerisation rises faster but the material is more compatible. Phase separation at constant χN just happens to mean constant reaction time because of

two compensating effects. The development of phase separation increases at a higher rate for higher temperatures, resulting in a more phase separated system for the poly(ether-isocyanurate) cured at higher temperature.

Figure 4.12 shows time - resolved SAXS patterns for 2200 Mw polyether soft segment poly(ether-isocyanates) with different hard segment contents. The d-spacing increases with hard segment content as with static experiments performed on samples with the same composition.

As hard segment content increases there is an increasing tendency for larger structures to appear in the scattering pattern at the start of microphase separation, after which the peak maximum moves to larger q values and remains constant while the phase separation completes. The appearance of the larger structures is not well understood, but may be explained by the decreasing the concentration of the isocyanate end capped polyol, which is acting as a surfactant in this system, therefore requiring the system to form larger structures to lower the interfacial energy.

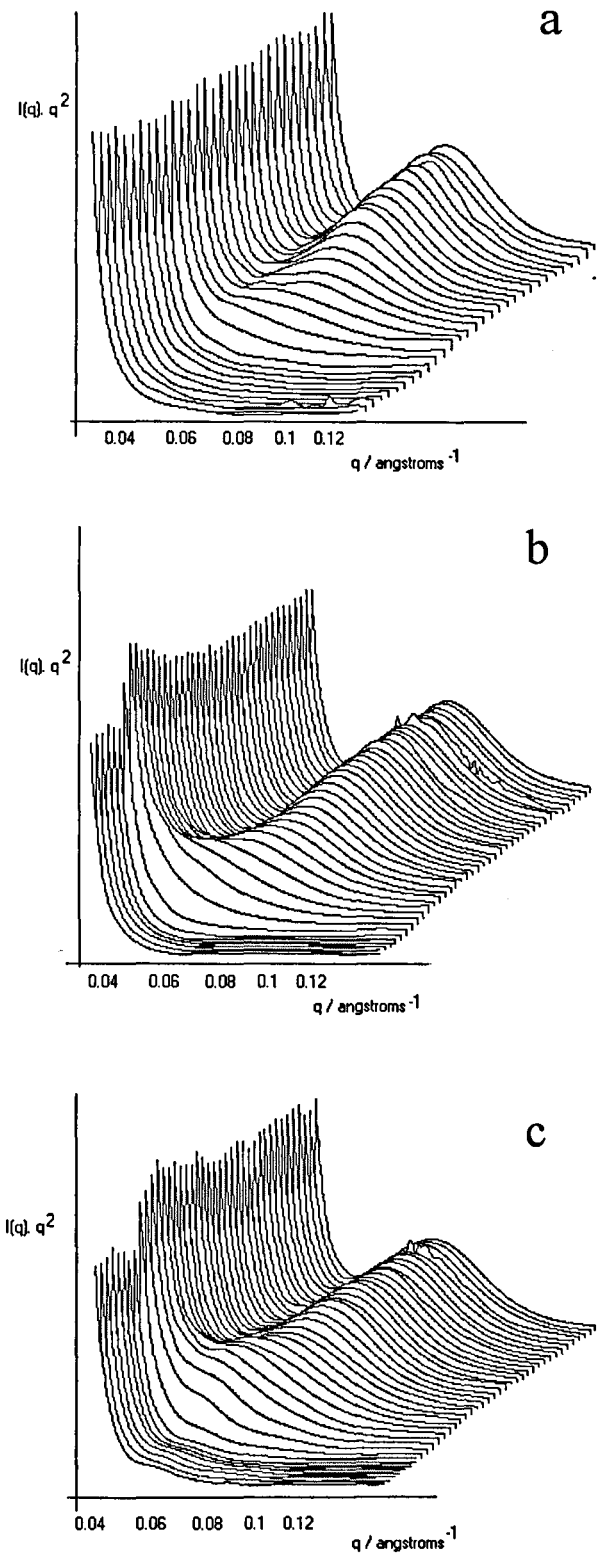

Fig. 4.12 Time resolved SAXS patterns a) 2200 40%, b) 2200 50% and c) 2200 60% at 95 °C

Mechanism of Microphase separation

Reaction induced phase separation (RIPS) may proceed via one of two mechanisms - nucleation and growth or spinodal decomposition, both of which were discussed in chapter 1. For RIPS in both cases phase separation proceeds until one phase vitrifies or a covalent network is formed.

The linearised spinodal decomposition theory of Cahn and Hilliard predicts that composition fluctuations and thus scattered intensity have a maximum for a given wavelength. If spinodal decomposition is the mechanism, q* should remain constant in the early stages of the separation, but the peak intensity should exhibit an exponential increase with time, according to equation 4.3.

$$I(q,t) = I(q,0)\exp[2R(q)t] \qquad 4.3$$

where R is the amplification rate of the composition fluctuations and depends on q. Figure 4.13 shows the plot of ln I(q*) vs time for sample 2200 40%.

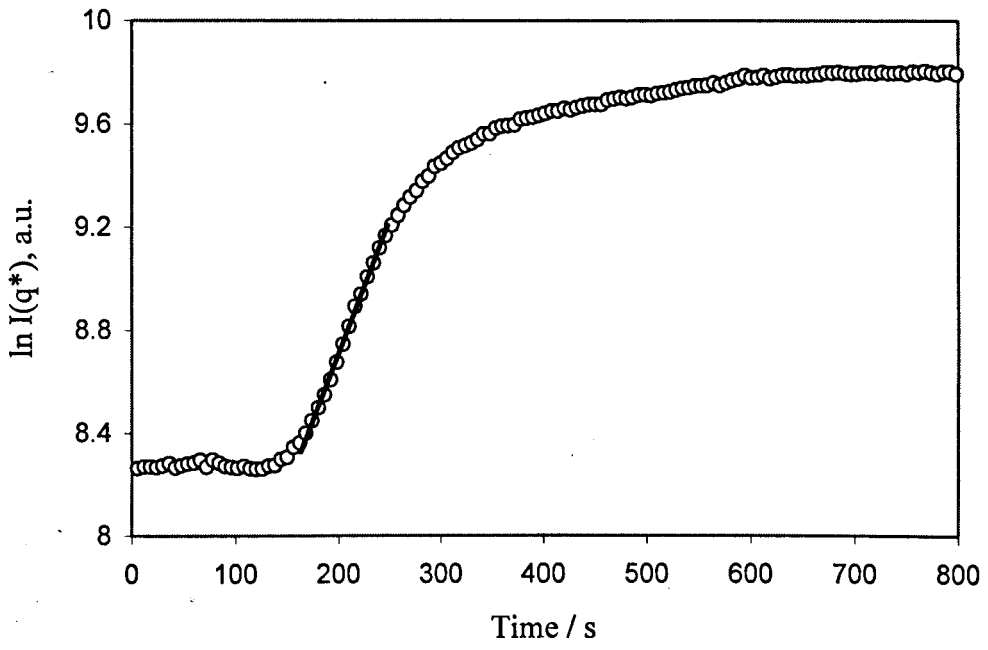

***Fig. 4.13** 2200 40% Increase in intensity of q_{max} with time*

A good fit of ln I(q*,T) data to a straight line is good agreement with the theory of Cahn - Hilliard.

Values of R(q) are calculated form the slopes of the lnI(q*) against time curves and taken as half the value of the gradient. R(q) is the rate at which the amplitude of q increases – a linear relationship between $R(q)/q^2$ and q^2 is predicted from the theory of Cahn and Hilliard. Values of $2R(q)/q^2$ against q^2 are plotted in figure 4.14.

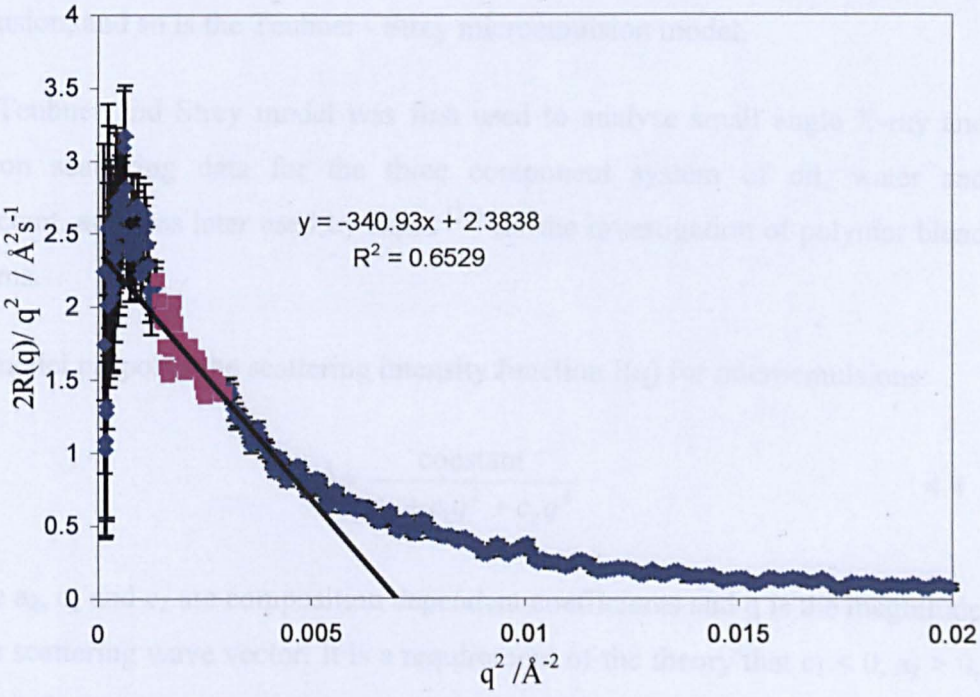

***Fig. 4.14** plot of $2R(q)/q^2$ against q^2 for sample 2200 40%*

Deviations from a straight line occur at higher values of q due to the fact that a reaction is occurring which increases the quench depth.

The time dependent Ginzburg - Landau model proposed by Hashimoto[19] used by Elwell and Li states that $2R(q)/q^2$ vs q^2 exhibits a maximum at a finite value of q if spinodal decomposition is the mechanism.

Spinodal decomposition is therefore identified as the mechanism of phase separation.

Teubner-Strey Microemulsion Analysis.

The phase separation mechanism of spinodal decomposition results in a bicontinuity of phase (although this may later be lost through Ostwald ripening). Confirmation of the existence of this phase bicontinuity may be sought by analysis of the scattering data using the Teubner - Strey model.[20]

Spinodal decomposition kinetics are based on the Ginzburg-Landau free energy expansion, and so is the Teubner - Strey microemulsion model.

The Teubner and Strey model was first used to analyse small angle X-ray and neutron scattering data for the three component system of oil, water and surfactant, and was later used by Bates [21] for the investigation of polymer blend systems.

The model proposes the scattering intensity function I(q) for microemulsions:

$$I(q) = \frac{\text{constant}}{a_2 + c_1 q^2 + c_2 q^4} \qquad 4.4$$

where a_2, c_1 and c_2 are composition dependent coefficients and q is the magnitude of the scattering wave vector. It is a requirement of the theory that $c_1 < 0$, $a_2 > 0$, and $c_2 > 0$.

Ultimately this gives two characteristic lengths, D and ξ. The length D represents the average periodic repeat distance of the system, and the correlation length, ξ represents the length over which the structural correlation exponentially decays.

Scattering data were selected a various times:

1. Just after onset of microphase separation
2. Before it starts to level off
3. Well after microphase separation is complete,

and fitted using equation 4.4. Figures 4.15 and 4.16 show where in the separation the data was taken and figures 4.17 and 4.18 show the fitting.

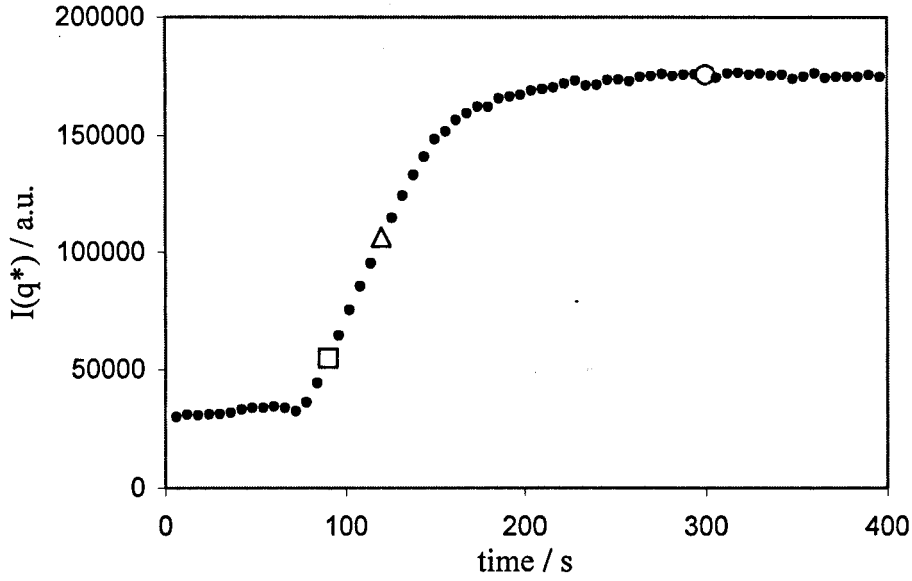

Fig. 4.15 *Integrated peak intensity showing frames selected for the Teuber-Strey analysis 2200 60%*

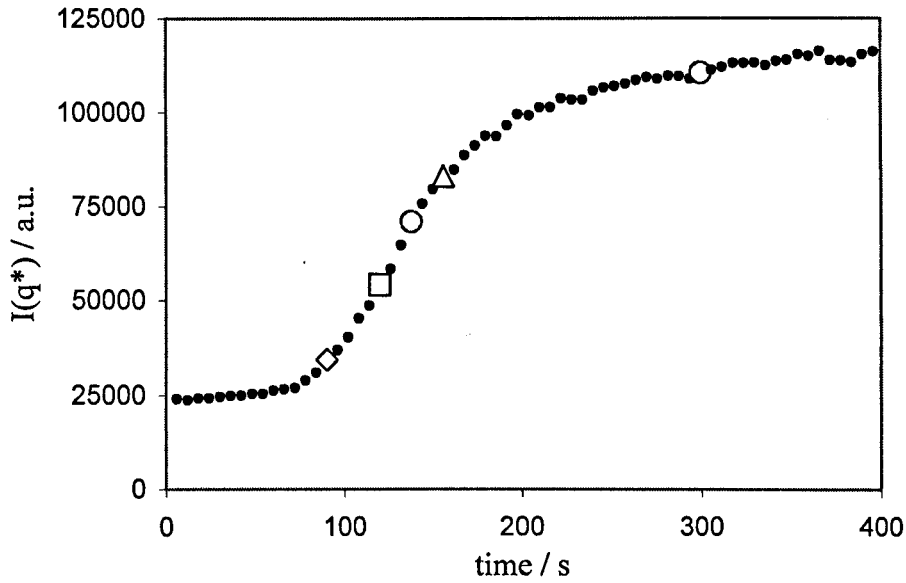

Fig 4.16 *Integrated peak intensity showing frames selected for the Teuber-Strey analysis 2200 40%*

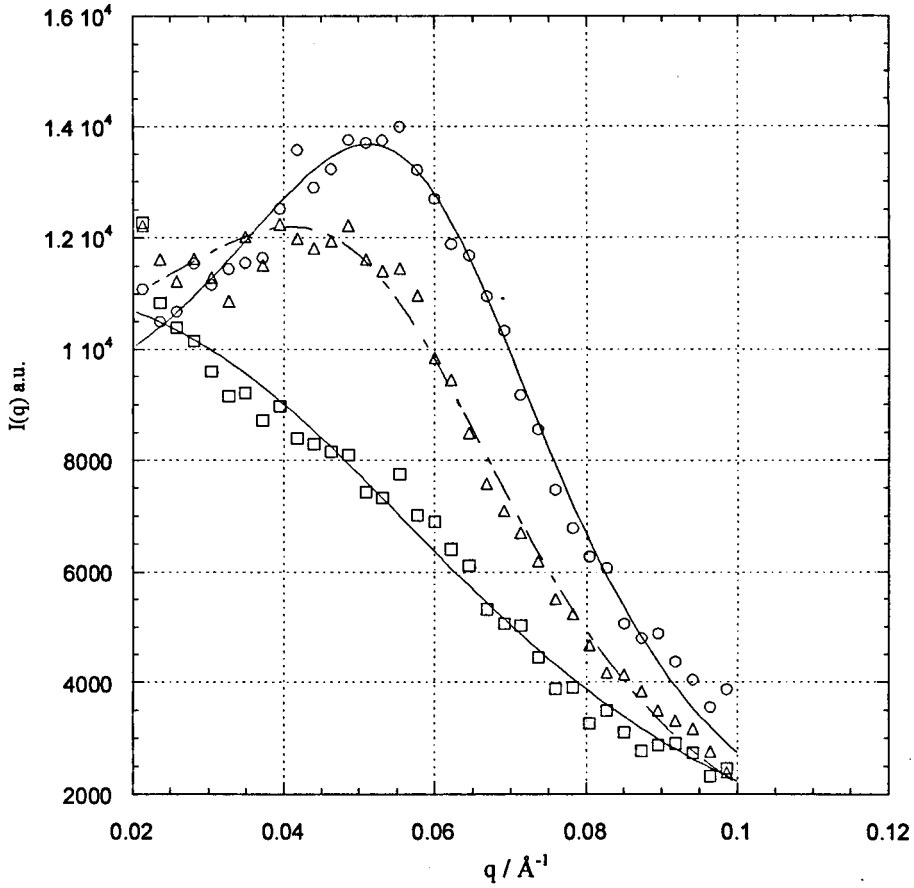

Fig. 4.17 *The scattering intensity I(q) at selected times from 2200 60 % and fitted curves as a function of q:○300 s, Δ 120 s and □ 90 s*

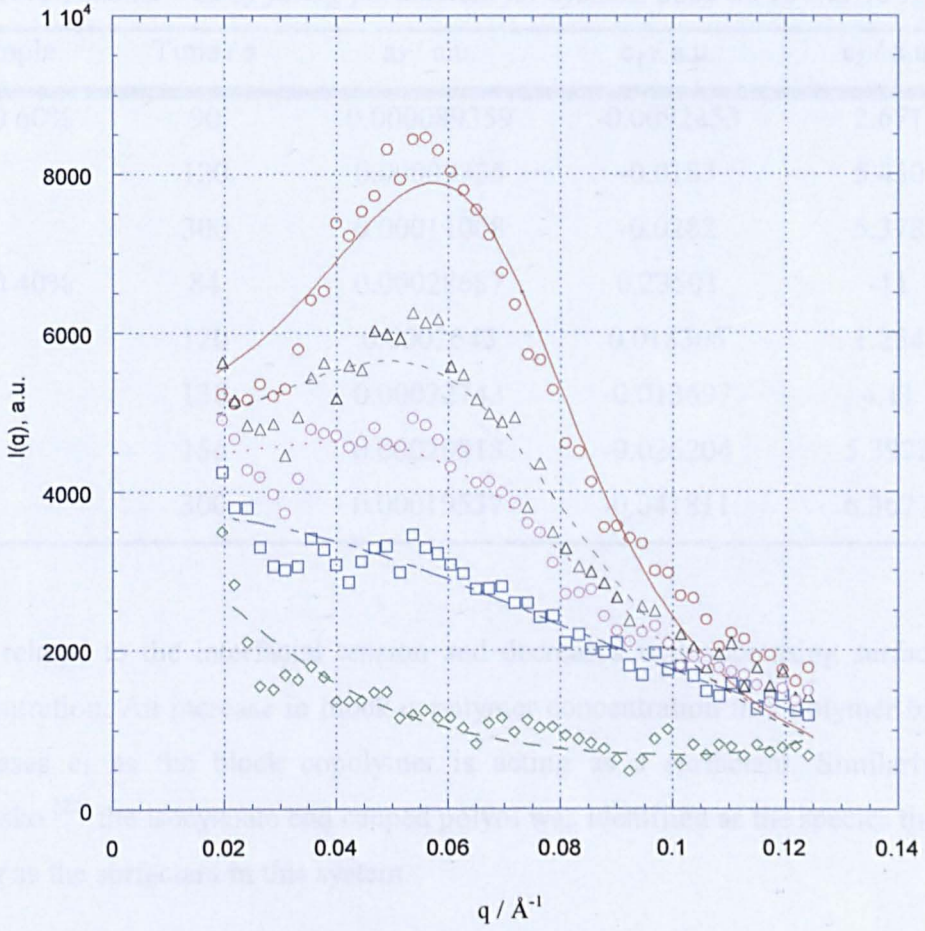

Fig. 4.18 *The scattering intensity I(q) at selected times from 2200 40 % and fitted curves as a function of q:* ○ *300 s,* Δ *156 s* ○ *138 s* □ *120 s and* ◊ *84 s*

The fitting of the Teubner-Strey structure factor is indicative of a bicontinuous morphology in the polyisocyanurate system. The fact that the fit is good well after the microphase separation is complete means that the bicontinuous morphology is preserved (i.e. Ostwald ripening is not occurring and phase separation has been arrested by the process of vitrification). Fitting parameters are shown in table 4.4.

Table 4.4 Teubner - Strey fitting parameters for systems 2200 60 % and 40 %

Sample	Time / s	a_2 / a.u.	c_1 / a.u.	c_2 / a.u.
2200 60%	90	0.000089359	-0.0092353	2.671
	120	0.00009735	-0.0183	5.430
	300	0.00011008	-0.0282	5.378
2200 40%	84	0.00028687	0.23501	-11
	120	0.0002643	0.018305	1.254
	138	0.00022743	-0.013697	4.11
	156	0.00020918	-0.026204	5.3972
	300	0.00019537	-0.041811	6.3677

c_1 is related to the interfacial tension and decreases with increasing surfactant concentration. An increase in block copolymer concentration in a polymer blend decreases c_1 as the block copolymer is acting as a surfactant. Similarly to Macosko [22] the isocyanate end capped polyol was identified as the species that is acting as the surfactant in this system.

c_2 is related to the behaviour at large q and subsequently the structure at the interface between the phases. An increase in c_2 before vitrification indicates a stiffening of the interface.

From a_2, c_1 and c_2, D and ξ may be calculated, where

$$D = 2\pi\left[\frac{1}{2}\left(\sqrt{\frac{a_2}{c_2}} - \frac{c_1}{2c_2}\right)\right]^{-1/2} \qquad 4.5$$

$$\xi = \left[\frac{1}{2}\left(\sqrt{\frac{a_2}{c_2}} + \frac{c_1}{2c_2}\right)\right]^{-1/2} \qquad 4.6$$

Increase of interdomain spacing due to increase in the concentration of hard segment. ξ/D increases with time i.e. increase in concentration of block copolymer as expected with the Teubner-Strey model.

For soft matter systems, a balance between entropy and interfacial energy controls ordering and mixing. The interaction strength of a surfactant controls the degree of mixing. The amphiphilicity of the surfactant may be quantified. In structured fluids the amphiphilicity factor, f_a is given by equation 4.7:

$$f_a \equiv c_1 / (4\, a_2 c_2)^{1/2} \qquad 4.7$$

Values of $f_a = 0 < f_a < 1$ indicate weak amphiphilicity and a poor microemulsion is formed. Values of $f_a = -1 < f_a < 0$ indicate slightly strong amphiphilicity and a good microemulsion is formed. Values of f_a for samples 2200 60 % and 2200 40 % were -0.87 and -0.59 respectively. Values for c_1, a_2 and c_1 used were from fits after microphase separation had finished. The stronger amphiphilicity factor for sample 2200 60 % adds further evidence to the increase in surfactant theory that was proposed to explain the formation of structures at lower q at the start of phase separation.

A distinguishing characteristic of a good microemulsion is a tendency to create an interface, due to a vanishing or negative value of c_1. A very strong amphiphilicity factor gives rise to an unstable microemulsion phase that tends towards a lamellar phase. The fact that c_1 decreases then levels off it is due to vitrification – i.e. the final equilibrium morphology is prevented from being attained.

4.4 Summary

Phase separation is seen in samples containing 2200 or higher molecular weight polyether soft segment. The higher the hard segment content the larger the d-spacing. The longer the polyether length, the larger the d-spacing

The addition of homopolystyrene to polystyrene-polyisoprene-polystyrene triblock copolymers increases the d-spacing until >50% weight of homopolystyrene when macrophase separation occurs.

Spinodal decomposition was identified as the mechanism of phase separation. Fitting of Teubner-Strey microemulsion structure factor showed that a bicontinuous morphology is preserved.

4.5 References

[1] N. Bliss, J. Bordas, B. D. Fell, N. W. Harris, W. I. Helsby, G. R. Mant, W. Smith, E. Townsandrews, *Review of Scientific Instruments* **1995**, *66*, 1311.

[2] R. L. Bilsborrow, N. Bliss, J. Bordas, R. J. Cernik, G. F. Clark, S. M. Clark, S. P. Collins, B. R. Dobson, B. D. Fell, A. F. Grant, N. W. Harris, W. Smith, E. Townsandrews, *Review of Scientific Instruments* **1995**, *66*, 1633.

[3] J. P. A. Fairclough, C. L. O. Salou, A. J. Ryan, I. W. Hamley, C. Daniel, W. I. Helsby, C. Hall, R. A. Lewis, A. J. Gleeson, G. P. Diakun, G. R. Mant, *Polymer* **2000**, *41*, 2577.

[4] W. Bras, G. E. Derbyshire, A. J. Ryan, G. R. Mant, A. Felton, R. A. Lewis, C. J. Hall, G. N. Greaves, *Nuclear Instruments & Methods in Physics Research Section a- Accelerators Spectrometers Detectors and Associated Equipment* **1993**, *326*, 587.

[5] R. Bonart, L. Morbitzer, G. Hentze, in *Journal of Macromolecular Science, Physics, Vol. 3*, **1969**, pp. 339.

[6] J. T. Koberstein, *Abstracts of Papers of the American Chemical Society* **1983**, *185*, 61.

[7] J. T. Koberstein, R. S. Stein, *Journal of Polymer Science Part B-Polymer Physics* **1983**, *21*, 1439.

[8] B. Chu, T. Gao, Y. J. Li, J. Wang, C. R. Desper, C. A. Byrne, *Macromolecules* **1992**, *25*, 5724.

[9] A. J. Ryan, W. R. Willkomm, T. B. Bergstrom, C. W. Macosko, J. T. Koberstein, C. C. Yu, T. P. Russell, *Macromolecules* **1991**, *24*, 2883.

[10] A. J. Ryan, J. L. Stanford, X. Q. Tao, *Polymer* **1993**, *34*, 4020.

[11] S. G. Musselman, T. M. Santosusso, J. D. Barnes, L. H. Sperling, *Journal of Polymer Science Part B-Polymer Physics* **1999**, *37*, 2586.

[12] D. J. Blundell, G. Eeckhaut, W. Fuller, A. Mahendrasingam, C. Martin, *Polymer* **2002**, *43*, 5197.

[13] A. N. Wilkinson, S. Naylor, M. J. Elwell, P. Draper, B. U. Komanschek, J. L. Stanford, A. J. Ryan, *Polymer* **1996**, *37*, 2021.

[14] L. Leibler, *Macromolecules* **1980**, *13*, 1602.

[15] J. W. Cahn, J. E. Hilliard, in *Journal of Chemical Physics, Vol. 28*, **1958**, pp. 258.

[16] M. J. Elwell, A. J. Ryan, H. J. M. Grunbauer, H. C. VanLieshout, *Macromolecules* **1996**, *29*, 2960.

[17] W. Li, A. J. Ryan, I. K. Meier, *Macromolecules* **2002**, *35*, 6306.

[18] W. Li, A. J. Ryan, I. K. Meier, *Macromolecules* **2002**, *35*, 5034.

[19] T. Hashimoto, *Macromolecules* **1987**, *20*, 465.

[20] M. Teubner, R. Strey, *Journal of Chemical Physics* **1987**, *87*, 3195.

[21] M. A. Hillmyer, W. W. Maurer, T. P. Lodge, F. S. Bates, K. Almdal, *Journal of Physical Chemistry B* **1999**, *103*, 4814.

[22] C. W. Macosko, *RIM Fundamentals*, Hanser, Munich, **1989**.

CHAPTER 5

MECHANICAL PROPERTIES

5.1 Introduction

Mechanical properties such as the modulus and loss tangent of solid materials can be measured in a variety of ways, for example by dynamic mechanical thermal analysis or by tensile testing. The eventual use of the material and therefore its form (thin film, foam or bulk elastomer) may influence the type of technique used for analysis.

Investigating sample surfaces becomes very important not only when dealing with very thin films but also when looking at adhesion. The surface properties of a material can be measured using different techniques depending on the length scale under investigation.

5.1.1 Scanning Probe Microscopy (SPM) methods

The first SPM machine was invented in 1981 by Gerd Binning and Heinrich Rohrer at IBM in Zurich.[1] Since then the growth in this area has been huge as this type of technique allows structural measurements to be taken that are smaller than the wavelength of light, without the need for staining, and various different types of surface interactions can be investigated.

SPM is now a general term covering several related technologies for imaging and measuring surfaces. All SPM techniques are based on the same principles – that of a scanning local probe with a sharp tip and its interaction with the sample surface, as shown in figure 5.1.

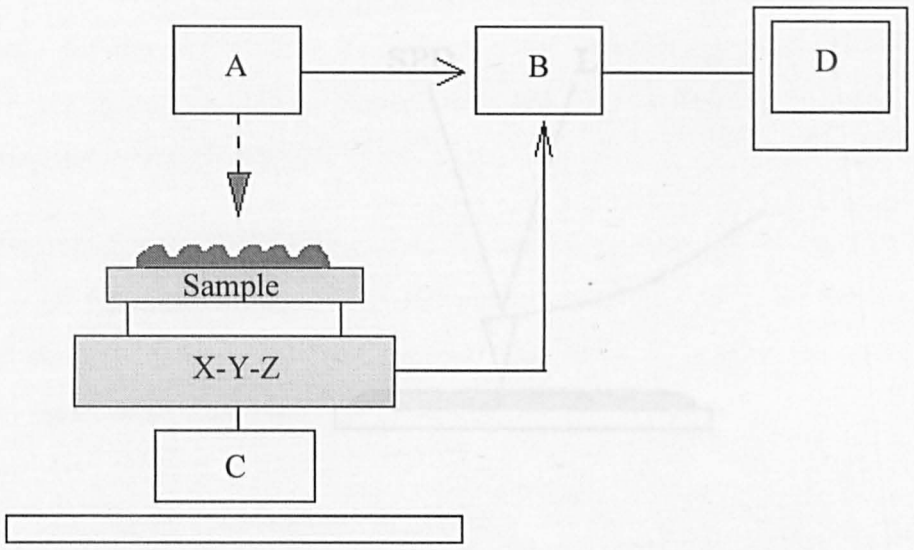

Fig. 5.1 *The principles of SPM, where A is the probe detection mechanism, B is the feedback mechanism, C is the coarse approach positioning, D is the display and X-Y-Z is the fine positioning.*

Types of SPM now in common use include Atomic Force Microscopy (AFM), Scanning Tunnelling Microscopy (STM) and Shear Force Microscopy (ShFM). A brief review of the AFM technique is given to compare with the methods used in the study of polyisocyanurate elastomers.

5.1.1.1 Atomic Force Microscopy

Atomic Force Microscopy was invented in 1986 by Binning, Quate and Gerber.[2] A schematic diagram is shown in figure 5.2. AFM utilises a sharp tip mounted on the end of a cantilever which bends in response to the sample – tip force. Light (L) is reflected onto a split photo diode (SPD), which gives the changes in bending of the cantilever. As the cantilever obeys Hooke's law the interaction force between the sample and the tip can be found. Piezo electric ceramics control the positioning of the sample.

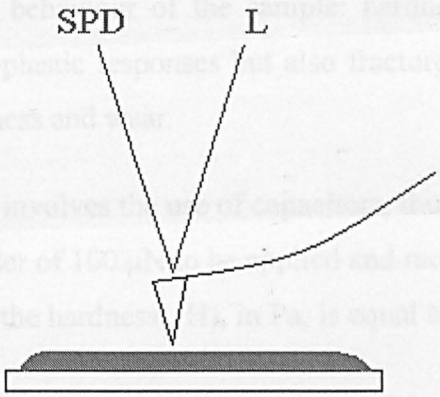

Fig. 5.2 Schematic diagram of AFM tip

The AFM can be operated in one of three modes: contact mode, tapping mode and non-contact mode.

Contact mode has the feedback control switched on; constant force between the tip and sample is maintained, which gives a topographical image. Without the feedback control constant height is maintained which gives a 'phase' image. Tapping mode can then be performed; the cantilever is oscillated at resonant frequency, but only taps the surface for a very small fraction of the oscillation. Phase images can be studied due to differences in stiffness or viscoelasticity of the sample surface.

Tips used in AFM are usually made from silicon nitride, and are either pyramidal or conical in shape.

5.1.1.2 Nanoindentation

Classical indentation, carried out on a much larger scale than SPM techniques, has been performed for some time, and involves the use of a microscope to measure the size of an indent made on a material when a given force has been applied. The forces involved were hundreds of grams. Spherical indenters have been widely used for measuring the mechanical properties of materials since the

time of Hertz [3] in 1881. Indentation tests provide a whole wealth of results not only for the deformation behaviour of the sample: hardness, elastic modulus, yield strength, and elasto-plastic responses but also fracture behaviour of brittle materials, strength, toughness and wear.

The modern nanoindenter involves the use of capacitors, thus enabling very small forces, typically of the order of 100 μN to be applied and measured. The principle of nanoindentation is that the hardness, (H), in Pa, is equal to the load (P) divided by the contact area (A):

$$H = P / A$$

This works well for materials where there is total elastic recovery, for example metals and ceramics, but is much more difficult for viscoelastic polymers because the contact area alters upon unloading. Correcting for elastic effects then means that the load – unload curve can lead to useful information regarding not only the hardness, but also elastic modulus, yield strength, creep resistance and stress relaxation.

The modern technique for extracting data from the load – unload curve is presented by Oliver and Pharr,[4] and the use of the nanoindentation technique to measure the properties of polymers has been reviewed by VanLadingham *et al.*[5]

Current applications of the nanoindentation technique include; measuring the properties of thin films for microelectronic integrated circuits, thin films for disks, structure – property – performance characteristics for composite materials[6] and in the dental industry, which makes use of the mapping ability of the probe.[7]

When the AFM is operated in force mode, indentation tests can be performed to provide information on mechanical response. However, it can be difficult to achieve an accurate measurement for the probe spring constant, and the tip shape may not be easy to define. This means that AFM measurements of indentation are only really relative measurements. The use of nanoindentation with the tip

controlled by capacitance sensors overcomes this and absolute values for mechanical properties can be obtained.

The work presented in this chapter describes the use of the nanoindentation technique to measure the mechanical properties of the series of poly(ether-isocyanurate)s. This technique was chosen due to the ability to position the tip very precisely, and there were no gluing or clamping issues to overcome. The technique allowed both static and dynamic measurements to be performed on different areas of the samples. The results obtained were compared with results obtained from DSC and from DMTA as the dynamic experiments using the nanoindenter had not been performed on polymers of this nature before.

5.2 Experimental Set-Up

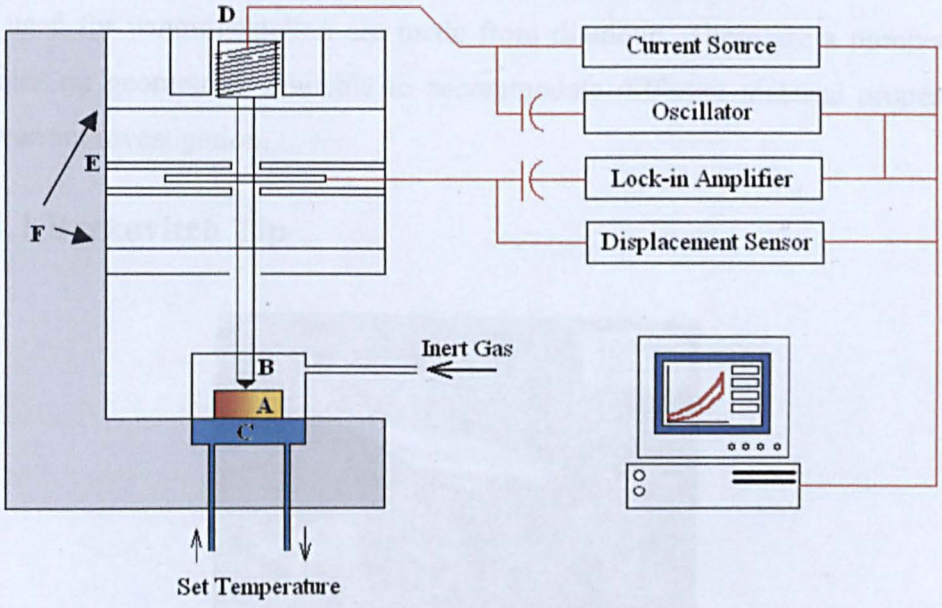

Fig. 5.3. *Diagrammatic representation of the Nanoindenter set-up where A is the sample, B is the nanoindentor tip, C is the environmental control system, D is the load application coil, E refers to the indentation column guide springs, and F is the capacitive displacement sensor.*

The nanoindenter used in this study is a Triboscope ® Nanomechanical test system manufactured by Hysitron Inc. The original SPM head (cantilever and detector system) is replaced with a Hysitron transducer that performs precise micro- or nano- indentations which can then be followed by *in situ* high resolution surface imaging. This has the advantage of being able to capture an image of the test site immediately after the test has been performed without disturbing the sample in any way. The capacitance sensors and thorough calibration allow the collection of accurate mechanical data. The whole instrument is protected from external vibrations by a soundproof hood. A schematic diagram of the set-up is shown in figure 5.3.

5.2.1 Tip Types

Tips used for nanoindentation are made from diamond. There are a number of different tip geometries available to accommodate different material properties that warrant investigation.

5.2.1.1 Berkovitch Tip

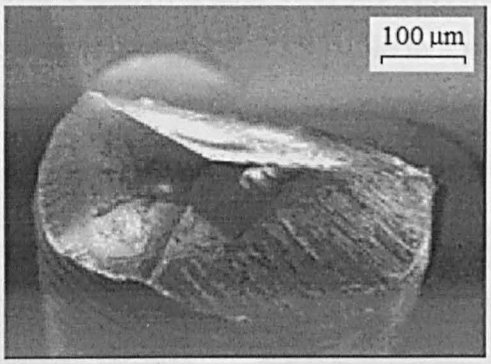

Fig. 5.4. *Image of the Berkovitch tip*

Figure 5.4. shows the Berkovitch tip – a three sided pyramid with a total included angle of 142.3°. This is the standard tip to use for bulk material nanoindentation and for films greater than 100 nm thick. The tip radius curvature is between 100 – 200 nm.

5.2.1.2 Cube Corner Tip

Figure 5.5 shows the cube corner tip with total included angles of 90°. The sharper angles and higher aspect ratio give radius of curvature much smaller than for Berkovitch so this is a better tip for ultra thin films, but they have the disadvantage that they blunt more quickly than Berkovitch tips.

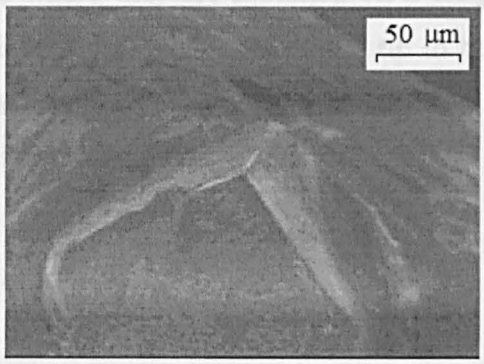

Fig. 5.5. Image of the cube corner tip

5.2.1.3 Cono-Spherical Tips

Figure 5.6 shows two cono-spherical tips with different radius angles. These tips are conically shaped with a spherical end. They are especially good for very soft polymers and biological samples. They are available in a variety of sizes – bigger ones being more suitable for softer samples.

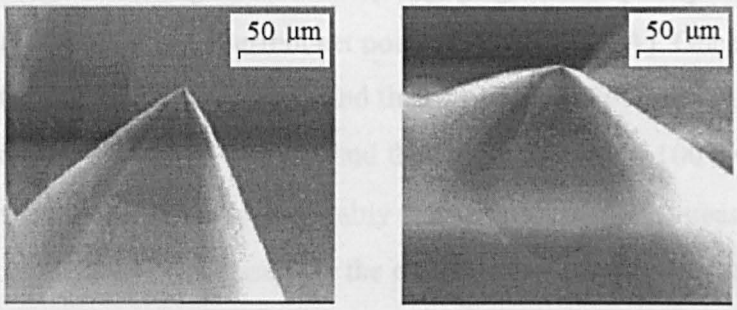

Fig. 5.6 Images of Cono-Spherical tips with a) <3µm radius and b) >3µm radius.

5.2.1.4 Other Tips

Other, more specialised tips available include the Vickers tip (a four - sided pyramid that gives a square - shaped indent) and the Knoop tip (a four sided pyramid that gives a diamond - shaped indent – these are especially good for looking at samples where there is some directional order). Most tips are also available as fluid tips where they are mounted on a long shaft, some distance away from the transducer head. This enables the tip to be immersed in a fluid, and so is useful for electrochemical experiments and for investigations of biological samples in their normal environment.

5.3 Testing Procedure

Nanoindentation was used to investigate bulk and graded materials. Samples were mounted with epoxy glue onto steel disks of approximately 10 mm diameter in order to position them on the sample stage, which has a small vacuum suction point. Suitable sample size is up to 8 mm^2 and 4 mm thick. The minimum sample thickness is three times the penetration depth. The sample surface must be flat to within ~100 nm to avoid contact with the side of the tip which would give an inaccurate contact area.

A suitable area for testing was found by engaging the sample tip with the surface of the material with a high current set point (typically 10 nA). Once at the surface the current was reduced to 1-3 nA, and the position of the tip recorded (X and Y). The scan size was set to 4 – 10 μm and the height to around 100 nm. The tip was then offset by a few μm and a suitably flat area to perform measurements was found. Berkovitch tips were used for the experiments described in this study.

5.3.1 Static Experiments

Triboscope® 3.6 software was used to programme variables for static measurements. The tip was brought into contact with the sample surface and a set

load applied. This load was then held to allow for creep and the tip withdrawn. Figure 5.7 shows schematic representations of load / time graph and load / unloading curves. The rate of loading / unloading and the holding time for which the load was applied was varied.

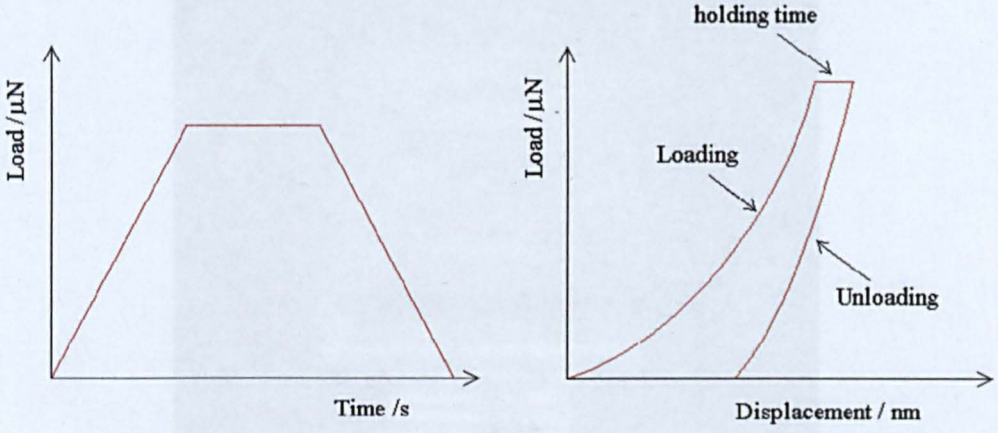

Fig. 5.7. Loading and unloading profiles.

In order to gain knowledge of the required load needed to overcome surface effects, a series of indentations were made on each sample with increasing load force. The tip was repositioned to a new area after each indent had been performed.

The properties of graded samples could be investigated by moving the tip a known distance across a cut cross section of graded polyisocyanurate sample.

5.3.2 Dynamic Experiments:

The device was fitted with an environmentally - controlled stage (Hysitron inc.) with a Melchor Thermoelectric temperature controller. The temperature was controlled using TECVIEW software. This enabled measurements to be made at temperatures from -25 °C to 125 °C. This has two advantages – the speed that data can be collected is greatly improved if a low temperature compensates for very low frequency oscillations, and there is a reduced danger of the tip-sample contact area heating up with very fast oscillations. A dry nitrogen flow prevents the formation of condensation at low temperatures, which would affect the

surface properties dramatically, and a thermocouple is attached to the sample to monitor the set temperature. The environmentally - controlled stage is shown in figure 5.8.

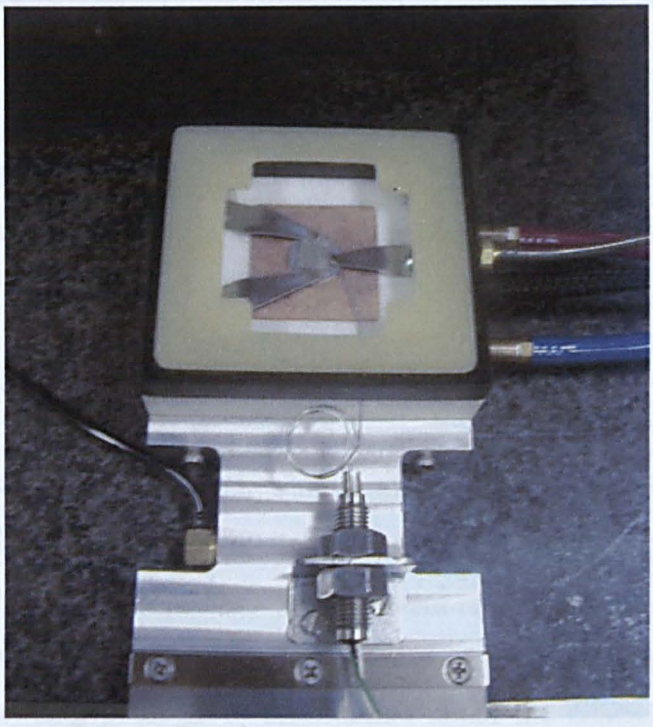

Fig. 5.8. *Photograph of the specially constructed heating stage showing sample mounted on steel disk and secured on copper plate (C in figure 5.3).*

DSM2 software was used to control parameters of dynamic testing. Using results obtained from performing a series of static indentations, a suitable load force was applied. The tip was then set to oscillate at ± 5% about this set force at a series of frequencies. Data concerning amplitude and phase were collected, enabling the calculations of the storage and loss modulus, stiffness, damping and tan . This procedure was then repeated for a range of temperatures at a new position on the sample surface.

The poly(ether-isocyanurate) series of samples with a range of polyether soft segment length and hard segment content were tested under both static and dynamic conditions.

5.4 Data Analysis

5.4.1 Static Measurements

The technique for analysing the data obtained from load - unload indentation curves is based on the method developed by Oliver and Pharr[4], where the relationship between penetration depth, h and applied load, P is given by equation 5.1:

$$P = \alpha(h - h_f)^m \qquad 5.1$$

α contains geometric constraints, sample elastic modulus, sample Poisson's ratio, (ν_m), the indentor's elastic modulus and Poisson's ratio(ν_i). h_f is the final unloading depth, and m is a power - law exponent related to the geometry of the indentor. The unloading curve is fitted by a power - law expression, then dP/dh at the maximum loading point gives information about the contact at that point which is termed the contact stiffness, S.

$$S = 2aE_r = \frac{2\beta}{\sqrt{\pi}}.\frac{E_r}{\sqrt{A}} \qquad 5.2$$

The β term is used to account for different geometries of indentor tip, a is the contact radius and A is the projected area of the tip – sample contact. E_r is the 'reduced' modulus, which accounts for both the deformation of the sample (m) and the indentor, (i), the relationship of which is shown in equation. 5.3.

$$\frac{1}{E_r} = \frac{\left(1-\nu_m^{\,2}\right)}{E_m} + \frac{\left(1-\nu_i^{\,2}\right)}{E_i} \qquad 5.3$$

where E_m is the modulus of the sample and E_i is the modulus of the indentor. The results obtained from the nanoindentation testing procedure are usually given as reduced modulus results, as the Poisson's ratio for the new material is not known exactly. If the Poisson's ratio is assumed to be 0.35 (that of an elastomeric

material), then the values of the reduced modulus are approximately 20% higher than the real modulus. The values obtained are sometimes referred to as "indentation" moduli.

Figure 5.9 shows the terms used for the various parameters before, during and after indentation.

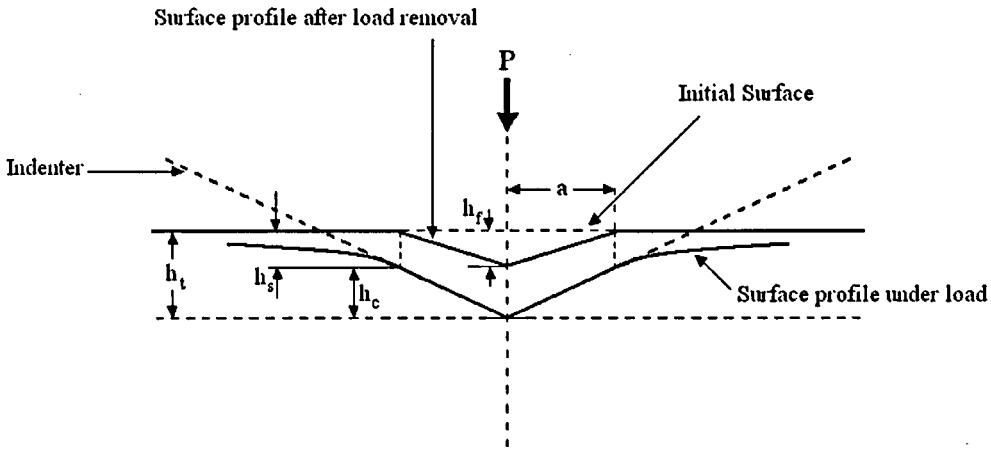

Fig. 5.9. *Sample surface geometry, where h_c is the vertical distance along which contact is made, h_s is the displacement at the surface at the perimeter of the contact. At peak load, the load and displacement are P_{max} and h_{max} respectively, and the radius of the contact circle is a. When the indenter is fully withdrawn, the final depth of the residual hardness impression is h_f.*

The Triboscope® 3.6 software enabled the chosen load, loading rate, and holding time to be accurately controlled. Figure 5.10 shows the analysis window where the unloading section of the load / unload curve is fitted.

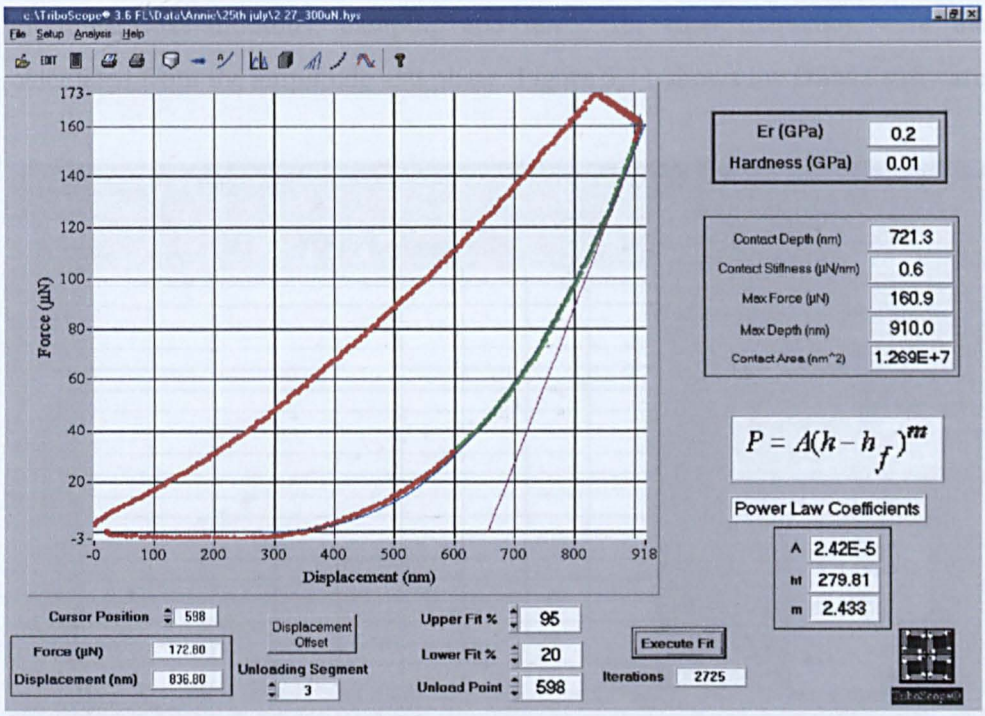

Fig. 5.10 *Triboscope software window showing the fitting of the unload portion of the load / unload curve.*

5.4.2 Dynamic measurements

Equations 5.4 to 5.6 are used for dynamic analysis:

$$\text{Storage modulus, } E' \quad \frac{k_s\sqrt{\pi}}{2\sqrt{A}} \qquad 5.4$$

$$\text{Loss modulus, } E'' \quad \frac{\omega C_s\sqrt{\pi}}{2\sqrt{A}} \qquad 5.5$$

$$\text{Damping factor, } \tan\delta \quad \frac{\omega C_s}{k_s} \qquad 5.6$$

where k_s is the spring constant, is the frequency A is the contact area and C_s is the compliance.

The DSM2 software controlled the experimental parameters of frequency range, load force, load amplitude, and ramp rate. The values of stiffness, storage

modulus, loss modulus, damping and tan for each frequency were then calculated from the amplitude and phase. Figure 5.11 shows the DSM2 software.

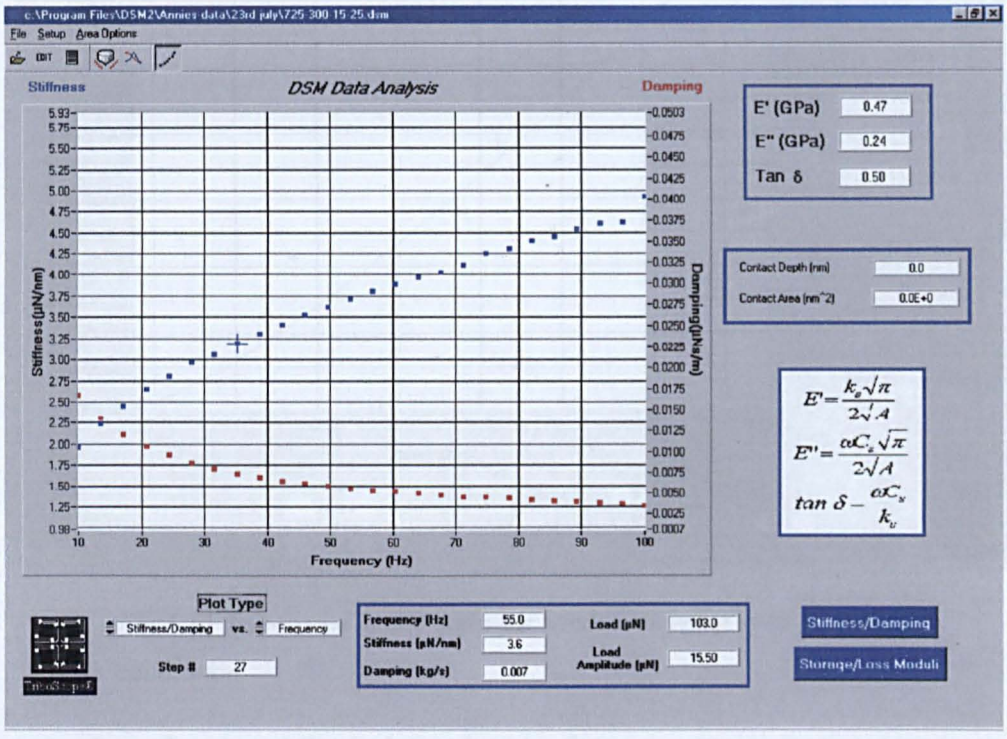

Fig. 5.11 DSM2 software window

5.4.3 Calibration

Before data could be taken the tip had to be calibrated for both types of testing procedure.

5.4.3.1 Static Calibration

To calibrate the tip for static measurements an area function calibration was performed using fused silica quartz crystal. This was chosen as there is no oxide layer formation and thus no variations in modulus and hardness with penetration depth. A series of indents covering a wide range of maximum load and penetration depth were made. The results of area against contact depth are shown in figure 5.12.

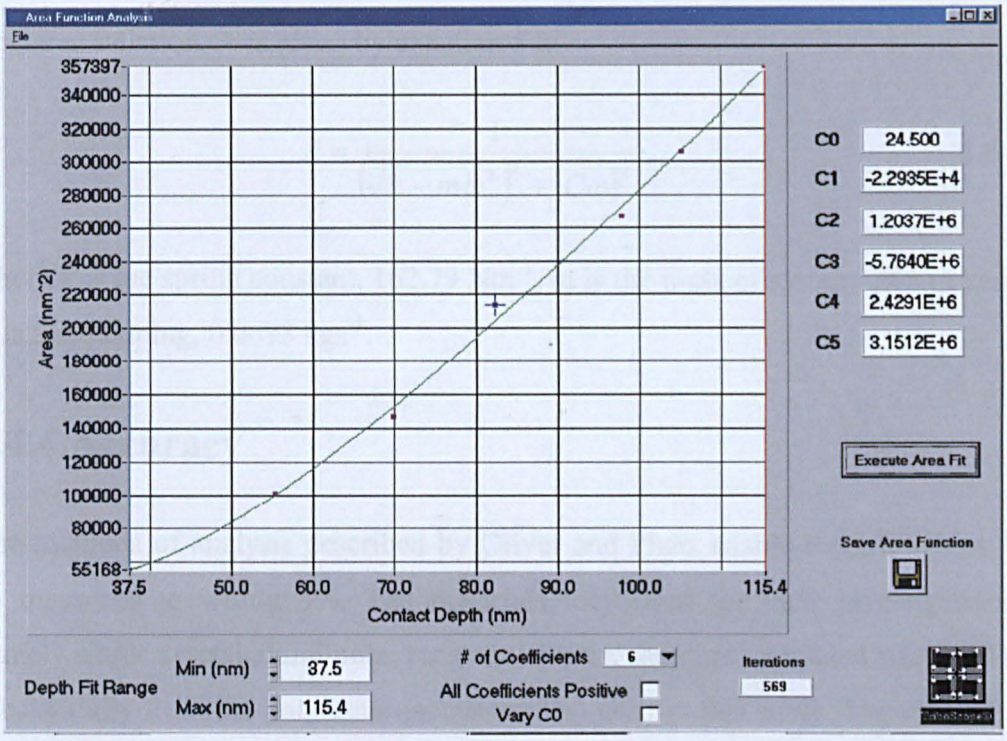

***Fig.5.12** Triboscope ® 3.6 software window showing area function calibration*

A tip shape function, $A(h_c)$ is determined by fitting the area against contact depth (h_c) using a polynomial fit of the form:

$$A(h_c) \quad C_0 h_c^2 \quad C_1 h_c \quad C_2 h_c^{1/2} \quad C_3 h_c^{1/4} \quad \ldots \qquad 5.7$$

where $A(h_c) = 24.500 h_c^2$, the area function of a perfect Berkovitch indentor, and the following terms (C_1 onwards) account for deviations from ideal geometry.

5.4.3.2 Dynamic calibration

To calibrate the indentor for dynamic measurements an air test was performed using variables similar to those used for the experiments.

The force applied was 150 N, then the force amplitude was set to ±5 N about the applied load. The frequency sweep was from 10 to 200 Hz with a loading rate of 10 Ns^{-1}.

The area function, A is given by equation 5.8:

$$A = \frac{1}{\left(\sqrt{k} - m\omega^2\right)^2 + (C\omega)^2} \qquad 5.8$$

where k is the spring constant, 162.79 Nm^{-1}, m is the mass of system, 265 mg and C is the damping, 0.0693 kgs^{-1}.

5.4.4 Accuracy

The methods of analysis described by Oliver and Pharr enable moduli values to be measured to within 5%. The materials they used for their investigations, namely single crystal aluminium, tungsten, quartz, sapphire and fused silica differ substantially from the poly(ether-isocyanurates) used in this study. The two main errors that contributed to the inaccuracy of the measurements were the sharpness of the tip (probe deconvolution), and the fact that it was very difficult to get the sample surface level. These factors increase the error in the modulus measurement to about 8%.

When performing the dynamic experiments the system was left for up to half an hour to equilibrate between temperature changes. This allowed for thermal expansion of the sample, but the temperature was still only accurate to ± 0.05°C.

When mapping the sample surface the experiment relied on the resolution of mechanical components to move tip and measure its position. This was accurate to ±0.5 μm.

5.5 Results

The following section describes results obtained from different types of tests performed on poly(ether-isocyanurates), polystyrene-polyisoprene-polystyrene / homopolystyrene blends and graded poly(ether-isocyanurate) samples.

5.5.1 Static Measurements

These include variable load force, constant load with variable ramp and variable position tests.

5.5.1.1 Variable Load Force

For each sample measured a series of load / unload curves are generated as the tip moves to a new position and the load force increases. Figure 5.13 shows load / unload curves for a series of load forces on sample 425 54%.

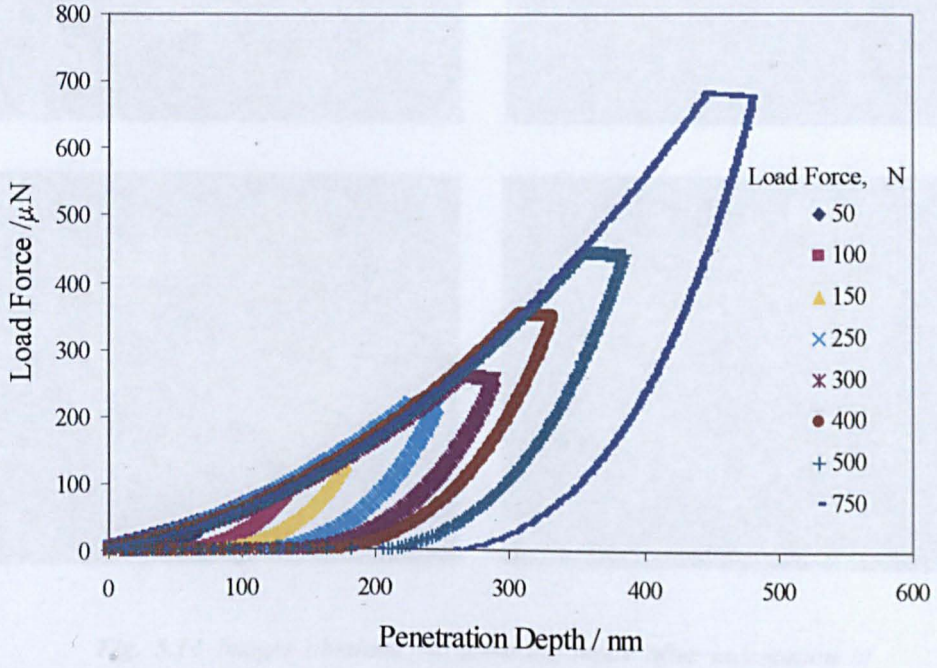

Fig. 5.13 *Load unload curves for a series of increasing loads for sample 425 54%*

In situ imaging by the tip records the shape of the indentation after the load has been applied. A series of these images shows clearly the increase in contact area with load force, as seen in figure 5.14.

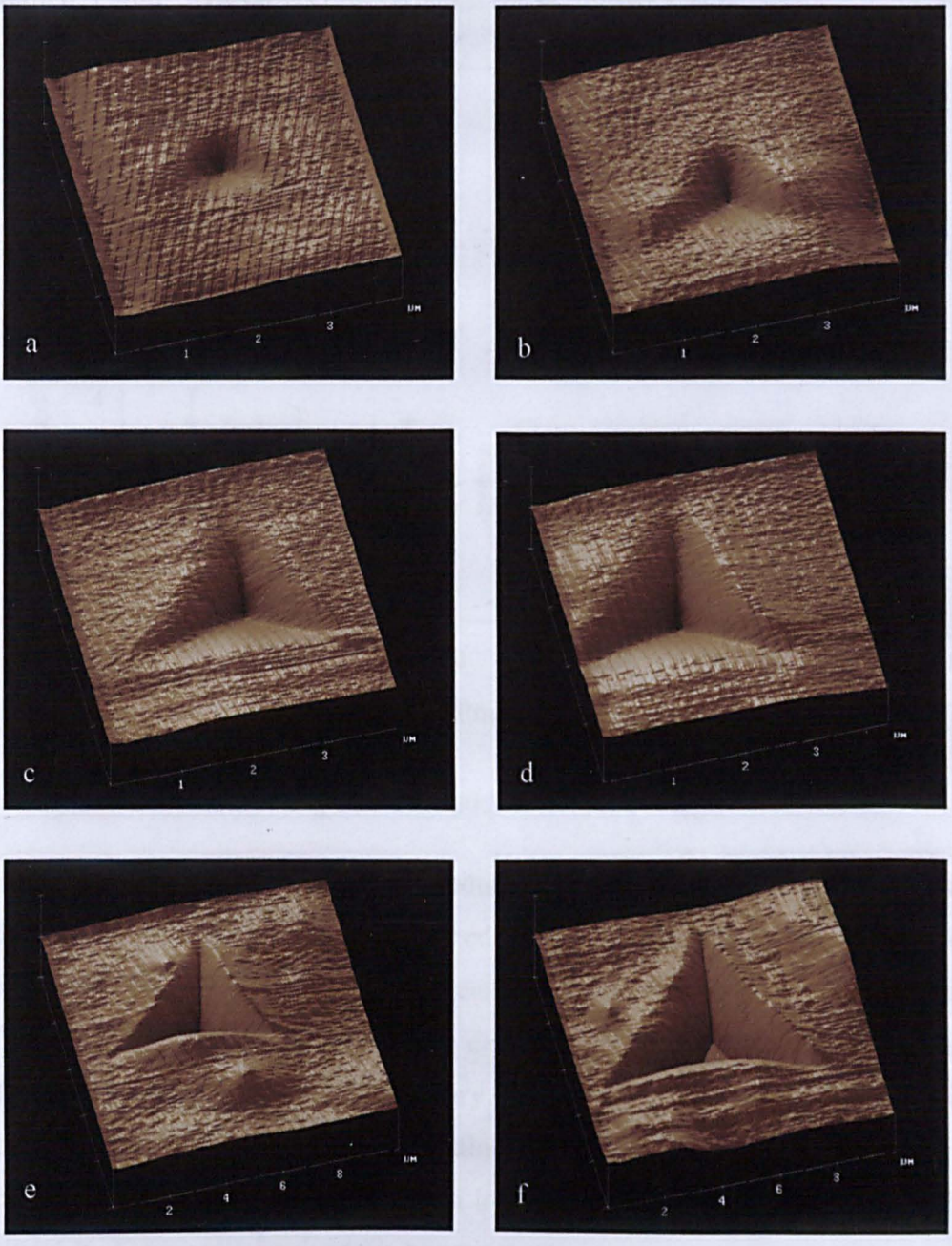

Fig. 5.14 *Images obtained via scanning mode after indentation of a)50μN, b)100μN, c)150μN, d)200μN, e)500μN and f)1000μN.*

Each of the unloading curves is fitted according to the analysis described in section 5.4. The variation in reduced modulus with load force can then be studied. Figure 5.15 shows this variation for sample 425 54%.

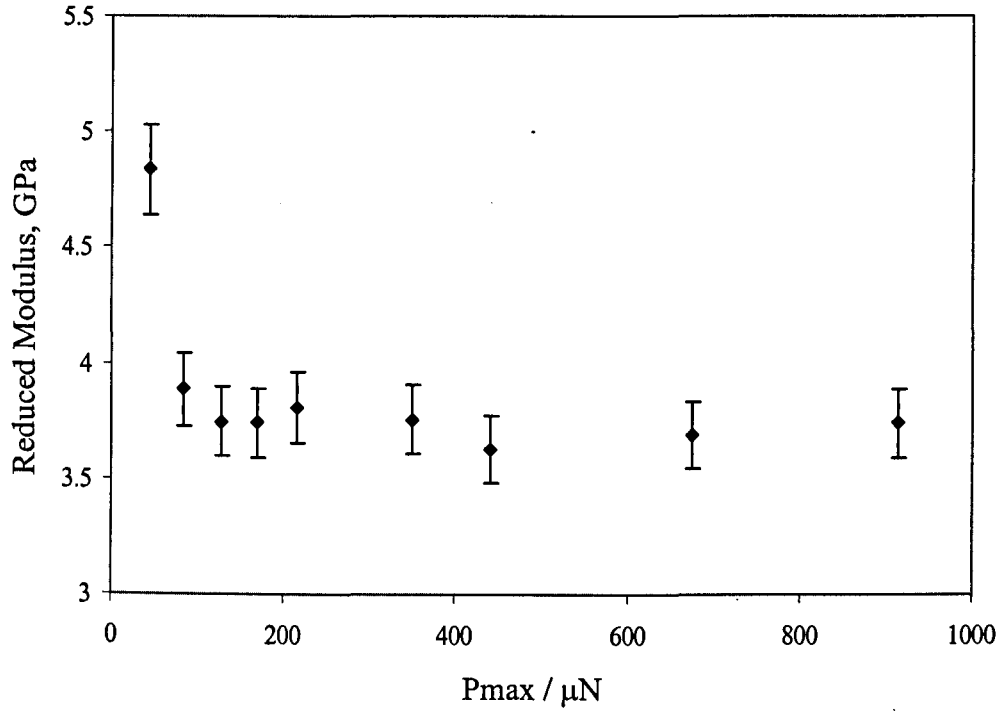

Fig 5.15 Load profile for 425 54%

Figure 5.15 shows a typical trend in reduced modulus obtained when varying the load force. The large value of reduced modulus obtained at the start of the experiment may be due to surface effects or to inaccurate measurement of the tip contact area. Currently there is some debate as to the true reasons behind the effects at low load forces (see summary in this chapter). Once this initial effect has been overcome, however, the values of reduced modulus become more constant. For each sample this "critical load" was noted and a value of twice the critical load was used for dynamic experiments.

Tables 5.1 and 5.2 show moduli obtained for all samples measured.

Table 5.1: Reduced moduli obtained for all poly(ether-isocyanurates), at 25 °C.

Polyether M_w	% Hard segment	Catalyst system	Reduced Modulus (GPa)
425	54	1	3.7
425	54	2	1.0
725	62	1	2.3
725	69	1	2.7
725	76	1	2.9
725	40	2	0.1
2200	40	1	0.1
2200	50	1	0.2
2200	53	1	0.5
2200	57	1	1.0
2200	60	1	1.2
2200	70	1	1.6
2200	73	1	1.9
4200	30	1	0.03
4200	37	1	0.05
4200	50	1	0.1
4200	54	1	0.15
8200	40	1	0.005

Table 5.2: Moduli obtained for PS-PI-PS / PS system

Weight % Triblock	Weight % Homopolymer	Total Volume fraction of polystyrene	Reduced Modulus (GPa)
0	100	1	4.4
50	50	0.496	0.2
80	20	0.255	0.03
90	10	0.183	0.003
100	0	0.114	0.001

5.5.1.2 Variable Loading Rates and Holding Times

For two test samples loading and holding times were varied.

Figure 5.16 shows the reduced modulus results obtained with sample 725 76% when subjected to different loading rates.

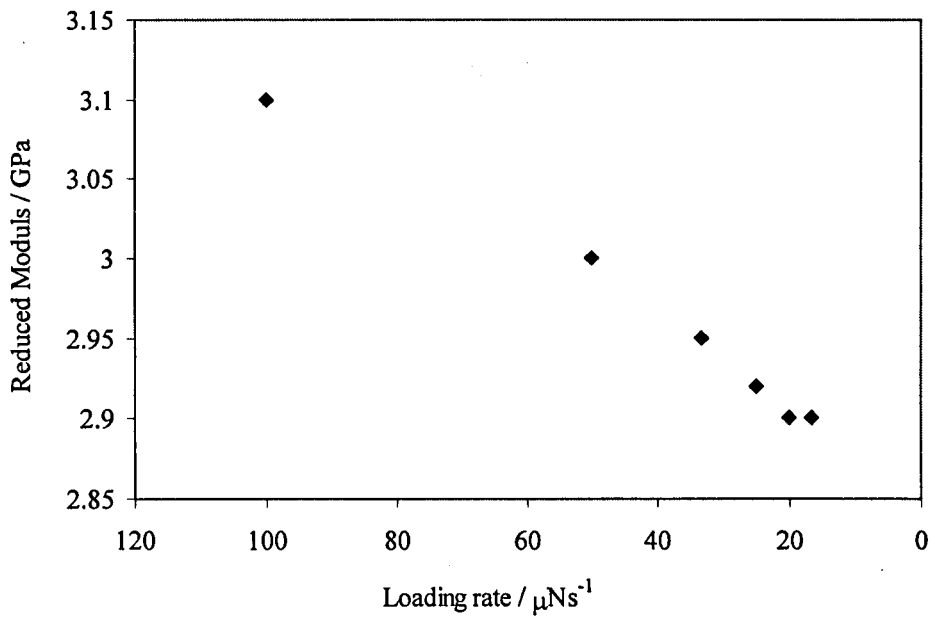

Fig. 5.16 Reduced modulus obtained with variable load rate using 500 μN load on sample 725 76%

The constant modulus reached at faster loading rates is similar to that attained with higher loads.

Slow loading rates and long holding times were avoided to reduce inaccuracy of the measured area due to creep / elastic recovery.

5.5.1.3 Graded Samples

Figure 5.17 shows the results of static indentations performed every 50 – 100 μm along a microtomed cross section of a graded sample. A steady value of 3.5 GPa was achieved for 700 μm before the results were plotted.

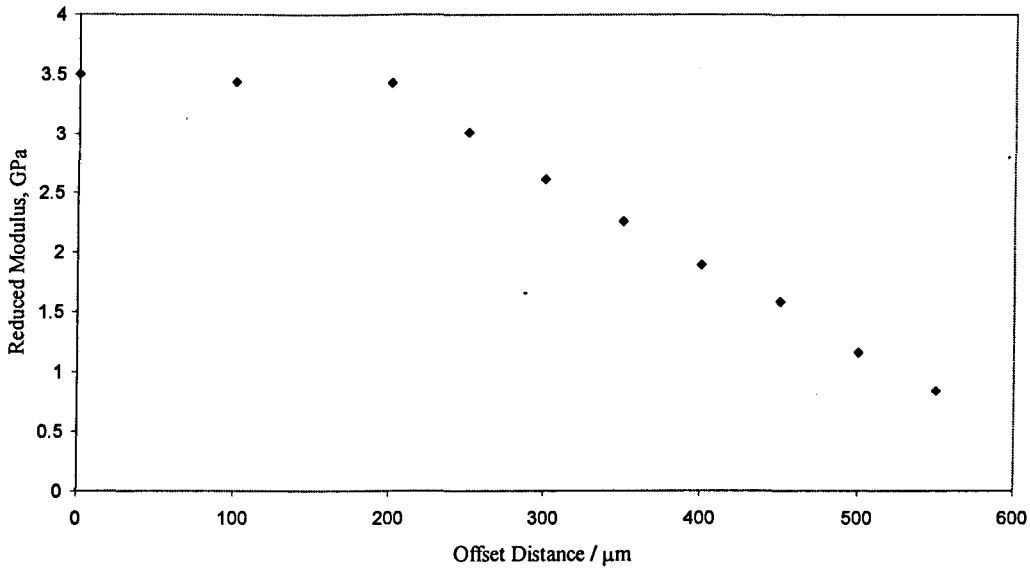

Fig. 5.17 The variation in reduced modulus with distance through cross section of graded sample G192-2200.

The obvious change in the value for reduced modulus occurs at a distance of 900μm, after which there is a steady decrease in the value of the reduced modulus. The gradient of the reduction in modulus is the same as the gradient obtained from the LAMS experiment – figure 3.6 in chapter 3. Further measurements could not be taken due to the roughness of the sample surface.

5.5.2 Dynamic Measurements

For samples measured in dynamic mode, a frequency sweep was performed at range of temperatures from -10 to 70 °C.

Samples with T_g's within this range were especially studied to investigate the measurements made by the nanoindentor and compare these with these obtained by other methods. Measurements of amplitude and phase gave tan δ, storage and loss modulus, stiffness and damping. Any values obtained at 50 Hz were removed.

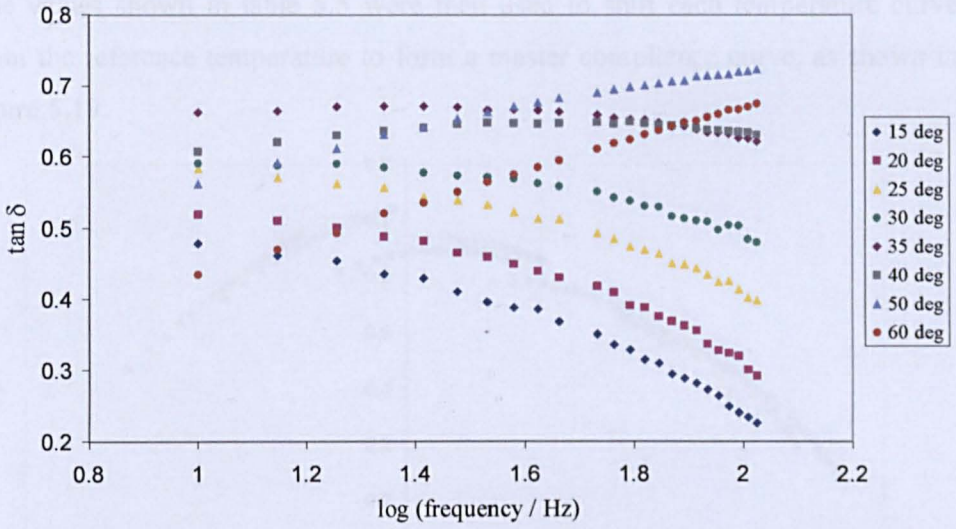

Fig. 5.18 *Variation of tan δ with log frequency at different temperatures for sample 725 40%*

The frequency dependence that would have been obtained over a much wider range of frequencies at a single temperature can be obtained by using the WLF equation to perform time – temperature – superposition. The reference temperature, T_0 used was 20 °C.

$$\log a_T \quad C_1^0(T \quad T_0)/C_2^0 \quad (T \quad T_0) \qquad 5.8$$

Values of C_1 and C_2 for WLF equation taken from polybutadiene.[8]

Table 5.3*: WLF parameters for sample 725 40%*

Temperature / °C	T-T_0	Shift factor a_T
15	-5	0.25
20	0	0
25	5	-0.35
30	10	-0.7
35	15	-1.3
40	20	-1.5
50	30	-2.1
60	40	-2.6

The values shown in table 5.5 were then used to shift each temperature curve from the reference temperature to form a master compliance curve, as shown in figure 5.19.

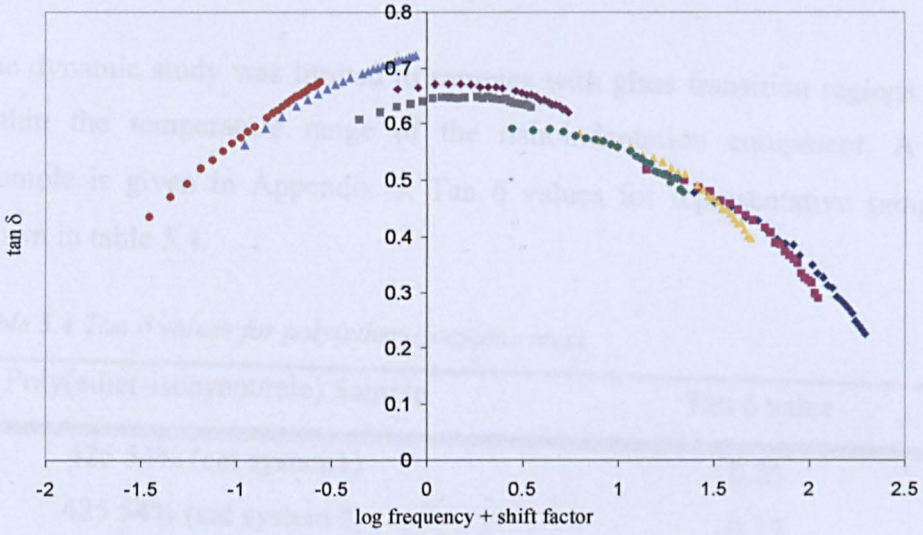

Fig. 5.19 *Use of the WLF equation to perform Time-Temperature-Superposition with data obtained for sample 725 40%.*

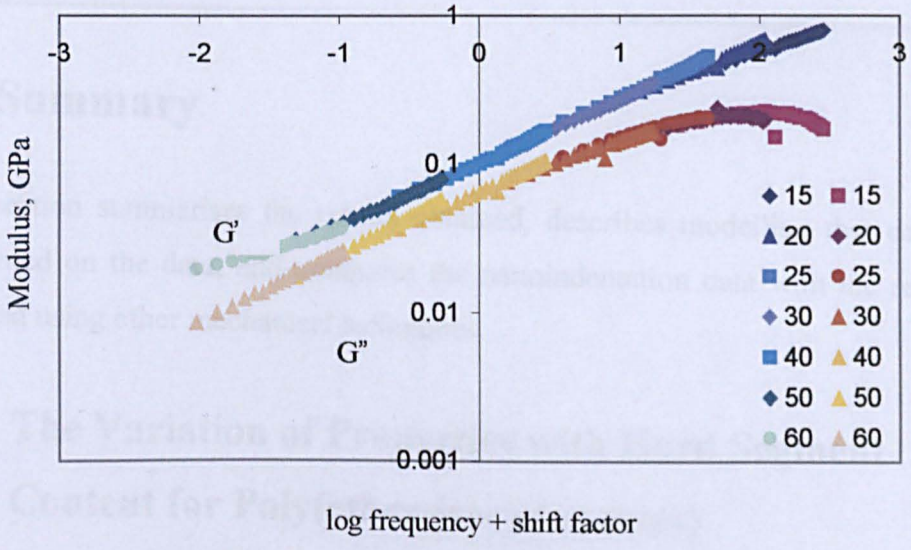

Fig. 5.20 *Time – Temperature – Superposition of storage (green / blue) and loss (red / yellow) moduli for 725 40%*

The time-temperature-superposition plots of the modulus, shown in figure 5.20 give a slope of the storage modulus to be a half, indicative of cross linked network [9].

The dynamic study was limited to samples with glass transition regions that lay within the temperature range of the nanoindentation equipment. A further example is given in Appendix 5. Tan δ values for representative samples are shown in table 5.4.

***Table 5.4** Tan δ values for poly(ether-isocyanurates)*

Poly(ether-isocyanurate) Sample	Tan δ value
425 54% (cat system1)	0.25
425 54% (cat system 2)	0.37
725 40%	0.72
4200 30%	0.9
4200 37%	1.3
4200 54%	0.5

5.6 Summary

This section summarises the results obtained, describes modelling that can be performed on the data, and compares the nanoindentation data with the results obtained using other mechanical techniques.

5.6.1 The Variation of Properties with Hard Segment Content for Poly(ether-isocyanurates)

For poly(ether-isocyanurates), as the hard segment content increases the (reduced) modulus increases. As the polyether length increases the (reduced) modulus decreases, shown in figure 5.21. This can be seen more clearly when the log of the modulus is plotted – figure 5.22.

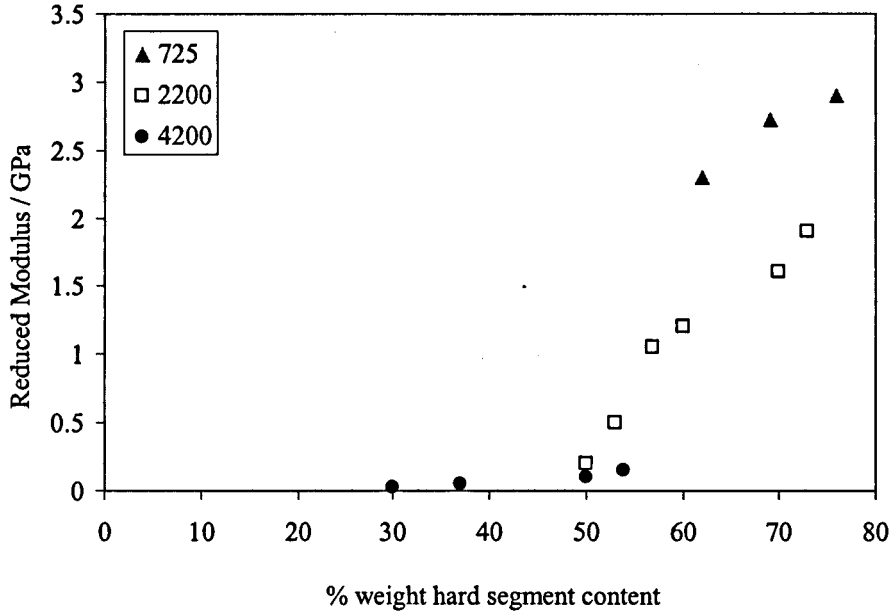

Fig. 5.21 The variation in reduced modulus with hard segment content and polyether length in poly(ether-isocyanurates).

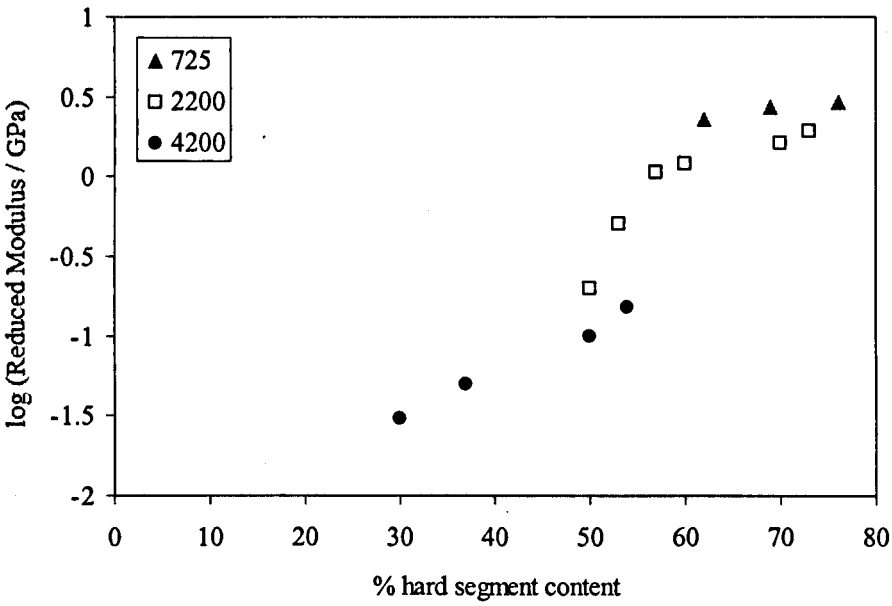

Fig. 5.22 The variation in the log of reduced modulus (GPa) with hard segment content and polyether length in polyisocyanurates.

Models for the structure may be used to predict the modulus of the material. Models used consider the material to be a polymer-polymer composite; a

multiphase material consisting of polymer matrix and polymer filler. The modelling of these composites has been reviewed by Nielsen [10].

The modified Kerner equation,[11] equation 5.9, gives the upper and lower bounds of a polymer material with two phases.

$$G = G_1 \left(\frac{\frac{\phi_1}{15(1-\upsilon_1)} + \frac{\phi_2 G_2}{(7-5\upsilon_1)G_1 + (8-10\upsilon_1)G_2}}{\frac{\phi_1}{15(1-\upsilon_1)} + \frac{\phi_2 G_1}{(7-5\upsilon_1)G_1 + (8-10\upsilon_1)G_2}} \right) \qquad 5.9$$

Where G is the composite shear modulus, ϕ is the volume fraction (where $\phi 1 + \phi 2 = 1$), υ is the Poisson's ratio, and the subscripts 1 and 2 refer to the matrix and filler components respectively. A requirement of Kerner's theory is that the particles are spherical in the mean.

Davies'[12] expansion of the theoretical treatment of the dielectric constant of two phase materials predicts the shear modulus of materials with two interpenetrating continuous phases in the expression:

$$G^{1/5} = \phi_1 G_1^{1/5} + (1-\phi_1) G_2^{1/5} \qquad 5.10$$

This method has previously been used for poly(urethane-ureas) formed by RIM by Ryan *et al.*[13]

Figure 5.23 shows the volume fraction of hard segment versus Young's modulus for various samples. The upper and lower curves are solutions to the Kerner equation (equation 5.9) for soft, rubber spheres in a hard, glassy matrix and glassy spheres in a rubber matrix. The value of Young's modulus used for rubber, E, = 10^6 Pa and Poisson's ratio υ of 0.5, and for glass 10^9 Pa for Young's modulus and 0.35 for Poisson's ratio. The central curve is the solution to the Davies equation (equation 5.10).

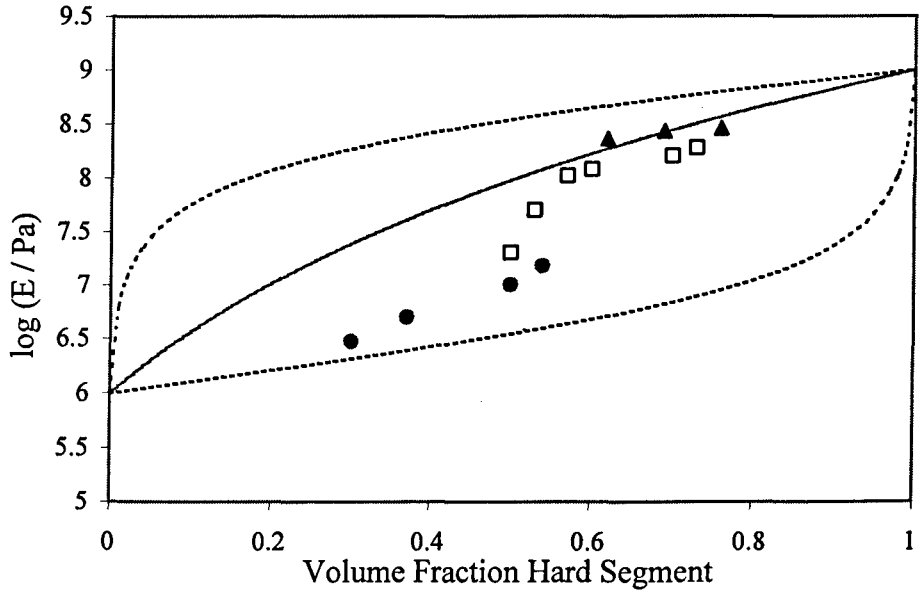

***Fig. 5.23** Upper and lower bounds of the Kerner equation (dashed lines), and the Davies equation (solid line) with the measured indentation moduli (solid points) for 725 (▲), 2200, (□) and 4200,(•) poly(ether-isocyanurate) elastomers*

The data points all lie within the boundaries predicted by the Kerner equation. The fact that they do not reach the upper and lower limits of modulus for the determined hard segment fractions may be due to a number of reasons. Firstly, the data collected is indentation modulus, rather than Young's modulus. Secondly, there may be some degree of phase mixing within the sample.

The Davies equation is not a good fit to the data collected for polyisocyanurates with higher molecular weight polyether segments. It makes no adjustment for the size of the phases or the interfacial area, which does change with hard segment content (as shown in Chapter 4) The higher the hard segment content the more likelihood of premature phase separation and thus a coarser hard segment phase.

The data points for 2200 polyether segment suggest that phase inversion occurs at around 55% hard segment content. This has previously been observed in Poly(urethane-urea) with 3,5-diethyltoluene diamine chain extender systems by Ryan *et al.* [14]

For each sample series the highest tan δ values were obtained for elastomers with ~40% hard segment content. The highest tan δ values were seen in the 4200 ether segment poly(ether-isocyanurates). A high tan δ value was also measured for sample 725 40% – a non - phase separated sample, with a single phase T_g.

5.6.2 Modulus variation for Triblock / Homopolymer Blends

As the polystyrene homopolymer content increases in the polystyrene - polyisoprene - polystyrene / polystyrene blend the (reduced) modulus increases, shown in figure 5.24. The morphology of the system changes from spheres of polystyrene in a polyisoprene matrix at low hard segment fractions, and the modulus increases as these spheres become rods with higher hard segment fractions. Eventually rubber polyisoprene spheres would form but the system macrophase separates before this happens.

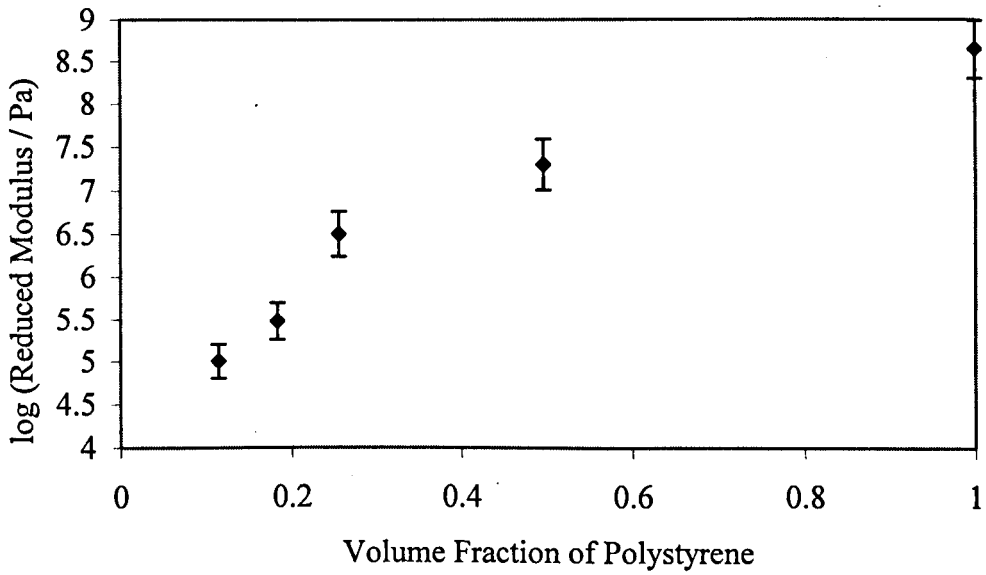

Fig. 5.24 The variation in (reduced) modulus (GPa) with added homopolystyrene content in PS-PI-PS / PS blends

5.6.3 The Nanoindentation Technique

In order to verify results obtained from the nanoindentor it was necessary to compare them with measurements made using alternative, standard equipment. Sample 4200 37% was subjected to Dynamic Mechanical Thermal Analysis and Differential Scanning Calorimetry and the results compared to those obtained from the nanoindentor in Dynamic Scanning Mode (DSM). This is shown in figure 5.25.

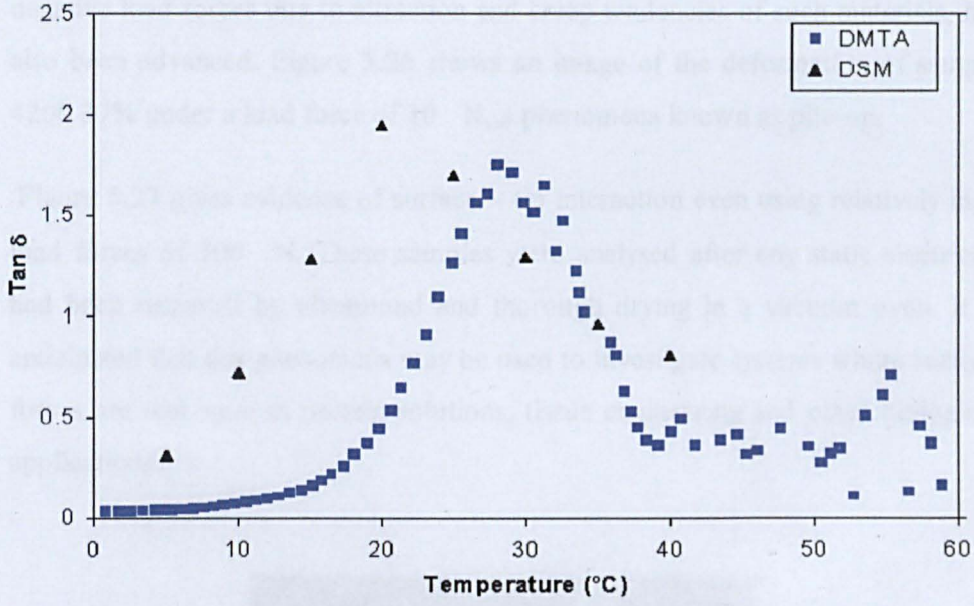

Fig 5.25 *Comparison of results obtained from DMTA and DSM for sample 4200 37%*

The T_g for sample 4200 37% obtained from DSC was 18 °C, from DMTA it was 27 °C and from DSM it was 21 °C. So the T_g obtained from the nanoindentation technique is in between the two other standard techniques.

The use of the nanoindentation technique to study properties of polymers is not well established.[5] Recent work has concentrated on PTFE [15] and benzocyclobutane.[16] The DSM technique with environmental sample control is unique and these results are included in a paper being published [S.Hayes, A-L Abbott, paper submitted].

The mechanical properties of samples with a known microstructure, by use of the same sample as SAXS experiments has been established and will be discussed in chapter 6. Progress in the understanding of the nanoindentation technique, particularly the dynamic testing procedure has been made, and it has been shown that the results are comparable to other techniques (DMTA). The very high moduli observed with small forces for some materials has been attributed to inaccuracies in the tip contact area not accounted for by calibration with quartz. The understanding of tip – sample interactions for viscoelastic materials, giving negative load forces due to attraction and creep tendencies of such materials, has also been advanced. Figure 5.26 shows an image of the deformation of sample 4200 37% under a load force of 10 N, a phenomena known as pile-up.

Figure 5.27 gives evidence of surface – tip interaction even using relatively high load forces of 300 N. These samples were analysed after any static electricity had been removed by ultrasound and thorough drying in a vacuum oven. It is anticipated that this phenomena may be used to investigate systems where surface forces are real such as protein solutions, tissue engineering and other biological applications.

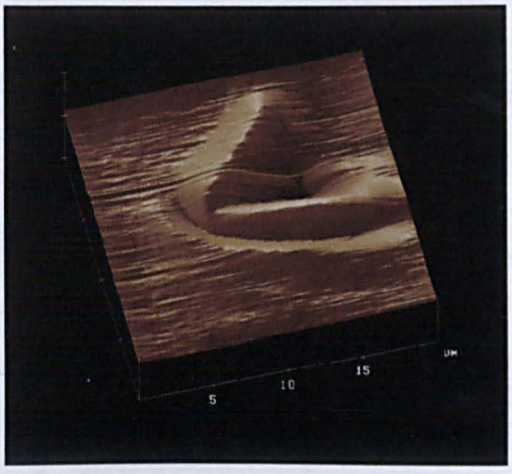

***Fig. 5.26** Example of "pile – up"*

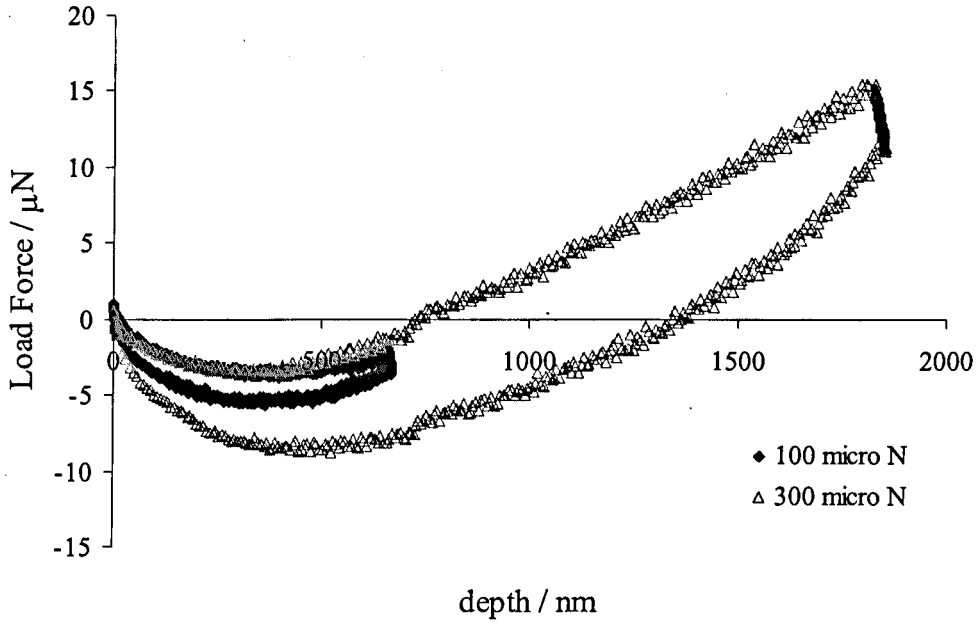

Fig. 5.27 Example of negative load forces obtained for sample 8200 40%

5.7 References

[1] G. Binnig, H. Rohrer, *Scanning Electron Microscopy* **1983**, 1079.

[2] G. Binnig, C. F. Quate, C. Gerber, *Physical Review Letters* **1986**, *56*, 930.

[3] H. Hertz, *Hertz's Miscellaneneous Papers Vol. Ch 5 and 6*, McMillan, London, **1896**.

[4] W. C. Oliver, G. M. Pharr, *Journal of Materials Research* **1992**, *7*, 1564.

[5] M. R. VanLandingham, J. S. Villarrubia, W. F. Guthrie, G. F. Meyers, *Macromolecular Symposia* **2001**, *167*, 15.

[6] X. W. Fan, M. K. Park, C. J. Xia, R. Advincula, *Journal of Materials Research* **2002**, *17*, 1622.

[7] J. L. Cuy, A. B. Mann, K. J. Livi, M. F. Teaford, T. P. Weihs, *Archives of Oral Biology* **2002**, *47*, 281.

[8] R. H. Colby, Fetters, L.J., Graessley, W.W., *Macromolecules* **1987**, *20*, 2226.

[9] M. Ilavsky, in *Polymer Networks Principles of their Formation, Structure and Properties*, 1st ed. (Ed.: R. F. T. Stepto), Blackie Academic and Professional, London, **1998**.

[10] L. E. Nielsen, *Predicting the properties of mixtures*, Dekker, New York, **1978**.

[11] E. H. Kerner, in *Proc. Phys. Soc. (London), Vol. 69B*, **1956**, pp. 808.

[12] W. E. A. Davies, in *Journal of Physics D: Applied Physics, Vol. 4*, **1971**, pp. 318.

[13] A. J. Ryan, J. L. Stanford, R. H. Still, *Plastics and Rubber Processing and Applications* **1990**, *13*, 99.

[14] A. J. Ryan, J. L. Stanford, R. H. Still, *British Polymer Journal* **1988**, *20*, 77.

[15] B. N. Lucas, *Materials Research Society* **1998**, *505*, 7.

[16] M. R. VanLandingham, Villarubia, J.S., Meyers, G.F., Society of Engineering Mechanics, Bethel, CT., **2000**, p. 912.

CHAPTER 6

STRUCTURE - PROPERTY RELATIONSHIPS

6.1 Introduction

The work described in the previous chapters details the preparation, investigates the mechanical properties and probes the structure of a series of polyisocyanurate elastomers with varying polyether soft - segment length and hard - segment content. It is now possible, therefore, to relate the mechanical properties of the elastomers to their microstructures, and to compare the findings with those obtained from the smaller series of PS-PI-PS / PS blends. This was the subject of a recent article by the author.[1]

6.2 How Mechanical Properties Change with Structure.

6.2.1 Glass Transition

The absence of any scattering intensity in the patterns obtained from samples with only one T_g indicates that microphase separation into hard and soft domains had not occurred. Samples formulated from POP 725 and below were single phase materials. All samples formulated from POP 2200 and longer were two phase systems, regardless of hard segment content.

An estimate of the Flory-Huggins interaction parameter, χ was calculated using 2200 50% - the first polyether soft segment poly(ether-isocyanurate) to phase separate at 50%. Here $\chi N = 10.5$, so if $N = 3300$, χ is 0.003. This is a very rough estimate as no polyether soft segments with M_n between 725 and 2200 were investigated. The phase diagram of χN against composition, ϕ is plotted in figure 6.1.

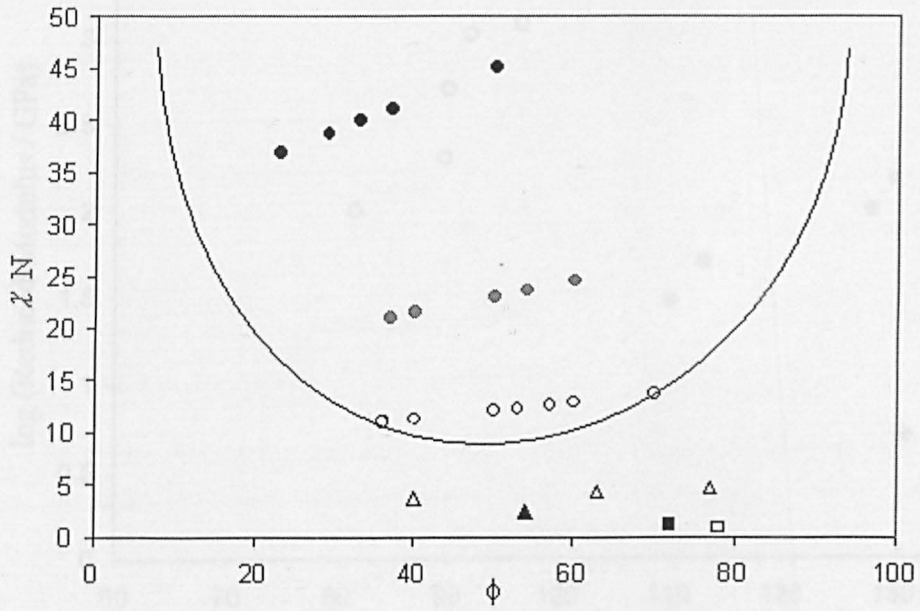

Fig. 6.1 *Phase diagram for poly(ether-isocyanurate) elastomers □ 134, ■192, ▲ 425, Δ 725, ○ 2200, • 4200, ● 8200 Mw polyether soft segment.*

The d-spacing in the triblock copolymer blends investigated was swollen with addition of homopolystyrene, which is similar to the addition of hard segment in the poly(ether-isocyanurate) elastomers.

6.2.2 Nanoindentation Modulus

The change in modulus with d-spacing for poly(ether-isocyanurate) elastomer is shown in figure 6.2. The d-spacing increases with hard segment content and polyether length, but the modulus only increases with hard segment content – it decreases with polyether length. It is apparent that there is a significant degree of overlap with the samples prepared- i.e. two samples with approximately the same d-spacing can have entirely different moduli, and samples with the same moduli may have different d-spacing. However, this only occurs between samples with different polyether soft segments. d-spacings from the series of samples made from the same polyether soft segment increase with hard segment content.

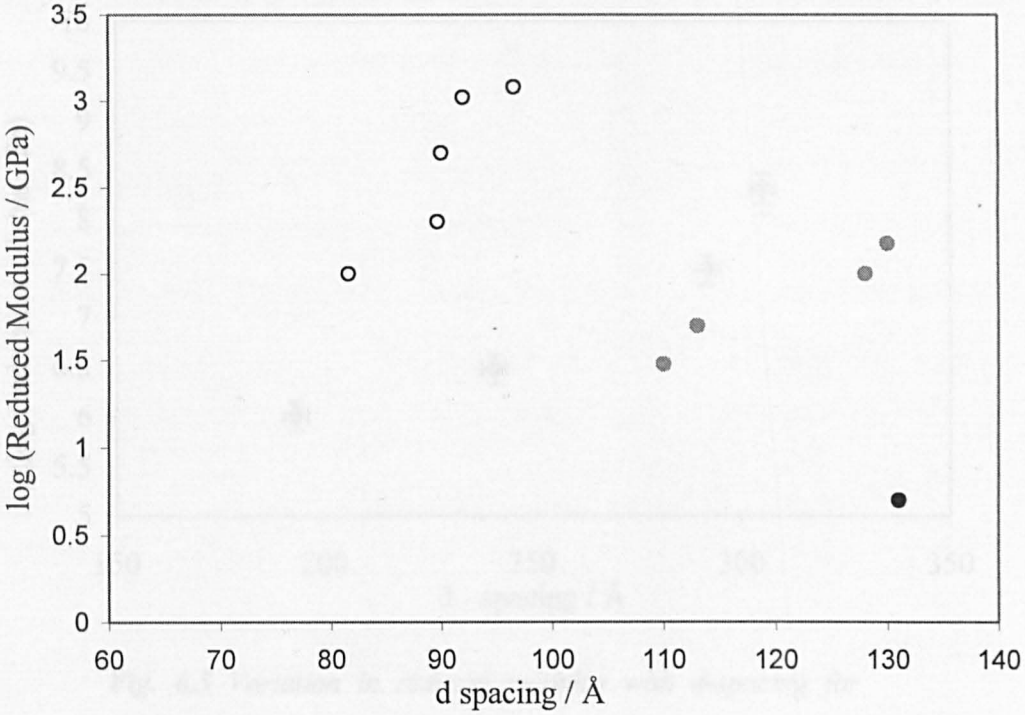

***Fig. 6.2** The increase in modulus with d-spacing for ○ 2200, ● 4200 and ● 8200 polyether soft segments.*

The change in modulus with hard segment was studied in chapter 5 by using the Kerner equation. It was seen that phase separated samples fell within the limits of the model, but that the Davies equation was not a good fit for higher molecular weight polyether soft segment samples. As shown in figures 6.1 and 4.6 the domain spacing varies quite considerably with additional hard segment content. The higher the hard segment content the more likely that premature phase separation will occur, resulting in a coarser hard segment phase. This is seen in the data presented in chapter 4, where phase separation does happen earlier for higher hard segment content samples. Structures at lower q are formed before the mechanism of spinodal decomposition takes over and phase separation forms in the same way as for lower hard segment content samples.

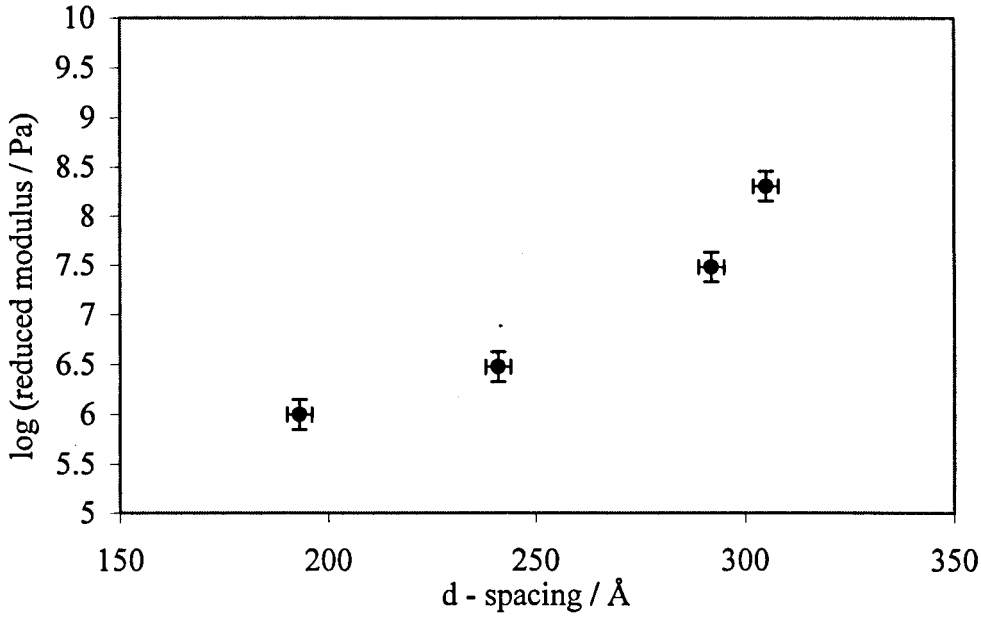

Fig. 6.3 Variation in reduced modulus with d-spacing for triblock copolymer blends.

Figure 6.3 shows the variation in modulus with d-spacing for the triblock copolymer blends. Although the spacing is much larger for this system a similar trend in results to the poly(ether-isocyanurate) system is observed.

6.3 Damping capability

tan δ values were obtained from dynamic nanoindentation. High damping capability was observed from samples that had moduli of approximately 50-200 MPa but had large d-spacings, greater than 100 Å. Samples that were not phase separated, e.g. 725, 40% were also good dampers, having a broad Tg in the temperature range under investigation.

The development of phase separation was fitted using the Teubner – Strey microemulsion structure factor in chapter 4. No shift to low q was seen, indicating that a bicontinuous microemulsion was preserved by vitrification of the hard segment phase. This bicontinuity may contribute to the high tan δ values

seen in the samples investigated, as this structure would allow the stress and strain components of the vibration to be well distributed throughout the material.

6.4 Reference

[1] Abbott, A-L, Turner, M.L., Ryan, A.J. *Fibre Diffraction Review* **2003**, 113.

CHAPTER 7

CONCLUSIONS AND FUTURE WORK

7.1 Conclusions

The work performed for this thesis concentrates on a poly(ether-isocyanurate) system with comparisons to a blend of polystyrene-polyisoprene-polystyrene triblock co-polymer with polystyrene homopolymer. The preparation of isocyanate end - capped polyether prepolymers enabled the isocyanate content to be measured during sample preparation by titration.

Bulk, layered and graded samples were all prepared. The catalyst and curing temperatures were optimised to give reproducible samples suitable for various types of testing.

Differential Scanning Calorimetry was employed to measure the thermal transitions – especially the glass transition in the prepared samples. The appearance of two Tg's in samples prepared from 2200 molecular weight polyether soft segment indicated that these samples were phase separated. A lower T_g of about -60°C was observed for those with a polyether - rich phase.

Techniques were developed for the chemical analysis of the layered and graded samples. Laser Ablation mass spectroscopy analysed the relative nitrogen content across a cross section of the samples, and the FT-IR microscope was used to investigate how the various carbonyl, ether and C-H bands changed in position and intensity along microtomed sections of the materials. Good correlation was seen between the two techniques. The formation of graded samples was attributed to a separation due to gravity.

The bulk samples prepared were analysed more thoroughly using scattering and nanoindentation experiments. This enabled the relationships between the structure and the properties to be established.

Structure was evaluated from small - angle X-ray scattering performed at synchrotron radiation sources. Above polyether Mn 2200, 30% hard segment content two - phase systems were obtained, the d-spacing of which increased as

the hard segment content increased and as the polyether length increased. The addition of homopolymer to triblock copolymer resulted in swelling of d-spacing, and changes in structure from glassy spheres in rubbery matrix to rubbery spheres in glassy matrix were observed. More than 50% added homopolymer (53% total polystyrene) resulted in macrophase separation.

The kinetics of phase separation for poly(ether-isocyanurates) were investigated by performing time - resolved measurements as the samples were heated to activate the catalyst in the X-ray beam. The system was found to phase separate by means of spinodal decomposition, forming a microemulsion which was modelled using the Teubner-Strey microemulsion analysis.

The technique of nanoindentation was employed to study the mechanical properties of the materials. Nanoindentation on 'soft' polymers (rather than 'hard' metals and ceramics) is not well documented, and no other research on phase - separated polymer systems has been published to date. The indentation modulus for all samples was obtained, and was found to increase with hard segment content and decrease with increasing polyether length.

Modulus results obtained ranged from 3 GPa to 1MPa and were fitted to the Kerner equation where phase inversion in the 2200 Mn polyether segment was seen. Modulus results for the PS-PI-PS / PS blends ranged from 1 to 200 MPa. These were plotted against total PS content where the different modulus obtained was attributed to the formation of different structures in the material.

The modulus variation with change in depth was measured for the graded samples. The positionability of the nanoindenter tip enabled mapping of the modulus of the cross section. This was compared to results obtained from the IR microscope and laser ablation mass spectroscopy to see the chemical changes in the gradient with the changes in modulus.

A specially constructed environmental stage was constructed to be used in conjunction with the nanoindentor tip. Previous work had been performed using the tip in an oscillatory mode to study the dynamic mechanical properties of

materials but very little research has been done using changes in temperature as another variable. This enabled time-temperature-superposition to be performed on the mechanical data obtained. The results generated from time-temperature-superposition were compared with those acquired from dynamic mechanical thermal analysis and differential scanning calorimetry. T_g's observed were found to lie above the T_g from DSC but below that obtained from DMTA.

Samples that displayed the best damping were those with higher molecular weight polyether soft segment and lower hard segment content, and single phase materials with room temperature T_g's. The single phase materials may have displayed good damping properties in the experimental conditions (10 to 70 degrees), whereas the two - phase systems that displayed good damping properties had a well - defined interlocking phase - separated structure, which was able to dissipate both the stress and strain components of the vibration through the material.

7.2 Suggestions for Future Work

Modulus measurements on materials cured at different temperatures would enable further studies to be performed on how an increase in the degree of phase separation would affect the mechanical properties.

The structure of the triblock copolymer blends could be investigated by AFM. Figure 7.1 shows the phase image obtained from a thin film triblock copolymer spin coated on silicon from a solution in toluene. Figure 7.2 shows the fourier transform for this image which would enable the length scale of the structure to be elucidated.

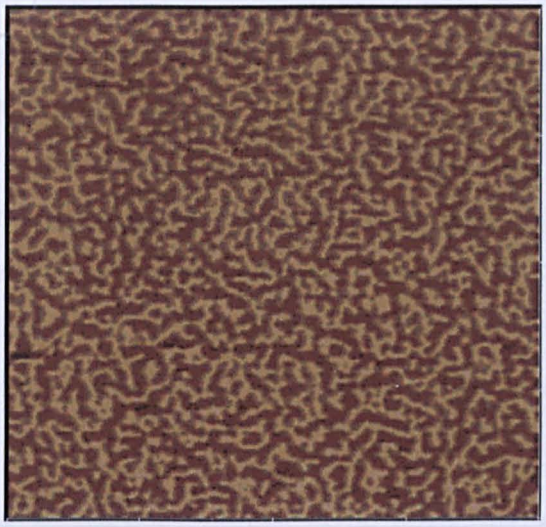

Fig. 7.1 *AFM image of polystyrene-polyisoprene-polystyrene*

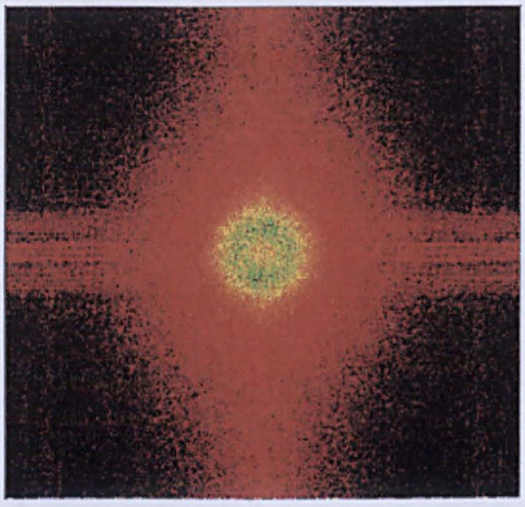

Fig. 7.2 *Fourier transform of the phase image*

These samples were difficult to image because the polyisoprene segment wets the surface and the tip gets stuck, but it would be possible to get a good indication of structure and length scale from the fourier transform. This confirms the presence of different structures in the PS-PI-PS / PS blends. AFM of poly(ether-isocyanurates) has not been attempted due to difficulties in preparing a suitably flat surface.

The formation of a graded poly(ether-isocyanurate) material was attributed to a separation due to gravity. In order to make use of this phenomenon a 'rotational mould' was made to separate end-capped polyethers to by centrifugal force. A schematic of this mould is given in figure 7.3. Preliminary studies show that this method works. However, a different d-spacing of the material with the same formulation was obtained. This could be attributed to different curing times, but further research would enable the full mechanism of the type of separation to be quantified.

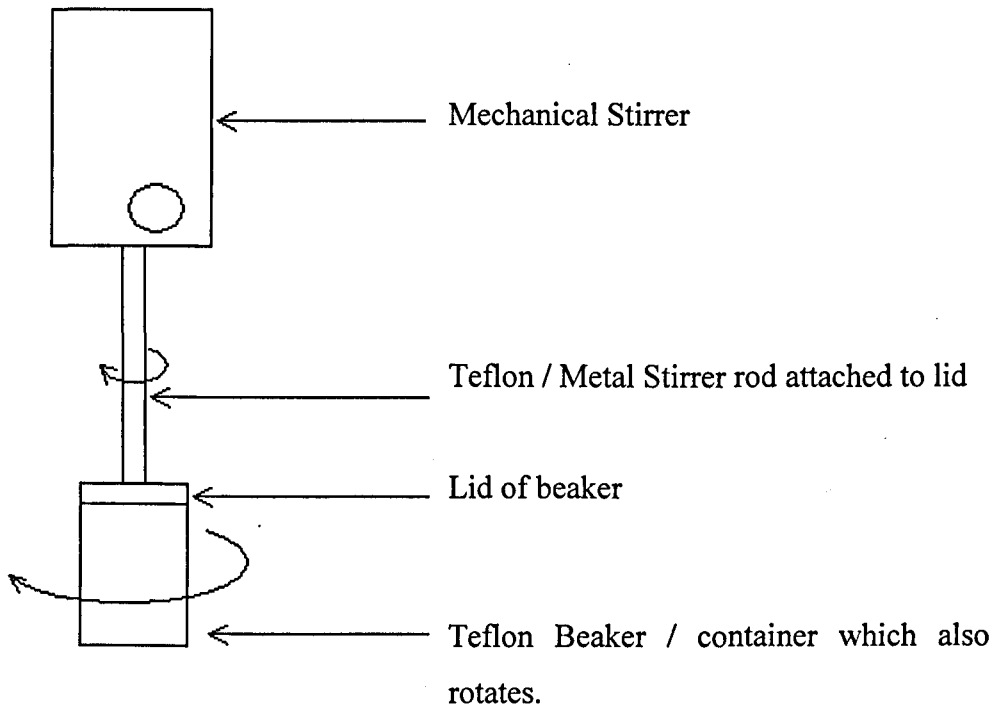

Fig. 7.3 Rotating mould

The use of the rotational mould would mean that this was a very effective way of coating the inside of parts that required vibrational damping. Work is being carried out to compare the damping capability with the gradient direction, as with the current system the prepolymer with shorter polyether segments would coat the substrate, with longer polyether prepolymers layering on top, nearer the centre of rotation

The material could be used to coat metal bars of various thickness. Preliminary studies show that poly(ether-isocyanurates) have good adhesion to most surfaces. DMTA could then be used to investigate the full damping capability.

The material may be suitable for testing using a photothermal FT-IR microscopy technique developed by Pollock *et al.* An AFM - type tip is used to measure the temperature when an IR beam has been deployed. Effectively an inverse spectrum is obtained which very useful as imaging can be performed beyond the limitations of the wavelength of light giving much better resolution than conventional FT-IR microscopy. There is definite scope for imaging over changing concentration gradients and, possibly, for imaging over different phases in phase - separated materials.[1,2]

7.3 References

[1] L. Bozec, A. Hammiche, H. M. Pollock, M. Conroy, J. M. Chalmers, N. J. Everall, L. Turin, *Journal of Applied Physics* **2001**, *90*, 5159.

[2] M. Reading, D. M. Price, D. B. Grandy, R. M. Smith, L. Bozec, M. Conroy, A. Hammiche, H. M. Pollock, *Macromolecular Symposia* **2001**, *167*, 45.

Appendices

1. Teflon Mould specifications
2. IR
3. DSC
4. LAMS
5. Nanoindentation

Appendix 1 TEFLON MOULDS

View from top:

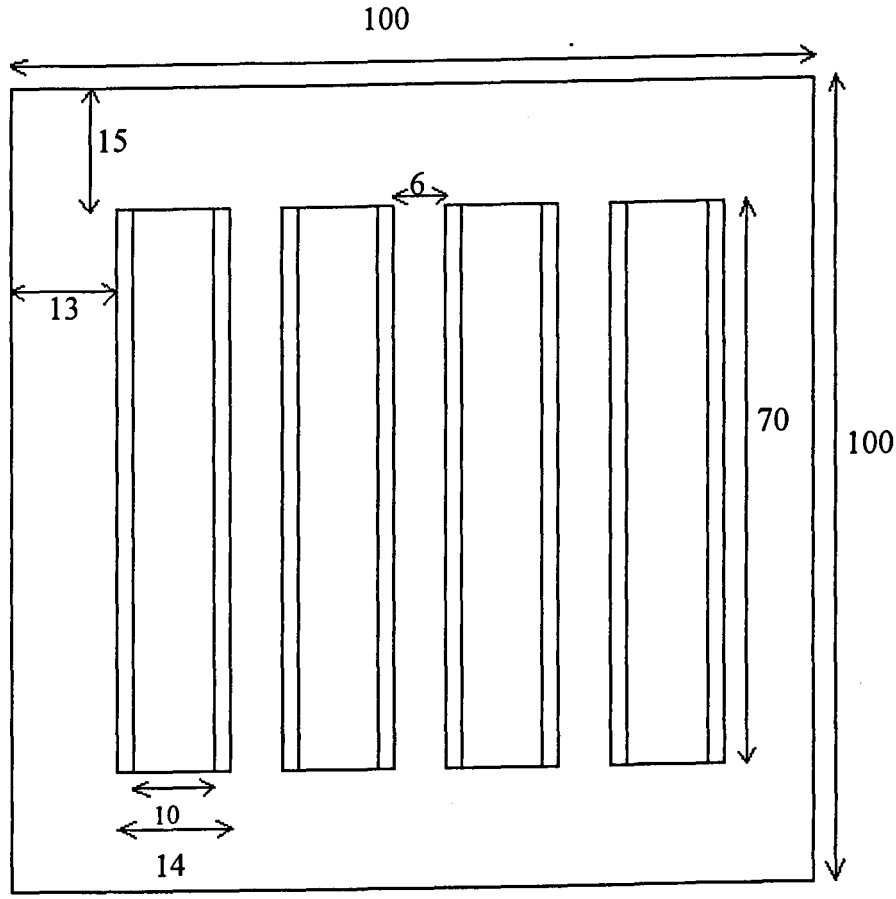

Cross Section:

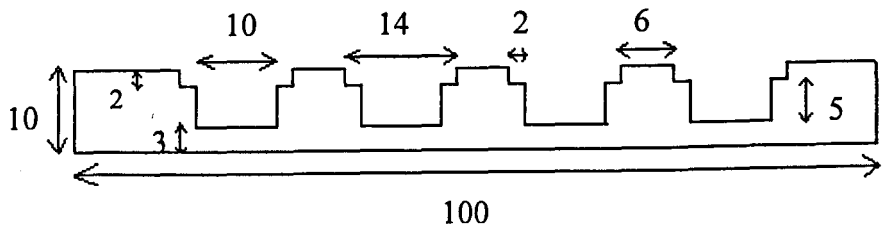

All measurements are in millimetres.

View from top:

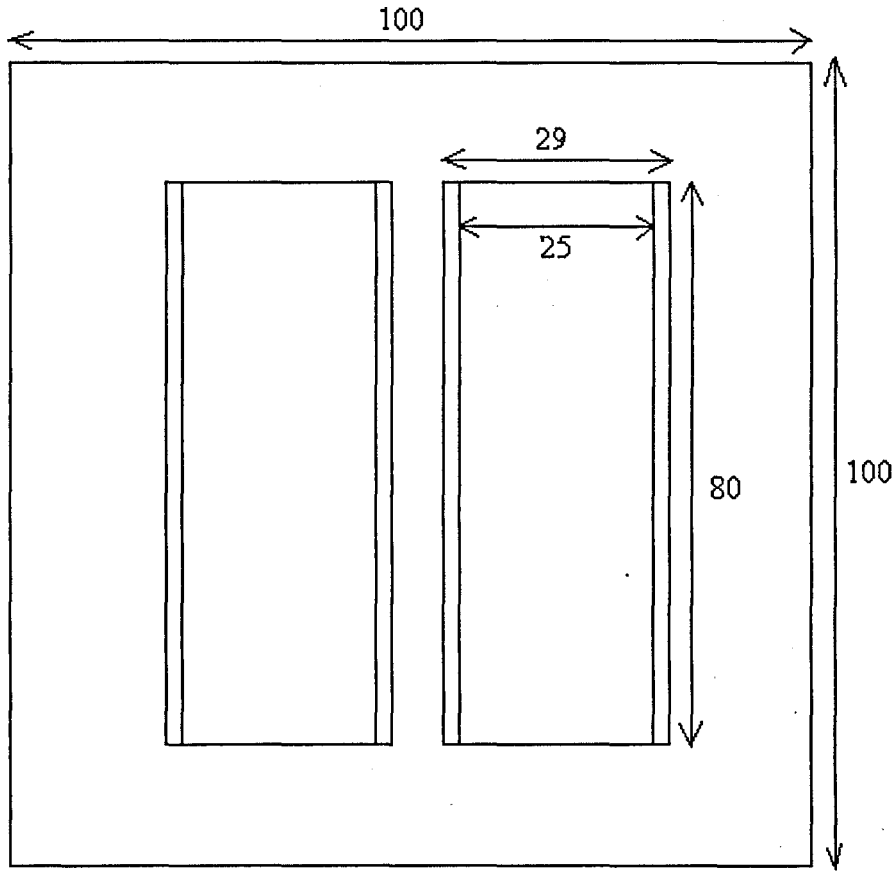

Cross Section:

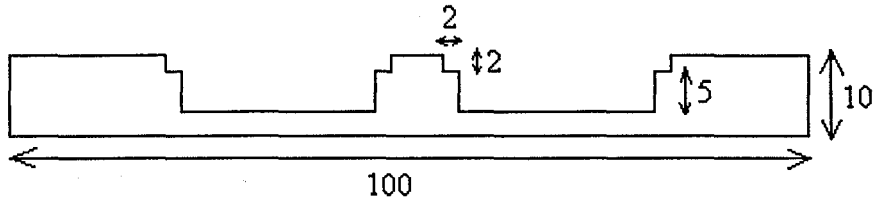

All measurements are in millimetres.

Appendix 2 IR

IR microscopy data

150 μm

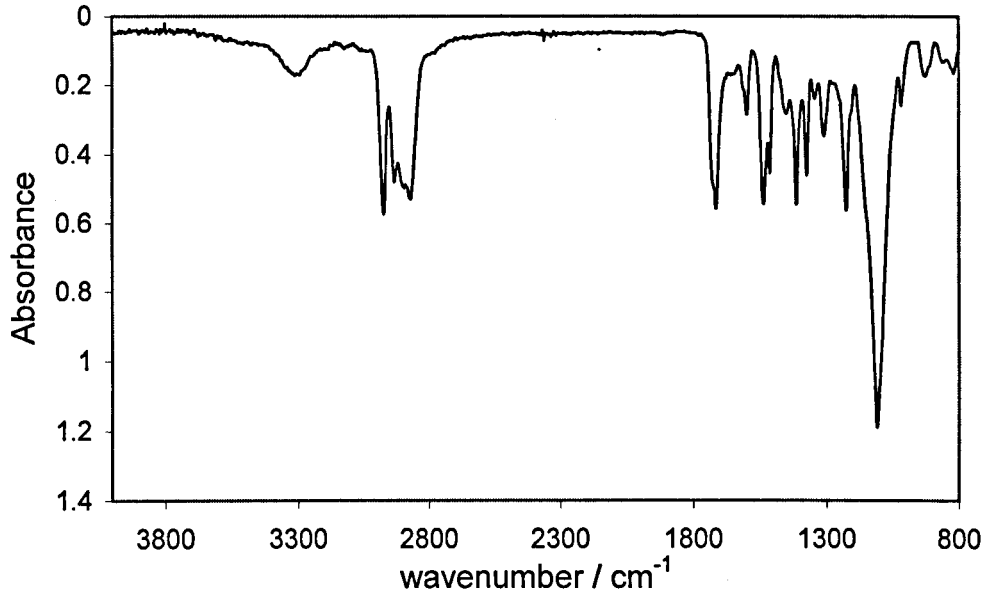

200 μm

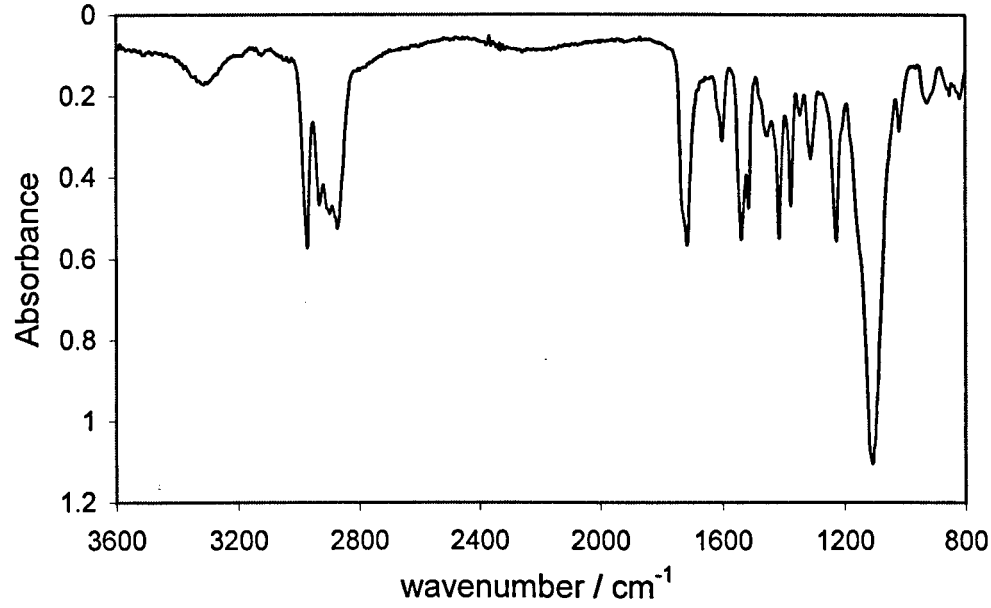

250 μm

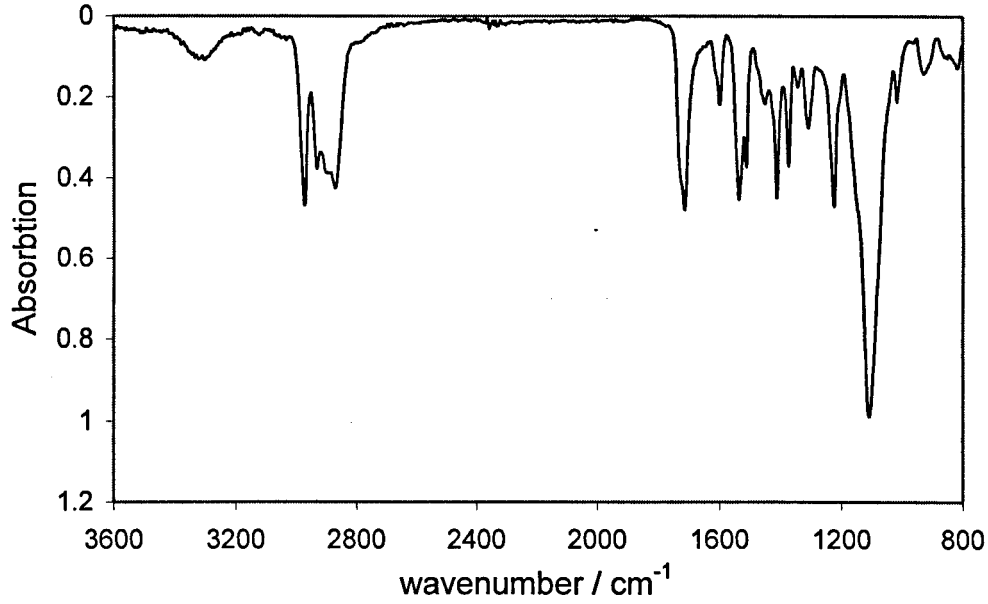
Absorbtion
0
0.2
0.4
0.6
0.8
1
1.2
3600
3200
2800
2400
2000
1600
1200
800
wavenumber / cm-1

300 μm

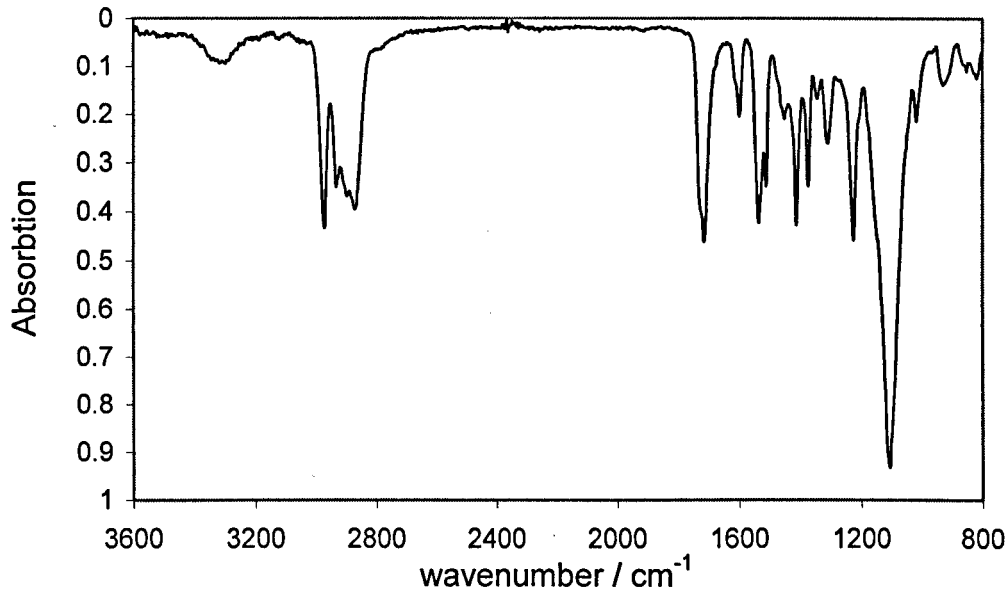
Absorbtion
0
0.1
0.2
0.3
0.4
0.5
0.6
0.7
0.8
0.9
1
3600
3200
2800
2400
2000
1600
1200
800
wavenumber / cm-1

350 μm

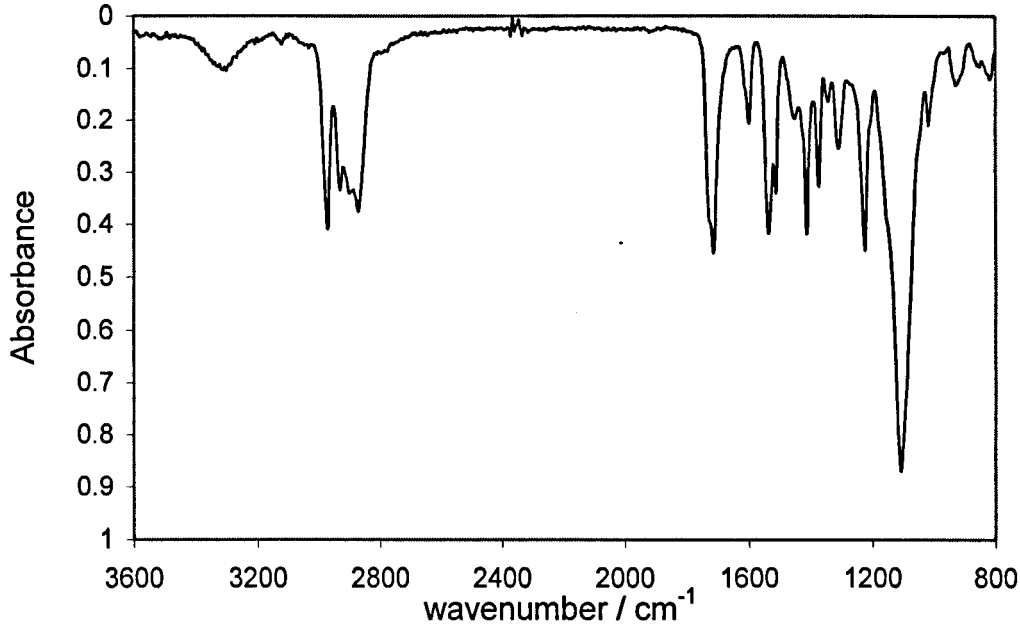
Absorbance
0
0.1
0.2
0.3
0.4
0.5
0.6
0.7
0.8
0.9
1
3600
3200
2800
2400
2000
1600
1200
800
wavenumber / cm-1

400 μm

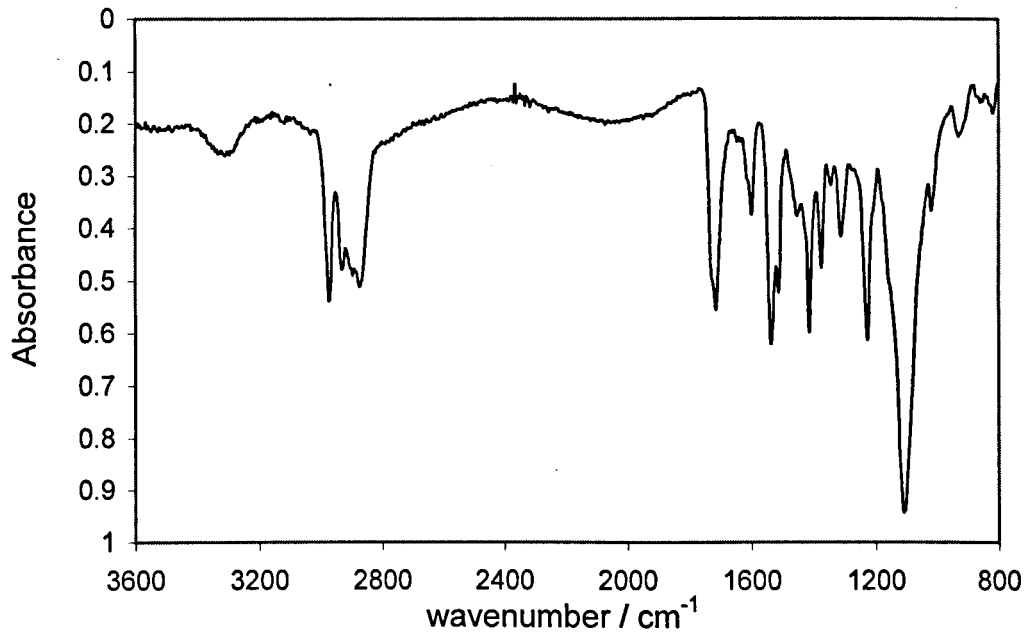
Absorbance
0
0.1
0.2
0.3
0.4
0.5
0.6
0.7
0.8
0.9
1
3600
3200
2800
2400
2000
1600
1200
800
wavenumber / cm-1

450 μm

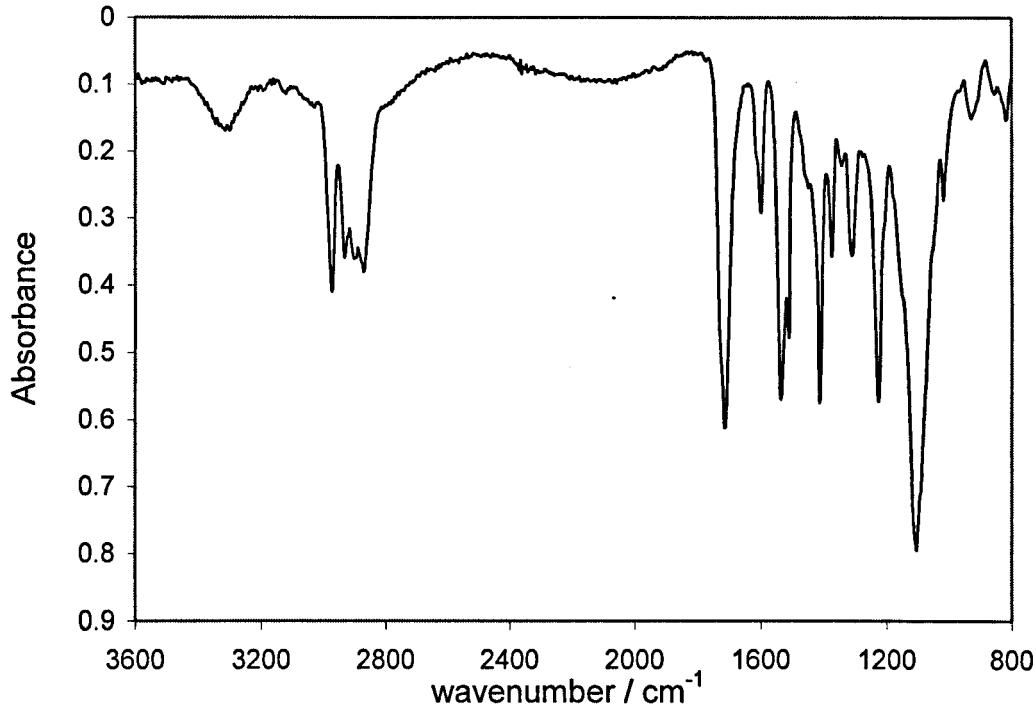
Absorbance
0
0.1
0.2
0.3
0.4
0.5
0.6
0.7
0.8
0.9
3600
3200
2800
2400
2000
1600
1200
800
wavenumber / cm-1

500 μm

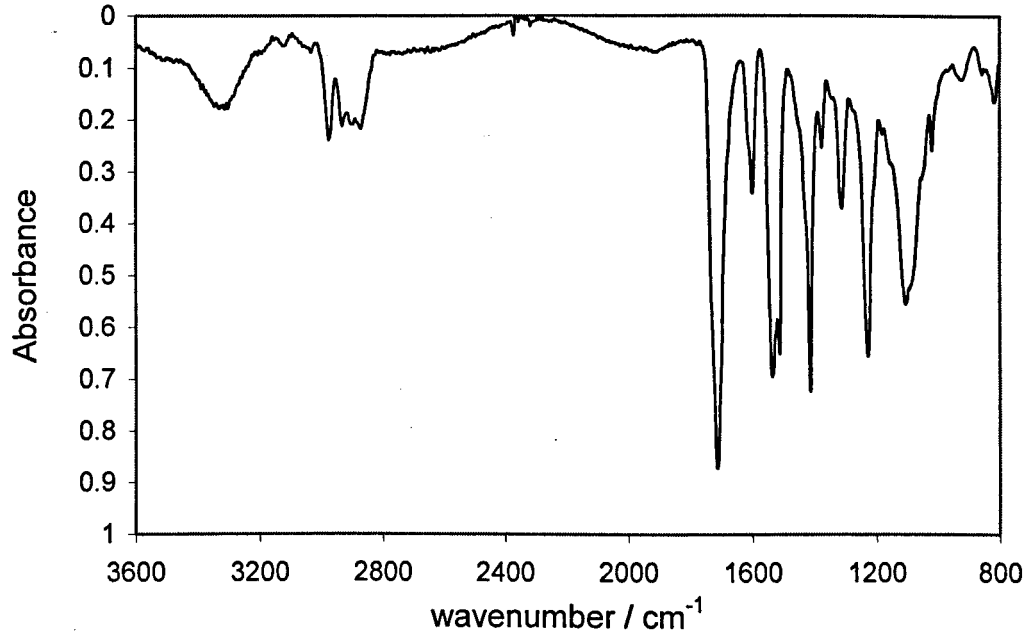
Absorbance
0
0.1
0.2
0.3
0.4
0.5
0.6
0.7
0.8
0.9
1
3600
3200
2800
2400
2000
1600
1200
800
wavenumber / cm-1

550 μm

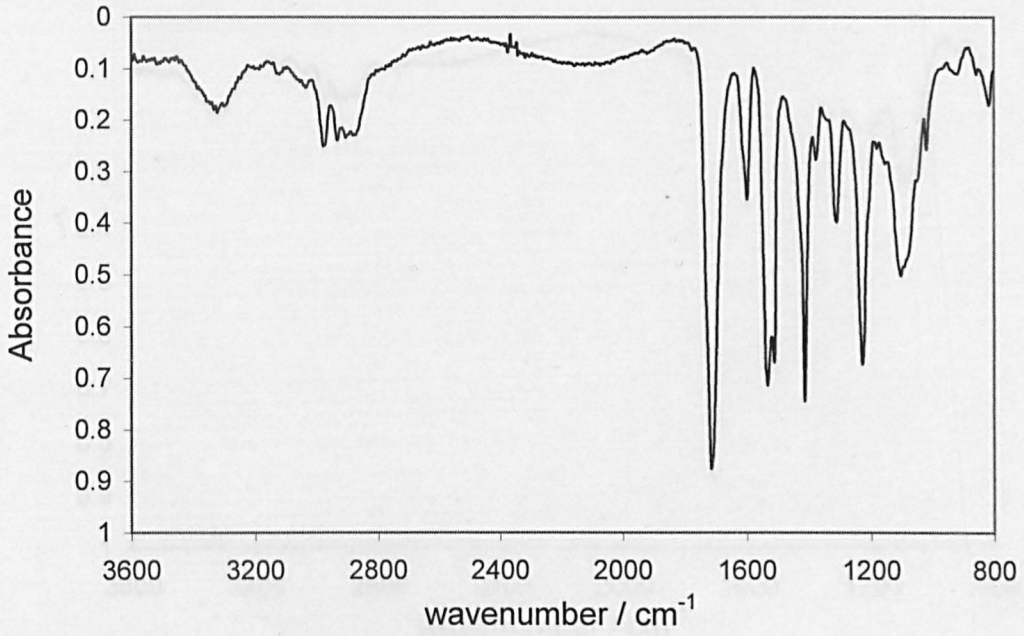
Absorbance
0
0.1
0.2
0.3
0.4
0.5
0.6
0.7
0.8
0.9
1
3600
3200
2800
2400
2000
1600
1200
800
wavenumber / cm-1

600 μm

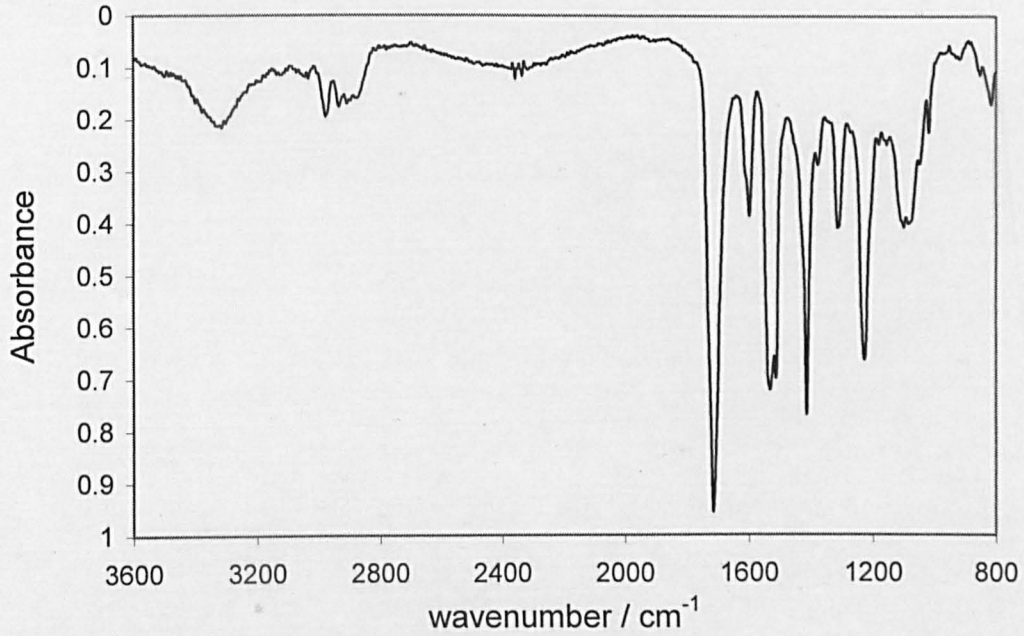
Absorbance
0
0.1
0.2
0.3
0.4
0.5
0.6
0.7
0.8
0.9
1
3600
3200
2800
2400
2000
1600
1200
800
wavenumber / cm-1

650 μm

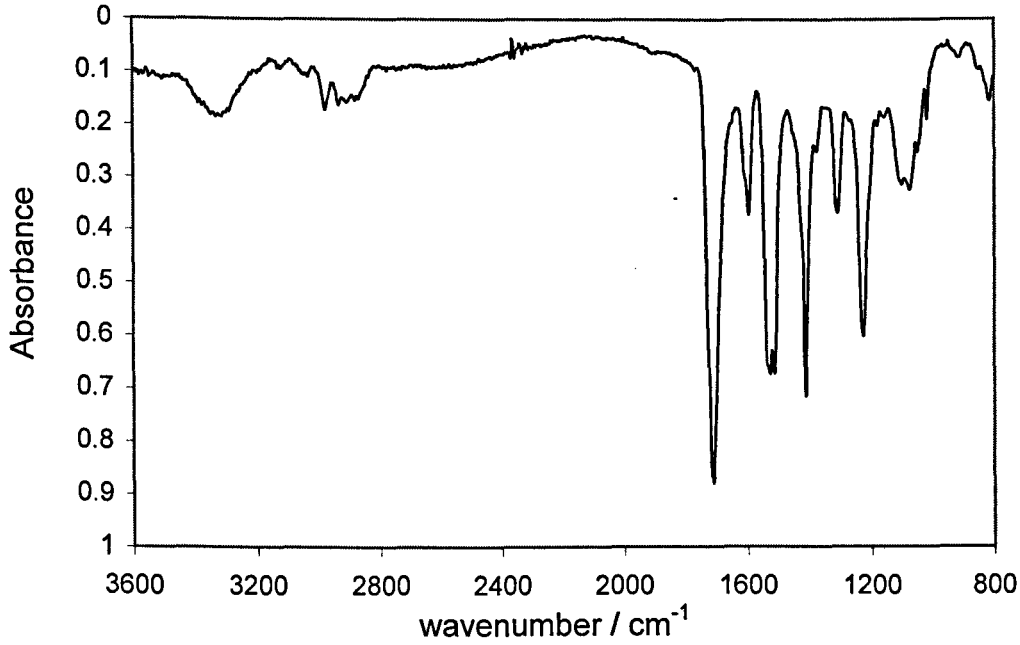
Absorbance
0
0.1
0.2
0.3
0.4
0.5
0.6
0.7
0.8
0.9
1
3600
3200
2800
2400
2000
1600
1200
800
wavenumber / cm-1

Appendix 3 DSC

4200 50%

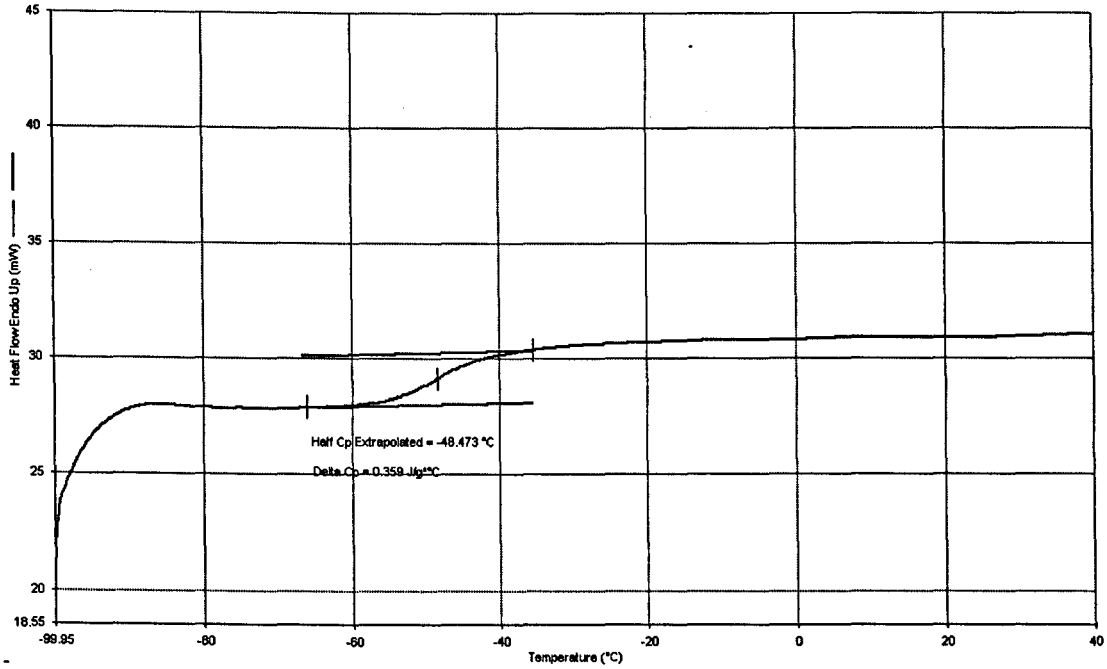

725 40%

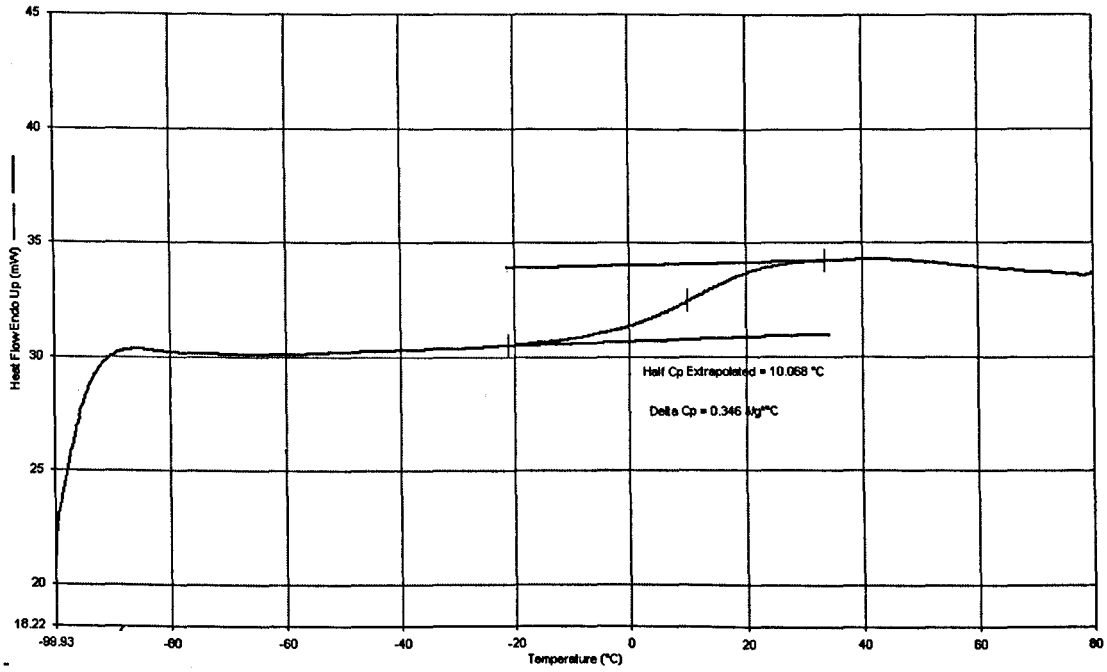

2200 40%

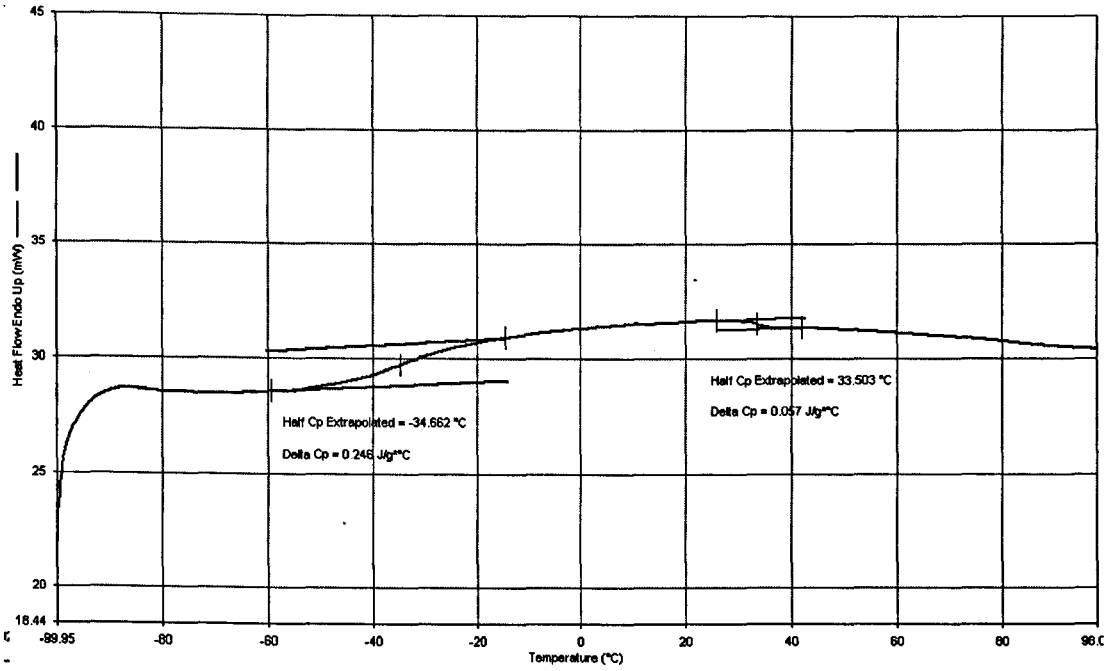
Heat Flow Endo Up (mW)
Temperature (°C)
Half Cp Extrapolated = -34.662 °C
Delta Cp = 0.246 J/g*°C
Half Cp Extrapolated = 33.503 °C
Delta Cp = 0.057 J/g*°C

Appendix 4 LAMS Data

Graded samples

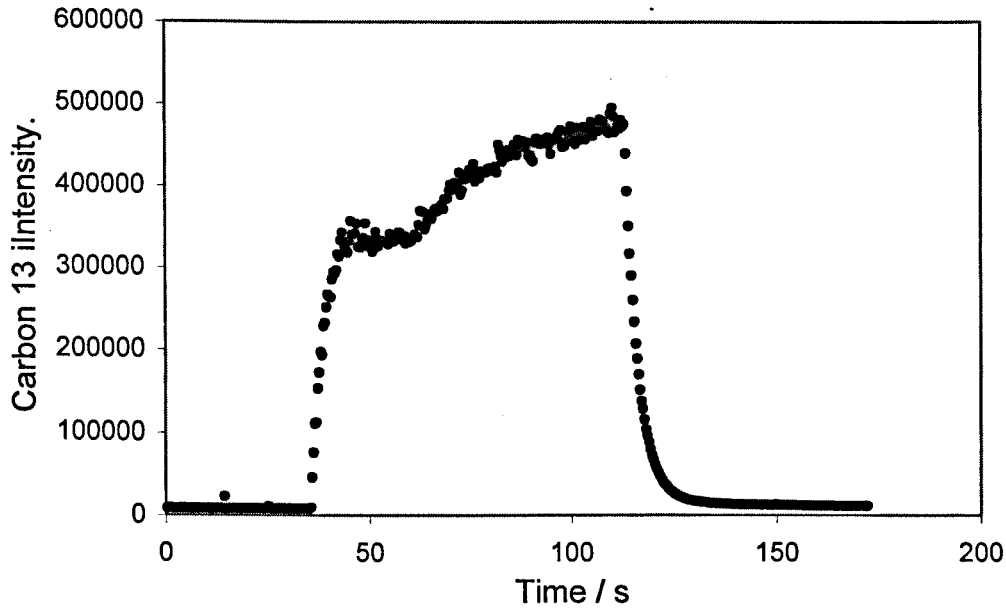

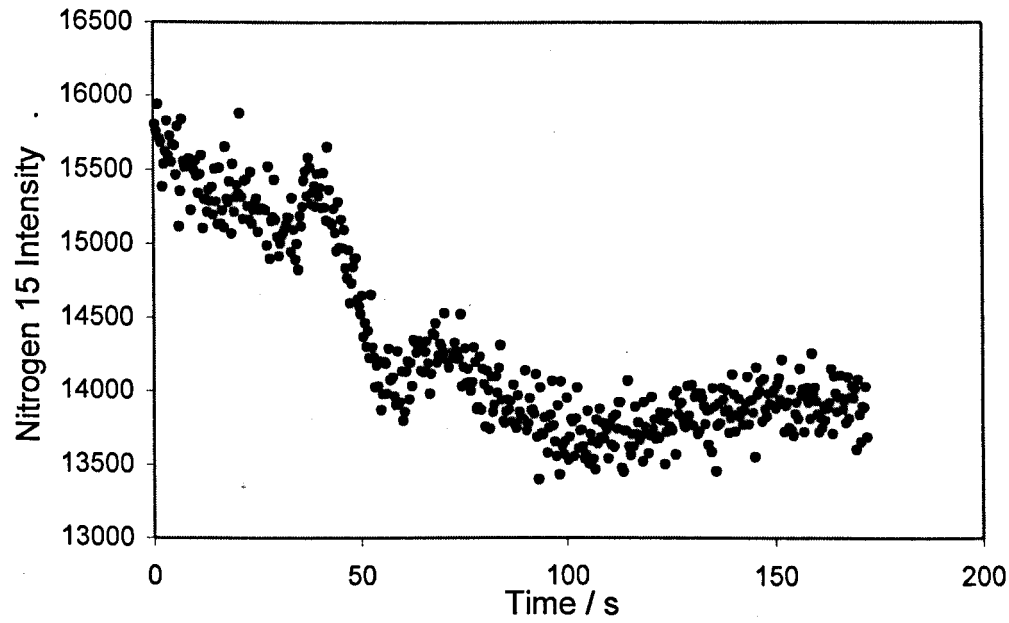

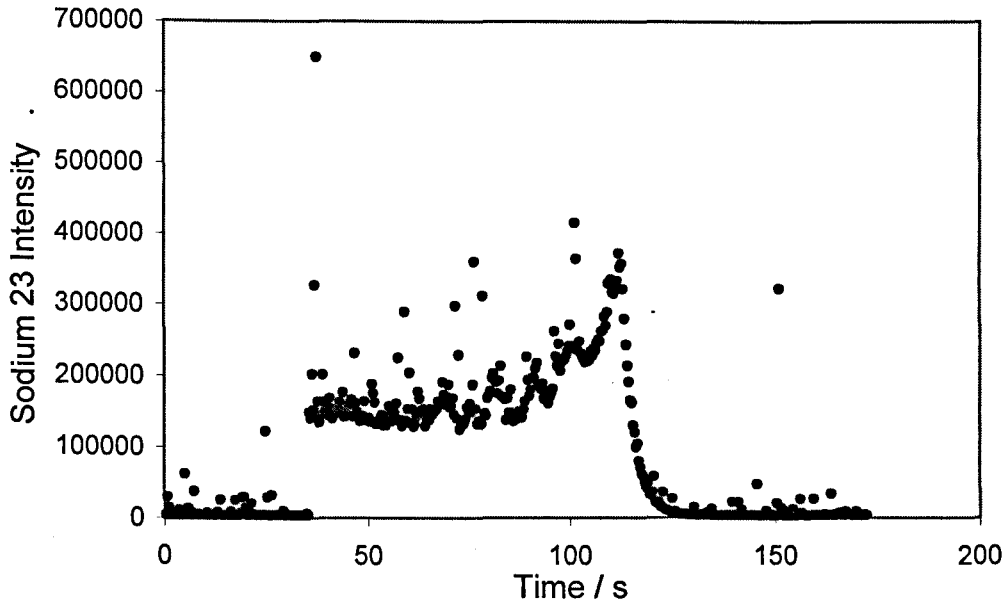
Sodium 23 Intensity
700000
600000
500000
400000
300000
200000
100000
0
0
50
100
150
200
Time / s

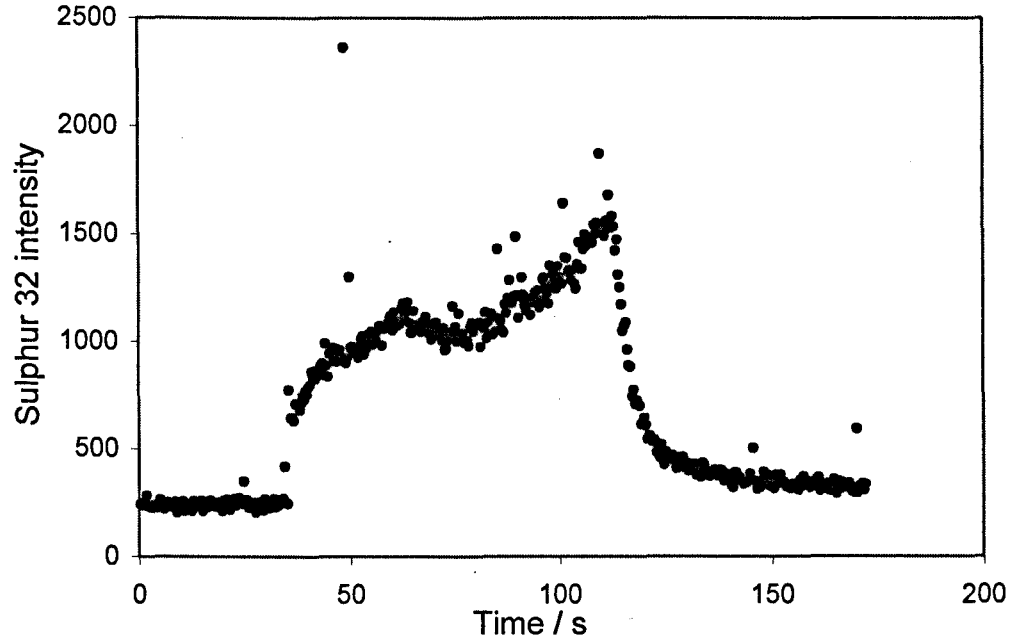
Sulphur 32 intensity
2500
2000
1500
1000
500
0
0
50
100
150
200
Time / s

Layered Samples

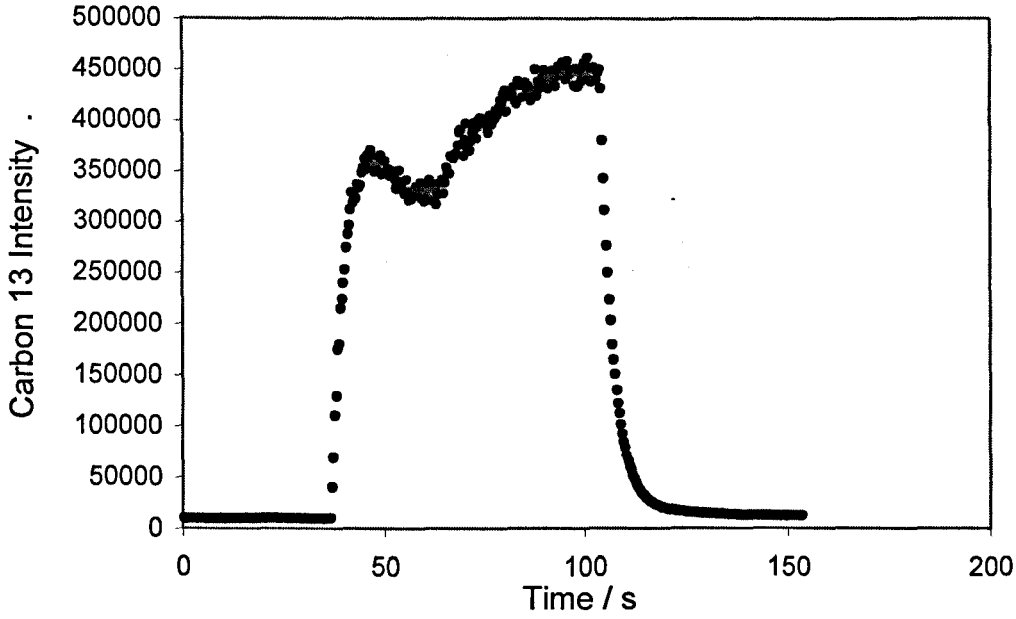

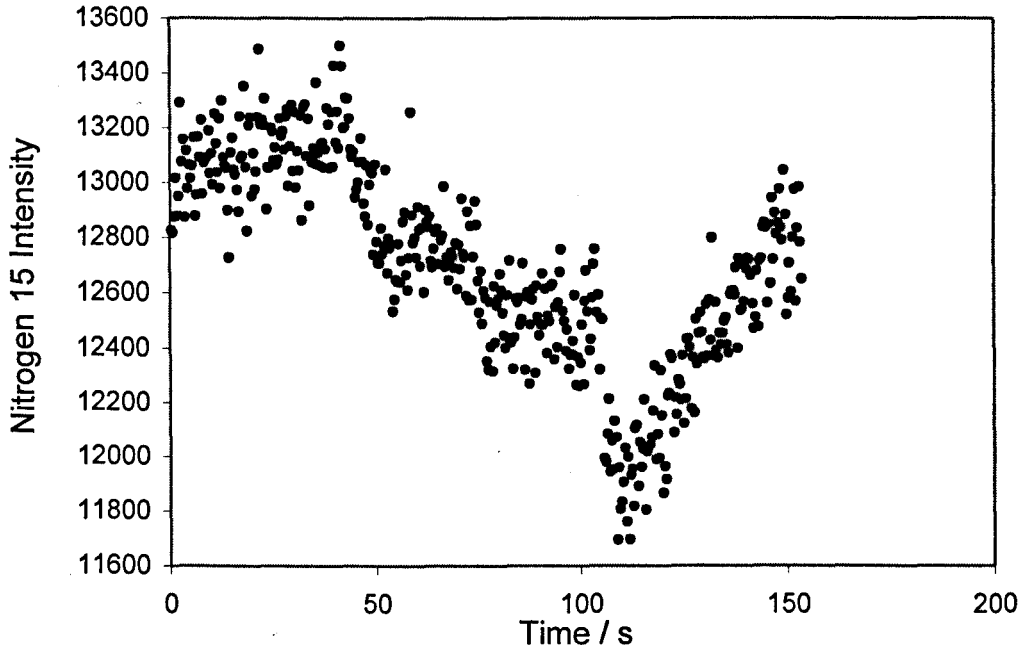

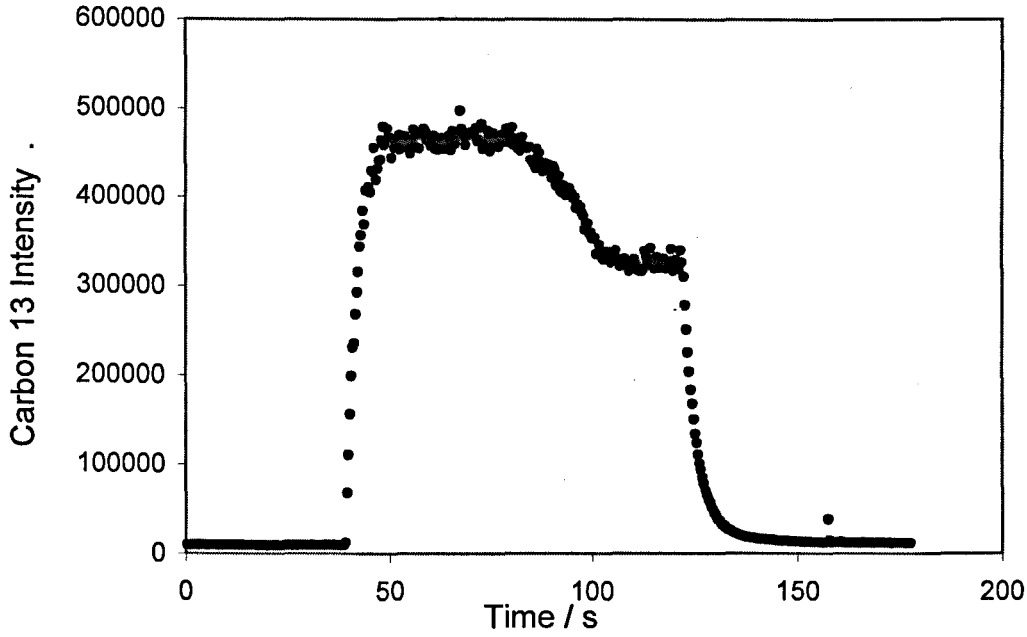
Carbon 13 Intensity
600000
500000
400000
300000
200000
100000
0
0
50
100
150
200
Time / s

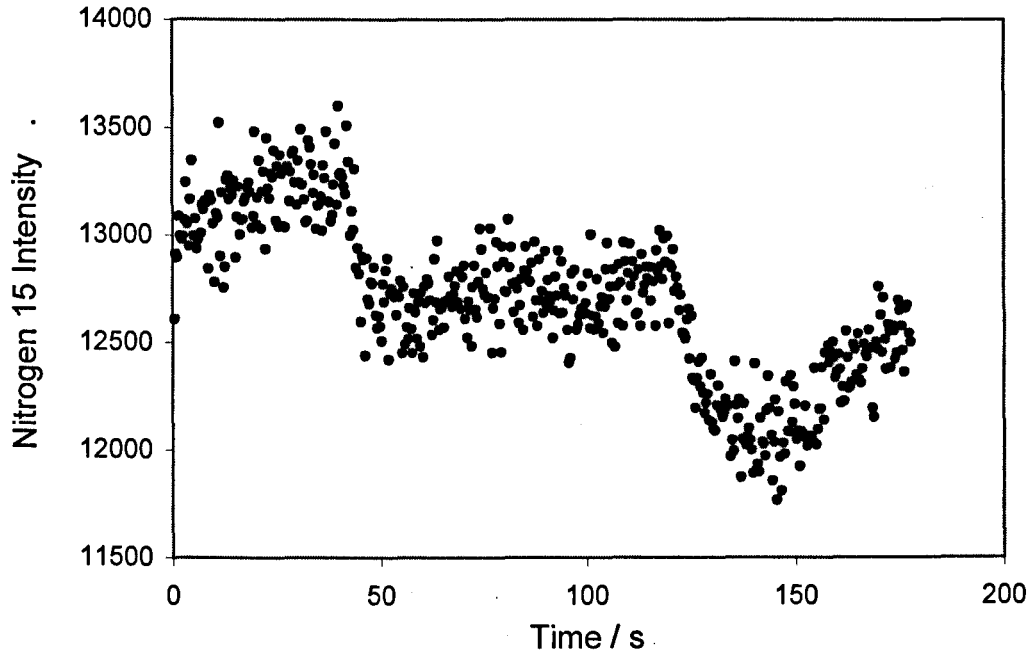
Nitrogen 15 Intensity
14000
13500
13000
12500
12000
11500
0
50
100
150
200
Time / s

Appendix 5 Nanoindentation

4200 30 % tan δ

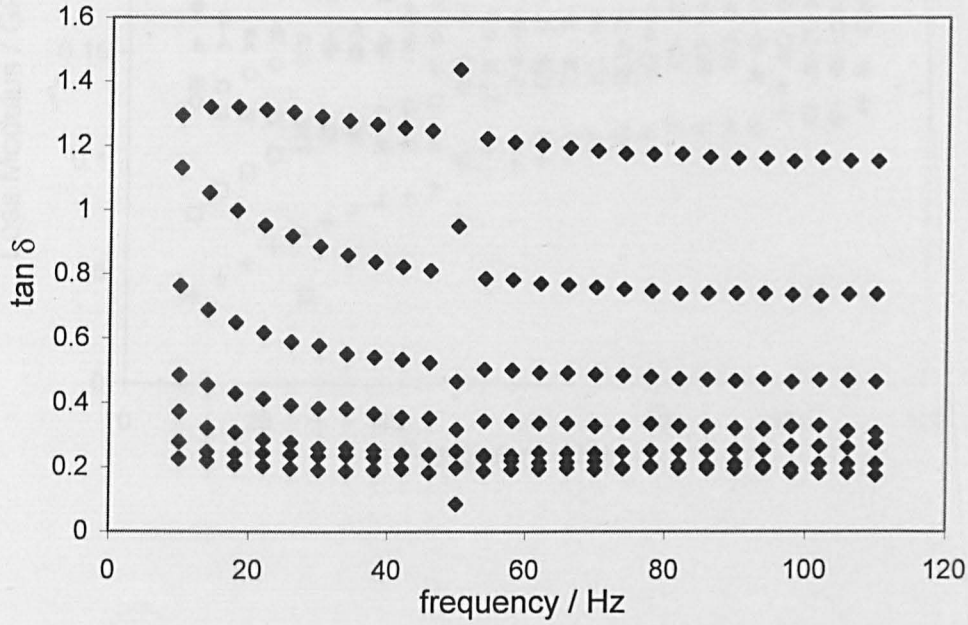

Storage Modulus 4200 30%

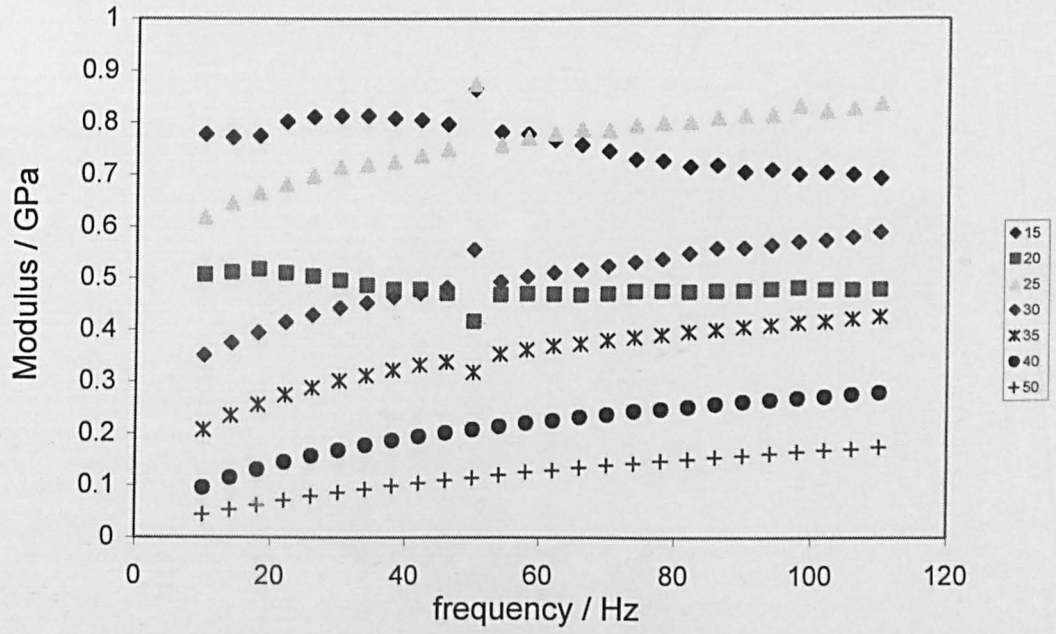

Loss Modulus 4200 30%